pennsylvania
DEPARTMENT OF TRANSPORTATION

Study of Glass Bead Gun Angle when Applying Glass Beads on Waterborne Paint

FINAL REPORT

October 8, 2009

By Eric T. Donnell, Zoltan Rado,
Barry E. Scheetz, Philip M. Garvey
and Ghassan Chehab

The Thomas D. Larson
Pennsylvania Transportation Institute

PENNSTATE
1855

COMMONWEALTH OF PENNSYLVANIA
DEPARTMENT OF TRANSPORTATION

Contract No. 510401
Work Order No. 016

DEPARTMENT OF TRANSPORTATION
UNITED STATES OF AMERICA

Technical Report Documentation Page

1. Report No. FHWA-PA-2009-017-510401-016	**2. Government Accession No.**	**3. Recipient's Catalog No.**
4. Title and Subtitle Study of Bead Gun Angle when Applying Glass Beads to Waterborne Paint		**5. Report Date** October 8, 2009 **6. Performing Organization Code**
7. Author(s) Eric T. Donnell, Zoltan Rado, Barry E. Scheetz, Philip M. Garvey, and Ghassan Chehab		**8. Performing Organization Report No.** LTI 2010-01 / PSU-2007-03
9. Performing Organization Name and Address The Thomas D. Larson Pennsylvania Transportation Institute The Pennsylvania State University 201 Transportation Research Building University Park, PA 16802-4710		**10. Work Unit No. (TRAIS)** **11. Contract or Grant No.** 510401, Work Order 16
12. Sponsoring Agency Name and Address The Pennsylvania Department of Transportation Bureau of Planning and Research Commonwealth Keystone Building 400 North Street, 6th Floor Harrisburg, PA 17120-0064 The Mid-Atlantic Universities Transportation Center 201 Transportation Research Building University Park, PA 16802-4710		**13. Type of Report and Period Covered** Final Report 4/09/2008 – 10/08/2009 **14. Sponsoring Agency Code**

15. Supplementary Notes

COTR: Matthew Briggs, 717-783-6268

16. Abstract

Retroreflectivity of pavement markings is an important measure of their nighttime effectiveness. In Pennsylvania, retroreflectivity is achieved by placement of spherical glass beads in the pavement marking paint using a bead gun attached to a paint truck. The purpose of this project was to investigate the application angle of glass beads on waterborne paint to determine which angle(s) result in optimal nighttime visibility from a paint truck moving at various speeds. A variety of laboratory and field experiments were conducted to evaluate pavement marking performance, including digital image processing, scanning electron microscopy, high-speed video imagery, end detection distance measurements from research participants, and retroreflectivity measurements. The laboratory tests were subjected to accelerated wear and weather exposure. The results indicate that the 12 mph truck application speed and -20 degree bead gun angle provides the optimal nighttime visibility based on the laboratory and field evaluations performed in the present study.

17. Key Words Pavement markings, delineation, retroreflectivity, waterborne paint, glass bead, bead gun angle, digital image processing, scanning electron microscopy, nighttime driving experiment	**18. Distribution Statement** No restrictions. This document is available from the National Technical Information Service, Springfield, VA 22161

19. Security Classif. (of this report)	**20. Security Classif. (of this page)**	**21. No. of Pages**	**22. Price**
Unclassified	Unclassified	110	

STUDY OF GLASS BEAD ANGLE WHEN APPLYING GLASS BEADS ON WATERBORNE PAINT

PennDOT/MAUTC Partnership Research Agreement No. 510401

FINAL REPORT

Prepared for

Commonwealth of Pennsylvania
Department of Transportation

By

Eric T. Donnell, Ph.D., P.E.
Zoltan Rado, Ph.D.
Barry E. Scheetz, Ph.D.
Phillip M. Garvey
Ghassan Chehab, Ph.D.

The Thomas D. Larson Pennsylvania Transportation Institute
The Pennsylvania State University
Transportation Research Building
University Park, PA 16802-4710

October 2009

This work was sponsored by the Pennsylvania Department of Transportation and the U.S. Department of Transportation, Federal Highway Administration.

ACKNOWLEDGEMENTS

The authors would like to acknowledge the Pennsylvania Department of Transportation for sponsoring this research. In particular, the authors thank Messrs. Kenneth Williams and Matthew Briggs from the Bureau of Highway Safety and Traffic Engineering, and Mr. David Kuniega from the Bureau of Construction and Materials, for their support, guidance, and many technical insights offered over the course of the study. Ms. Lisa Karavage from the Division of Research is acknowledged for her support and management of the project. Finally, the authors would like to acknowledge Ms. Robin Tallon and Mr. Dan Fura from the Larson Institute at Penn State for assisting in acquiring much of the laboratory data used in the study. Mr. Joe Kearns from the Materials Research Laboratory is acknowledged for his contribution running the scanning electron microscope. Ms. Ivette Cruzado, Ms. Erin Hlava, and Mr. Chris Kahler, all students at Penn State during this study, are acknowledged for their data collection efforts during the nighttime driving experiment. Ms. Lekshmi Sasidharan, a Ph.D. candidate at Penn State, is acknowledged for her assistance in analyzing the nighttime driving experimental data.

TABLE OF CONTENTS

LIST OF FIGURES

LIST OF TABLES

CHAPTER 1. INTRODUCTION

Longitudinal pavement markings are used to delineate the limits of a travel lane, convey regulations or warnings, provide guidance to road users, and/or supplement other traffic control devices. The coefficient of retroreflected luminance, R_L—herein referred to as retroreflectivity—is a measure of the amount of light reflected back to a source. In the case of longitudinal pavement markings, the light source is vehicle headlamps. Retroreflectivity of pavement markings is an important measure of their nighttime effectiveness. In Pennsylvania, retroreflectivity is achieved by placement of spherical glass beads in the pavement marking paint using a bead gun attached to a paint truck. A preliminary study conducted by the Pennsylvania Department of Transportation's (PennDOT) Bureau of Highway Safety and Traffic Engineering (BHSTE) indicated that some bead gun angles result in higher initial pavement marking retroreflectivity than others. The purpose of this project is to investigate the application angle of glass beads on waterborne paint to determine which angle(s) result in optimal bead embedment and maximize pavement marking retroreflectivity and visibility from a paint truck moving at various speeds. As it is possible that some truck speeds and bead gun angles will produce different levels of nighttime visibility quality over time, the pavement markings considered in the present experiment were evaluated shortly after application and at regular intervals over the study period.

1.1 Research Objectives and Scope

The primary objective of this study was to determine the paint truck application speed and bead gun angle combination that produces a high level of initial pavement marking visibility that is also maintained over a 1-year period. As such, initial pavement marking retroreflectivity is not the only measure of effectiveness considered; rather, this measure is combined with a measure of durability to assess pavement marking visibility.

The project was divided into three technical tasks as follows:

- Task 1: Synthesize the extant literature related to pavement marking application and evaluation methods, and develop an experimental plan to collect and evaluate various pavement marking visibility performance metrics.
- Task 2: Apply 18 white, longitudinal pavement markings at the Thomas D. Larson Pennsylvania Transportation Institute Test Track Facility at various bead gun angles and paint truck speeds. During the application process, high-speed video cameras were mounted on PennDOT's paint truck to record kinematic parameters of glass beads being discharged from the bead gun. Additionally, 36 sample test plates were fastened to the pavement surface and painted during the application process. These test plates were used for laboratory testing and evaluation.
- Task 3: Evaluate the 36 sample test plates and 18 in-situ pavement markings. The 36 sample test plates were split into separate samples of 18 test plates. One set of test plates was subjected to continuous traffic loadings using a Model Mobile Load Simulator (MMLS). The other set of 18 test plates was placed in an outdoor laboratory for full exposure to the weather for a period of 1 year. Both sets of sample test plates were exposed to a variety of evaluations that are described in more detail in Chapter 3 of this

report. Periodic retroreflectivity measurements were recorded on the 18 in-situ pavement markings and a two-phase nighttime driving experiment was conducted to evaluate the detection distance of each marking soon after application and then again after being weathered for nearly a 1-year period.

1.2 Organization of the Report

This report is organized into five subsequent chapters. Chapter 2 provides background information on PennDOT's waterborne pavement marking and glass bead specifications. Published literature related to nighttime experimentation of pavement markings, as well as various imagery and other laboratory and field evaluation methods of pavement markings, is summarized in Chapter 2. Chapter 3 describes the experimental plan used to evaluate the initial visibility and long-term durability of the pavement markings considered in this study. Chapter 4 contains a summary of the various laboratory evaluation methods used to perform the pavement marking evaluations, while Chapter 5 contains a summary of the various field evaluation methods. Chapter 6 describes various correlation analyses that were performed to determine the optimal bead gun angle/truck speed application combination. Chapter 7 includes a summary of the research and recommendations related to the optimal truck application speed and bead gun angle to achieve both high initial levels of visibility and long-term durability of the 18 pavement marking samples included in the present study.

CHAPTER 2. BACKGROUND AND LITERATURE REVIEW

The first section in this chapter provides background information related to PennDOT's waterborne pavement marking and glass bead specifications. The literature review is divided into three sections: (a) methods used to capture and evaluate static and dynamic images of pavement markings, (b) domestic and international accelerated wear testing of pavement markings, and (c) pavement marking human factors research methods. In the first section, methods to determine the surface area of glass beads in pavement markings are described based on static images. Additionally, methods used to evaluate the dynamic behavior of glass beads during the pavement marking application process are summarized. The second section of the literature review describes various accelerated wear pavement marking evaluation programs in use both domestically and internationally. The last section of the literature review describes numerous human factors experiments performed in the United States to determine driver perceptions of various pavement markings.

2.1 PennDOT Pavement Marking and Glass Bead Specifications

Waterborne traffic paint and glass beads in Pennsylvania are supplied by a variety of manufacturers. Longitudinal pavement markings are applied on highways in Pennsylvania at a wet-film thickness of 15 mils $\pm$ 1 mil, with the exception of edge line markings, which are applied at a wet-film thickness of 12 mils $\pm$ 1 mil. Glass beads are applied at a rate of 7 pounds per gallon of paint and satisfy the following gradation criteria (PennDOT, 2007):

- 100 percent of glass beads pass sieve size 16 (1.18 mm),
- 75 to 95 percent of glass beads pass sieve size 30 (600 μm),
- 15 to 35 percent of glass beads pass sieve size 50 (300 μm), and
- 0 to 2 percent of glass beads pass sieve size 100 (150 μm).

The glass beads are dispensed immediately after the paint film. The glass beads have a larger diameter than the wet-film thickness of paints and therefore are exposed to vehicle headlamps, which provide light reflection at night. As such, bead embedment and dispersion are two important issues related to waterborne pavement markings in Pennsylvania.

2.2 Imagery Analysis Methods

2.2.1 Static Images

Rich et al. (2002) used high-temperature pyrolysis and image processing methods in an effort to correlate glass bead properties in traffic paint to pavement marking retroreflectivity in Michigan. A set of 12-inch by 6-inch test plates were used to collect the pavement marking samples (five yellow and five white) – each marking was applied in a laboratory at a wet-film thickness of 15 mils. A premeasured amount of glass beads were applied to the paint using a saltshaker. The sample plates were dried at room temperature for two days and any glass beads that were not retained in the paint were removed and weighed prior to the analysis. The panels were pyrolyzed at 932 ^{o}F (500 ^{o}C) for 5 hours and weighed. Control panels without glass beads were subjected to the same process to determine the weight of the traffic paint. It was shown that the pyrolysis

method could determine the amount of glass added to the paint with less than 7 percent error. Because the pyrolysis analysis could not determine the location of the glass beads in the paint, image processing analysis was used. Test plates collected in the field were initially used to develop the image processing analysis method. A binary image of the sample was used to determine the percentage of the surface covered by glass beads. An example of a macrograph from a test plate is shown in Figure 1a, while the binary image is shown in Figure 1b.

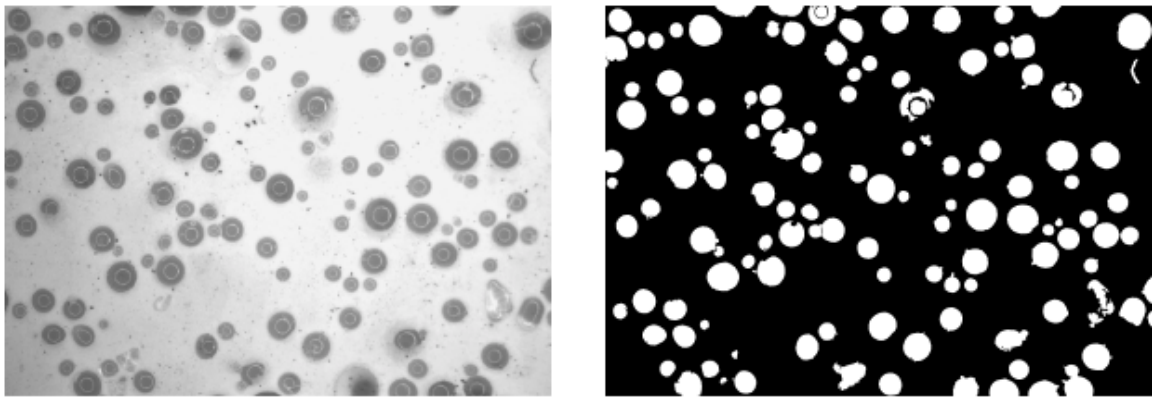

(a) Macrograph of Pavement Marking Sample. (b) Binary Image of Pavement Marking Sample.

Figure 1. Image Analysis of Pavement Marking Sample (Rich et al., 2002).

The image processing analysis was performed using the following procedures:

- Convert macrograph image to binary image;
- Sort objects based on an aspect ratio (circles have aspect ratio of one);
- Filter out particles that are too small or irregularly shaped such as dust and debris;
- Manually highlight glass beads on the edge of the macrograph or those touching each other.

The analyses performed by Rich et al. (2002) showed a strong correlation between the pyrolysis and image processing methods; however, the comparison was limited to only four test plates. A generally linear trend was found between pavement marking retroreflectivity and the percentage of the paint surface covered by glass beads using the image processing method. It was noted that the association of glass bead size and pavement marking retroreflectivity is not well understood and should be further investigated in future image processing analysis.

O'Brien (1989) subjectively evaluated the retroreflectivity and embedment characteristics of Illinois drop-on moisture-proofed and uncoated glass beads on various hot-applied thermoplastic pavement markings in a laboratory. Initial evaluations were performed using a glass bead application rate of 6 lb/100 ft^2 (29.4 kg/100 m^2). Subsequent evaluations were performed at various bead application rates. All retroreflectivity subjective evaluations were performed in a dark room with light emitted by a small flashlight at distances of 10 and 25 ft (3.1 and 7.6 m). Photomicrographs were taken to show glass bead dispersion and embedment; these images were also evaluated subjectively. Table 1 shows the subjective evaluation results for pavement marking retroreflectivity and glass bead embedment for white and yellow pavement markings. It

should be noted that there were two uncoated and a single moisture-proofed glass bead evaluated. The Type 1 and Type 2 uncoated glass beads had slightly different gradations, although both were based on the same specification.

Table 1. Subjective Evaluation of Pavement Marking Retroreflectivity and Glass Bead Embedment based on Application Rate of 6 lb/100 ft^2 (O'Brien, 1989).

System[a]	White Pavement Marking System (Retroreflectivity/Embedment)		
	Bead 1: Uncoated (70 % rounds)	**Bead 2: Uncoated (83% rounds)**	**Bead 2C: Moisture-Proofed**
A	Minimal/95-100	Moderate/80-85	Excellent/60-65
B	Minimal/95-100	Moderate/80-85	Excellent/60-65
C	Moderate/80-85	Moderate-Excellent/70-75	Excellent/60-65
D	Minimal/95-100	Minimal/95-100	Excellent/60-65
	Yellow Pavement Marking System (Retroreflectivity/Embedment)		
A	Minimal/95-100	Moderate/80-85	Excellent/60-65
B	Minimal/95-100	Moderate/80-85	Excellent/60-65
C	Minimal-Moderate/90-95	Moderate/80-85	Excellent/60-65
D	None/100	None/100	Excellent/60-65

[a] System refers to the four different thermoplastic markings supplied by different manufacturers.

Table 2 shows the subjective evaluation results for the moisture-proofed glass bead application rate analysis. The coverage and embedment, retroreflectivity, and visual acuity of the glass beads were all evaluated based on the application rates shown in Table 2.

Table 2. Subjective Evaluation of Glass Bead Coverage, Retroreflectivity, Glass Bead Embedment, and Visual Acuity Related to Glass Bead Application Rate (O'Brien, 1989).

Application Rate (lbs/100 ft^2)	Glass Bead Coverage	Retroreflectivity	Glass Bead Embedment	Visual Acuity
2	Minimal	Minimal-Moderate	60-65	Dull
4	Minimal	Moderate	60-65	Dull
6	Moderate	Excellent	60-65	Sharp
8	Excellent	Excellent	60-65	Sharp
10	Excellent	Excellent	60-65	Sharp
12	Excessive	Excellent	50-55	Scattered
14	Excessive	Excellent	40-45	Scattered

Based on the subjective analysis, O'Brien (1989) concluded that the use of moisture-proofed glass beads resulted in optimal embedment, coverage, retroreflectivity, and visual acuity when applied at a rate of 10 lb/100 ft^2 (26.9 kg/100 m^2). This application rate resulted in optimal embedment of 60 to 65 percent with excellent glass bead coverage and retroreflectivity.

2.2.2 Dynamic Images

Mizera et al. (2009) evaluated two different glass bead guns using a Photron Fastcam® SA-1 high-speed camera. The camera is capable of recording 5,000 frames per second and was set up in a static position perpendicular to the direction of the pavement marking application along an

in-service roadway. The application of glass beads in waterborne paint was recorded and the glass bead distribution, bead roll, initial pavement marking retroreflectivity, and glass bead trajectory were evaluated at application speeds of 8, 10, 12, and 14 mph (13, 16, 19, and 23 km/h). All pavement marking samples were applied on a 10-inch (25-cm) by 24-inch (60-cm) aluminum test plate.

In-place glass bead distributions were computed using 1-inch (2.5-cm) by 1-inch (2.5-cm) random samples from the aluminum test plates. These samples were photographed using a digital macro zoom camera. The number of Type III glass beads per square inch was highest at the slowest truck application speed and lowest when applied at the highest truck speed. The SpeedBeader™ from Potters Industries dispensed more beads at speeds between 8 and 12 mph (13 and 19 km/h) than the ZeroVelocity™ from EZ-Liner Industries because the application rate was set to 10 lb/100 ft^2 in the Speed Beader™ while the application rate of beads in the ZeroVelocity™ bead gun was set at 9 lb/100 ft^2 for an application speed of 14 mph (23 km/h). As a result, the SpeedBeader™ bead gun was shown to produce higher bead densities than the ZeroVelocity™ bead gun at lower speeds, but the densities were nearly equal at the higher application speed.

To evaluate bead roll, separate square-inch samples from each aluminum test plate were evaluated. As expected, no bead roll was observed when the glass beads were applied using the ZeroVelocity™ bead gun, except when applied at a speed of 14 mph (23 km/h), where only 2 percent of the beads rolled. Bead roll was observed when applying glass beads using the SpeedBeader™ bead gun, ranging from 7 percent at 8 mph (13 km/h) to 56 percent at 14 mph (23 km/h).

Initial pavement marking retroreflectivity levels were measured on the test plates 26 days after the panels were painted in the field. The SpeedBeader™ bead gun was used when applying white waterborne paint while the ZeroVelocity™ bead gun was used when applying yellow waterborne paint. As expected, the retroreflectivity for white pavement markings was higher when compared to yellow markings. There appeared to be a direct correlation between increased bead roll and truck application speed and lower levels of initial pavement marking retroreflectivity.

The high-speed video was used to subjectively evaluate the trajectory of glass beads from the two bead guns. Both appeared to produce nominal horizontal velocities.

2.2.3 Summary

Although much of the existing research does not directly relate to the objectives of the present study, there are several interesting findings worth noting based on past glass bead evaluations using static and dynamic imagery analysis methods. First, it appears that image processing provides an objective method to evaluate the percentage area covered with glass beads (number of beads per unit area) and to assess the uniformity of bead coverage over a specific area. Analyzing a series of photographs from the same application area taken at different time periods can allow for objective comparisons of bead loss as the pavement markings are subjected to both weather and traffic. Secondly, O'Brien (1989) notes that the optimal embedment of glass beads

in thermoplastic pavement marking systems is 60 to 65 percent. While waterborne pavement markings are the focus of the present study, it appears that greater levels of embedment do not necessarily improve pavement marking retroreflectivity. Finally, increasing truck application speeds appear to increase bead roll as glass beads are dispensed into waterborne paints. The increased roll appears to be linked to lower levels of initial pavement marking retroreflectivity.

2.3 Accelerated Wear Testing Evaluations

Donnell et al. (2009) performed exploratory testing to assess the feasibility of using a portable accelerated wear tester (Model Mobile Load Simulator, 3rd scale [MMLS3]) to evaluate the degradation of pavement markings over time. The experiment consisted of applying 10 different white pavement markings at an outdoor laboratory and the same 10 markings at a transverse test deck applied on a two-lane roadway. Pavement marking retroreflectivity was measured at various stages in between traffic loading cycles applied using the MMLS3 and compared to retroreflectivity levels measured periodically in the wheel path of the transverse pavement markings at the test deck. Both dry and wet testing was conducted using the MMLS3, and the results produced similar trends in the outdoor laboratory when compared to the transverse test deck. The authors concluded that the feasibility of using the MMLS3 to evaluate pavement marking retroreflectivity loss over time on transverse markings appeared to correlate well with the on-road test deck; however, additional testing was needed to validate the findings and to determine the transferability of the method to longitudinal pavement markings.

Choubane et al. (2006) investigated the feasibility of using a heavy vehicle simulator (HVS) to perform accelerated wear testing of raised pavement markers for the purpose of product qualification in Florida. A total of 32 raised pavement markers (RPMs), represented by four different classes (i.e., temporary work zone, work zone, temporary, and permanent), were evaluated under simulated traffic conditions. The performance metrics used in the analysis were the structural integrity of the RPMs and the retroreflectivity. All RPMs were of a similar design. Each RPM had eight replicates, randomly installed in two separate arrays of 16 RPMs. Each set of RPMs received either a full or half hit with the HVS tire. The HVS tire was 12 inches wide and loaded to 9,000 lb with a pressure of 115 psi – the loading was applied at a speed of 8 mph in one direction with a 42-inch wheel wander. Observations from the HVS evaluation indicated that no RPMs exhibited any structural failure; no RPMs settled into the asphalt pavement surface; rubber tire buildup was evident on all RPMs; and all testing (72,322 HVS passes) was completed in 1 week. Although the coefficient of luminous intensity was measured before and after the accelerated wear testing, the measurements were not correlated with any like measurements from in-service RPMs. However, it was concluded that accelerated wear testing was a feasible and efficient method to evaluate the long-term performance of RPMs.

In Europe, two accelerated pavement marking wear testing programs have been developed and evaluated. These include the Federal Highway Research Institute (BASt) wear simulator in Germany and the AETEC wear simulator in Spain. The BASt accelerated wear testing machine has a diameter of 21 ft (6.4 m), where up to 72 pavement marking test specimens can be evaluated simultaneously by applying up to eight wheel loads on a circular steel turntable (Keppler, 2003). Pavement marking wear testing always begins with new test tires. The pavement marking test specimens are applied along the outer edge of the turntable on top of cast

asphalt that has a texture depth of 0.004 to 0.02 inches (0.1 to 0.5 mm). One year of traffic loadings in an on-road setting can be simulated in the accelerated wear testing machine in approximately 1 week (50:1 ratio) (Baker and Ferragut, 2005). The pavement marking samples are evaluated based on physical chemical, endurance, and prototype tests. The physical chemical test evaluates the pavement marking sample on its resistance of alkalis. Although this test is not a criterion for exclusion of the pavement marking along German roads, failure to resist alkalis prevents the use of the specimen on concrete pavements (Keppler, 2003). The endurance test is undertaken with up to eight different traffic loading classifications based on the intended use of the pavement marking sample. Minimum levels of various pavement marking properties must be maintained throughout the endurance test. These include (Keppler, 2003):

- Dry coefficient of retroreflected luminance,
- Wet coefficient of retroreflected luminance,
- Coefficient of retroreflected luminance in rain (if requested by sample provider),
- Luminance coefficient in diffuse illumination (daylight reflection),
- Chromaticity of pavement marking sample based on standard CIE color chart,
- Skid resistance, and
- Remaining marking surface (durability).

If a pavement marking sample has met the requirements of the first two tests based on either permanent use (white markings) or temporary use (yellow markings), a prototype test is performed and the sample subjected to a variety of objective measurements based on German specifications. These tests include: wet and dry nighttime visibility (coefficient of retroreflected luminance), daytime visibility (luminance coefficient in diffuse illumination), skid resistance, durability, and drying time.

The AETEC wear simulator was developed jointly by four Spanish traffic marking companies and one glass bead company (Ferragut et al., 2005). Like the BASt accelerated wear simulator, the AETEC simulator can evaluate (pre-qualify) up to 72 test specimens on a turntable at a rate of nearly 1 million cycles per week. Four new wheels apply loads to the test specimens at a speed of 5 mph (10 km/h) or 35 mph (60 km/h). Pavement marking test specimens are selected based on the pavement marking type (e.g., edge line, centerline, etc.), pavement texture, roadway type (e.g., divided, undivided, lane width, etc.), and traffic volume (Ferragut et al., 2005). Pavement marking specimens are evaluated based on the following objective measures:

- Luminance coefficient in diffuse illumination (daylight reflection),
- Coefficient of retroreflected luminance in dry, wet, and rain conditions,
- Color based on standard chromaticity chart (white for permanent markings and yellow for temporary markings),
- Skid resistance based on pendulum test vehicle, and
- Alkalinity for pavement markings on concrete pavements and bleeding for pavement markings on asphalt pavements.

Both the AETEC and BASt accelerated wear testing simulators provide the advantage of pre-qualifying pavement markings for on-road use over a short time period. Additionally, the

simulators have been extensively tested and provide standard procedures in Europe for evaluating pavement marking samples.

Although limited accelerated-wear testing has been conducted in the United States related to pavement marking performance, recent research has shown that use of portable equipment to simulate traffic loading may be feasible. Accelerated wear testing programs in Europe have been extensively tested and validated. Both the AETEC and BASt simulators appear to be widely-accepted as pavement marking product performance evaluation methods.

2.4 Human Factors Evaluations of Pavement Markings

Research shows that pavement marking retroreflectivity (R_L) values alone may not consistently or accurately predict the level of pavement marking luminance (i.e., brightness) a driver experiences during nighttime driving (e.g., Burns et al., 2008). Also, variations in retroreflectivity, and for that matter, luminance, from one marking to another must be above a certain magnitude for drivers to notice a difference; this is known as the "just noticeable difference" (jnd). Studies of the jnd are concerned with determining through experimentation how perception changes as a function of changes in physical intensity. For every physical stimulus there is a physical measure of intensity associated with a psychological perception for each sense modality (light intensity yields brightness, weight yields heaviness, etc.). Early work in this field resulted in the development of Weber's Law, expressed as a very simple equation that can be used to determine the difference threshold between two stimuli. In Weber's Law, the ability to notice a change in stimulus intensity is a function of the intensity level of the original stimulus: $\Delta I/I = k$ where "I" is the initial stimulus intensity, "ΔI" is the change in intensity, and "k" is the Weber fraction or jnd.

Some of the past research identified for the present study evaluated only wet pavement markings (Gibbons and Hankey, 2007) or only centerlines (Zwahlen and Schnell, 1996). Several research studies, however, were identified that served the purpose of the literature review, namely to determine the levels of the following key factors in the present study:

- Number of research participants,
- Observation vehicle speed,
- Threshold criterion for research participant response,
- Length of pavement marking test lines, and
- Range of pavement marking detection distances.

Zwahlen and Schnell (1997) published a pavement marking detection study that evaluated the visibility of both centerline and edge line markings. End detection distance, defined as detection of the far downstream termination point of a pavement marking as the driver approaches, was their choice of dependent variable. The criterion for research participant response was a high degree of certainty, near 100 percent. The participants drove the observation vehicle between 5 and 10 mph (8 and 16 km/h). Ten young participants (average age of about 23 years) took part in the portion of the study that pertained to the present research. The 610 ft (186 m) long white edge line marking that was relevant to the present study had a retroreflectivity of 425 mcd/m^2/lx. The edge line was only 2 inches (5 cm) wide. None of the 10 participants could detect the end of

the pavement marking beyond 660 ft (201 m), nine beyond about 550 ft (168 m), and eight of the participants could not detect the end of the pavement marking beyond about 490 ft (149 m).

Zwahlen and Schnell (1999) published another study that evaluated pavement marking end detection distance. Again, the criterion for participant response was a high degree of certainty, near 100 percent. Among other conditions, but most relevant to the current research, was a white, 4-inch (10-cm) wide, 1,200-ft (366-m) long right edge line marking with a retroreflectivity level of 268 mcd/m^2/lux. Using low-beam head lamps, research participants drove the observation vehicle between 5 and 10 mph (8 and 16 km/h) toward the marking. Twenty research participants (10 young and 10 old) took part in the research. The researchers found that 20 percent of the younger participants and none of the older participants were able to detect the end of the markings beyond 650 ft (198 m), and that only 10 percent of the younger participants were able to detect it beyond about 900 ft (274 m). The longest detection distance for the oldest drivers was 581 ft (177 m), and the three longest for the younger drivers was 1,040 ft (317 m), 912 ft (278 m), and 632 ft (193 m), respectively.

Finley et al. (2002) published a study to evaluate pavement marking visibility from the perspective of commercial vehicle drivers. End of line detection distance was the dependent variable. The subjects "were instructed to notify the researcher when…he/she could clearly see the end of the pavement marking." Four-inch (10 cm) white right edge line pavement markings were used. A total of 28 research participants, one female, took part in the evaluation. The average age was 43 years. The research participants drove the experimental vehicle at a maximum speed of 30 mph (48 km/h). The edge lines were of low (R_L = 100 mcd/m^2/lux), medium (R_L = 300 mcd/m^2/lux), and high (R_L = 800 mcd/m^2/lux) retroreflectivity and extended 640, 860, and 1,000 ft (195, 262, and 305 m), respectively. The research participants were divided into young, middle, and older age groups. The mean end detection distances for the three groups were, 411, 414, and 355 ft (125, 126, and 108 m), respectively. The three levels of retroreflectivity (i.e., low, middle, high) resulted in mean end detection distances of 494, 401, and 285 ft (151, 122, and 87 m), respectively. The maximum end detection distance for the medium retroreflective condition was less than 700 ft (213 m), with 85 percent of the participants unable to detect the end of the line beyond about 500 ft (152 m).

Aktan and Schnell (2004) evaluated nighttime pavement marking detection distance under dry, wet, and rainy conditions. As with Zwahlen and Schnell (1997, 1999), they used pavement marking end detection distance as the dependent variable. A total of 18 research participants were recruited for the study, all between the ages of 55 and 75. The section of road that was used for the dry evaluation was 500 ft (152 m) long. Research participants drove the vehicles at night at or below 10 mph (16 km/h) with low beams activated. The participants were told "to be sure about seeing the end of the pavement marking" before responding. Aktan and Schnell used 4-inch (10-cm) wide white, right edge lines made of paint with large beads (300 to 400 mcd/m^2/lux), and two types of tape (high [1,100 mcd/m^2/lux] and low [600 mcd/m^2/lux] retroreflectivity, respectively). For the paint markings, none of the participants was able to detect the end of the marking beyond 350 ft (107 m) and for the tape markings no participants detected the end of the markings beyond 475 ft (145 m).

As part of a large pavement marking detection distance study, Edwards et al. (2005) evaluated the nighttime detection of dry pavement markings. The authors used detection of the beginning

and end of the pavement markings as dependent variables. With regard to research participant response criterion, the subjects were told "…your job will be to tell the experimenter when you detect the first and the last pavement marking in each section." The 30 participants in the study were divided into three age categories: ten were between the ages of 18 and 25 (young drivers), ten were between the ages of 40 and 50 (middle-aged drivers), and ten were aged 60 and over (older drivers). The research participants drove the observation vehicle at 25 mph (40 km/h). The researchers did not specify the retroreflectivity of the pavement markings tested; however, they described the 4-inch wide 1,010 ft (308 m) long white, right edge line markings as a liquid system with beads and ceramic reflectors. The average beginning detection distance using normal low-beam headlamps on asphalt was approximately 275 ft (84 m), while end detection distance was an average of about 225 ft (69 m).

Gibbons (2006) published a study that evaluated the effect of pavement material (i.e., concrete and asphalt) on nighttime pavement marking detection distance. Like Edwards et al. (2005), Gibbons asked participants "to detect the beginning or the end of the pavement markings" as the dependent variable. The markings were 4-inch (10-cm) wide white, right edge lines created using standard paint with regular or large beads, wet retroreflective tape, and thermoplastic profile-type markings. A total of six research participants took part in the dry portion of the study (the research was mainly focused on the effects of wet weather on pavement marking detection). The research participants drove the test vehicle at 25 mph (40 km/h). Combining all pavement marking materials tested (as they performed equivalently in dry conditions), Gibbons found that detection distances were about 6 percent longer on asphalt than on concrete (mean distances of 291 and 274 ft [89 and 84 m], respectively) for dry nighttime viewing. Given the small number of research participants, no inferential statistics were performed, so it is not possible to determine whether this was a statistically significant difference.

In summary, there is considerable human factors research related to pavement marking visibility experimentation. Several factors worth noting from the published research reviewed for the present study are as follows:

- The number of research participants ranged from 6 to 30;
- The observation vehicle speed ranged from 5 to 30 mph (8 to 48 km/h);
- The threshold criterion for subject response varied – common criteria were: (1) high degree of certainty that the research participant could detect the end of the pavement marking; (2) the research participant must clearly see the end of the pavement marking; (3) the research participant must be sure about seeing the end of the pavement marking; and (4) the research participant must respond when detecting the pavement marking.
- The length of pavement marking test lines ranged from 500 to 1,200 ft (152 to 366 m).
- The range of pavement marking detection distance ranged from 225 to more than 650 ft (69 to 198 m).

CHAPTER 3. PAVEMENT MARKING APPLICATION AND EXPERIMENTAL TEST PLAN

This chapter of the report describes the process used to apply the experimental pavement markings at the Larson Institute Test Track Facility to assess pavement marking performance as a function of truck speed and glass bead gun angle. Additionally, the laboratory and field evaluation methods that were used to evaluate the pavement markings are described in this chapter of the report.

3.1 Application of Pavement Marking Samples at Test Track

A total of 18 white, continuous pavement markings were applied to a paved asphalt section of the Larson Institute Test Track Facility. The asphalt pavement was approximately 5 years old and the surface was flat. The pavement markings were applied at a wet-film thickness of 15 mils ($\pm$ 1 mil). It should be noted that PennDOT applies white skip line pavement markings at this same wet-film thickness, but commonly applies white edge line pavement markings at a wet-film thickness of 12 mils ($\pm$ 1 mil). The thicker application was used in this study as a means to assess the more durable marking (e.g., skip line) that is exposed to traffic passages.

Glass beads (AASHTO Type M 247) were applied to each pavement marking at a rate of 7 lb/gallon (0.12 kg/L) of paint. Each marking was 4 inches (10 cm) wide and 100 ft (30 m) long so that all markings could be accommodated at the test track. PennDOT's Engineering District 3-0 paint truck and crews applied the markings. PennDOT technical staff was responsible for supplying the glass beads and paint, calibrating the pavement marking and glass bead pressures prior to application, and adjusting the dispensing pressures during the application process. The pavement markings were applied at three speeds (12, 15, and 18 mph [19, 24, and 29 km/h]) and six bead gun angles (-60, -40, -20, 0, 20 and 40 degrees). The bead gun angle was measured in relation to an orthogonal axis with the pavement surface. For example, a -60 degree angle is pointed opposite the direction of the pavement marking application, 60 degrees from a vertical axis. The pavement markings were applied on the test track at the location shown in Figure 2. Nine pavement markings were applied near the vehicle handling area and nine pavement markings were applied near the rail-guided crash test facility shown in Figure 2. Figure 3 shows a photograph of the pavement marking application process during the calibration procedure.

The markings were applied on a section of the test track that is used in an ongoing bus testing program operated by the Larson Institute at the test track facility. Drivers in the bus testing program were asked to vary their lateral lane position in the pavement marking test section to ensure that the pavement markings were equally worn from bus passes. The approximate number of bus passages over the experimental pavement markings applied at the test track was 37,500, uniformly distributed over a period of 1 year (3,125 passes per month). No snow removal activity occurred and no anti-skid material was applied to the pavement markings in the winter months. As such, all wear on the pavement markings over the analysis period was a result of vehicle tire passages (equal across all markings) and weathering.

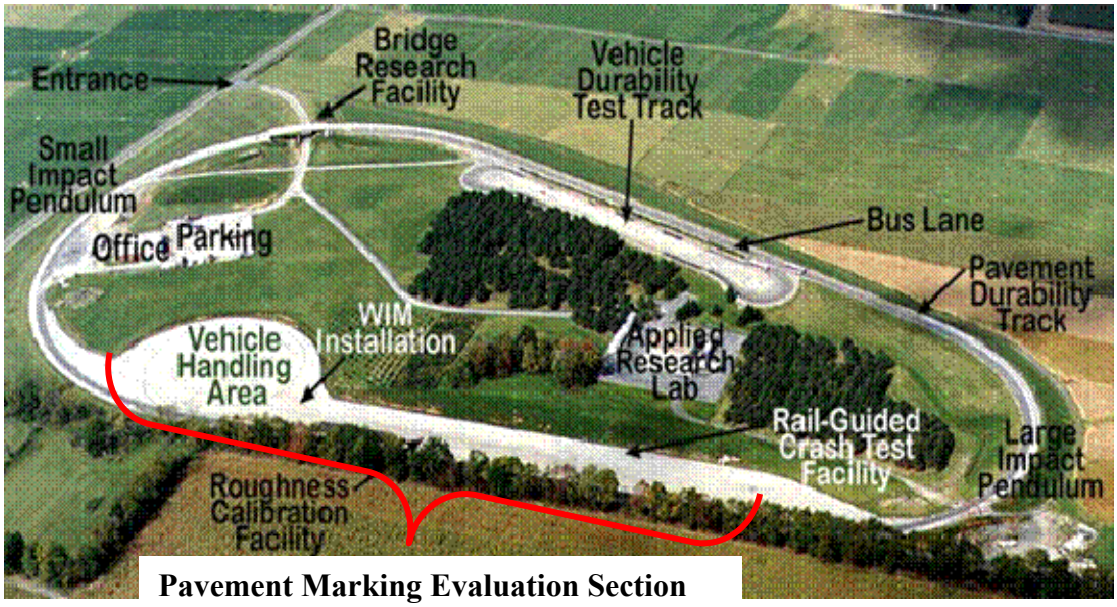

Figure 2. Location of Pavement Marking Application at Test Track.

Figure 3. Photograph of Pavement Marking Application Process.
(Photograph taken during calibration procedure)

During the application process of the 18 pavement markings at the test track, a high-speed digital camera and a light source were affixed to the pavement marking truck to record the application of glass beads. The camera and light source are shown in Figure 3. Both were covered with plastic bags to prevent the paint from splashing onto the camera lens and light source. The camera was set to record at 500 frames per second. A full-featured camera control and motion analysis software package was used to control, synchronize, and operate the camera during recording – this software was installed on a laptop computer contained in the paint truck operator compartment. A Larson Institute researcher operated the laptop computer during the pavement marking application process to record bead and paint dispensing.

During the marking application process, 36 test plates were fastened to the pavement surface to collect two samples of each of the 18 pavement markings. The test plates were made using an aluminum alloy that was one-half inch (1 cm) thick and sandblasted on one side to provide a surface that was abrasive and irregular in an attempt to closely represent an asphalt pavement surface. Figure 4 is a photograph of the test plates. The test plates were 12 inches (30 cm) wide by 6 inches (15 cm) long. The test plates contained several short, removable one-inch square (6 cm^2) sample coupons that could be removed for laboratory testing. The sample coupon dimensions were based on the size of a specimen that could be used to collect data in a scanning electron microscope.

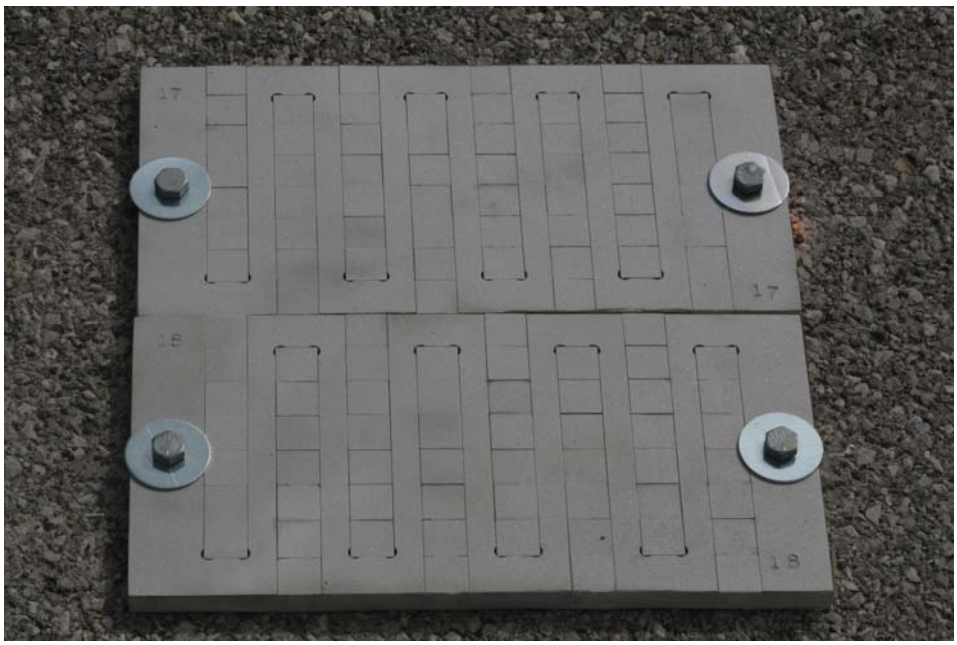

Figure 4. Sample Test Plates.

A 1-ft square (900 cm^2) was cut into a piece of one-half inch (1 cm) thick plywood, and the plywood was placed over the sample test plates prior to applying the sample pavement markings, as shown in Figure 5. The plywood served as a mechanism to help eliminate the vibration associated with the paint dispenser and bead gun apparatus prior to applying the pavement markings to the sample test plates.

Figure 5. Plywood Covering Sample Test Plates.

3.2 Experimental Test Plan

A graphical representation of the experimental test plan is shown in Figure 6. As shown in Figure 6, application of the 18 experimental pavement markings was the first step in the evaluation plan. Preparation of the 36 sample test plates was the second step in the process. Each of these is described in section 3.1 of this report. All other experimental tests are described in this section of the report. Specific details concerning the field and laboratory tests are described, as are the measures of effectiveness that were collected during each test.

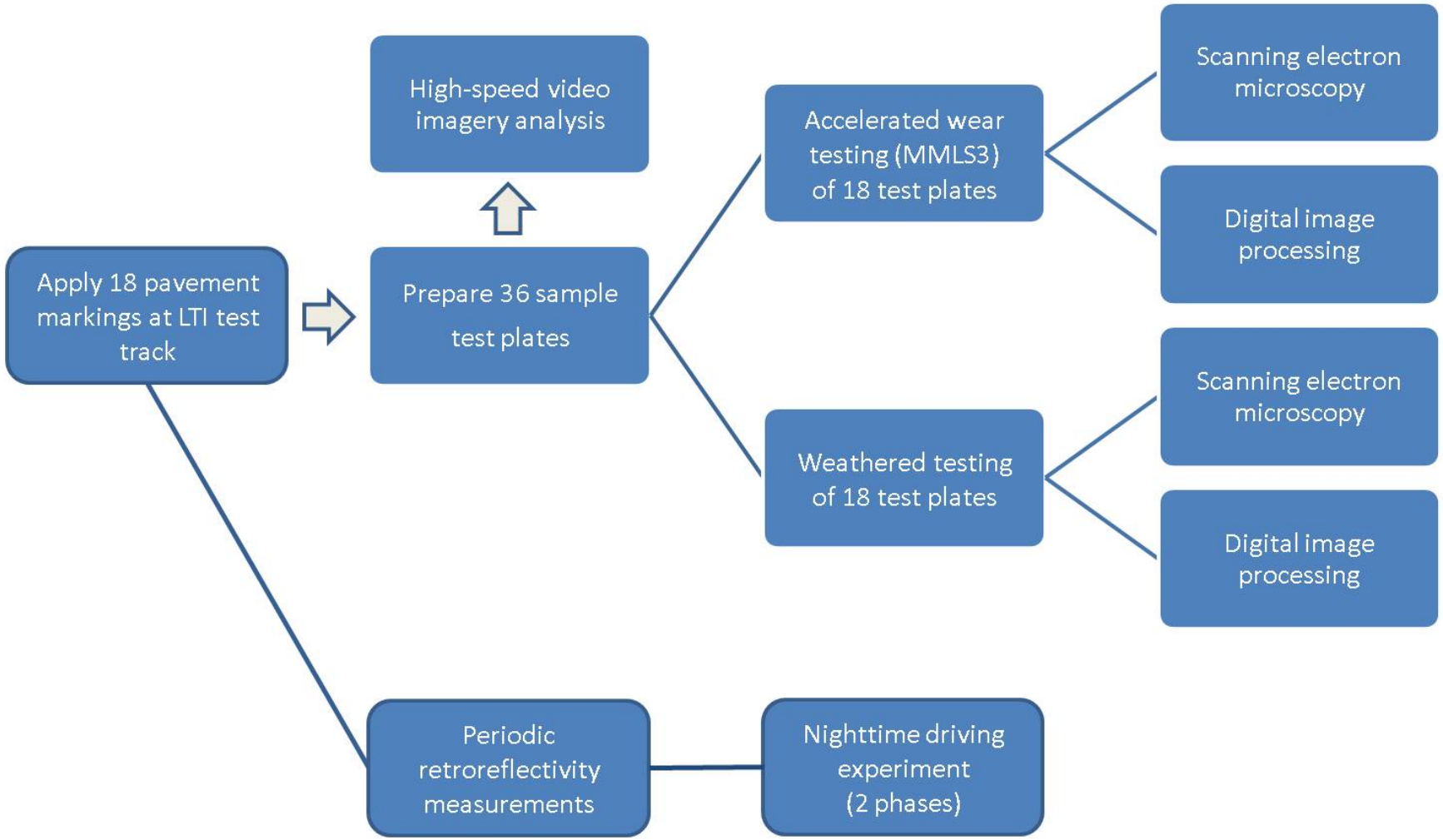

Figure 6. Experimental Testing Process.

3.2.1 High-speed Video Imagery Analysis

A special mounting and support frame was developed by the research team and was capable of supporting the video camera head and two high intensity discharge lamps to illuminate the area of the glass bead stream contacting the waterborne paint. The frame was designed and manufactured in order to rigidly attach to the paint truck's pavement marking application assembly, while holding the two lights and the video camera head safely above the ground. The frame was designed to hold the high-speed video camera head in line with the predicted contact point of the glass bead stream and the ground. The camera head was moveable, permitting it to be repositioned on the frame when the glass bead gun angle was changed. A schematic of the camera and lighting setup is shown in Figure 7.

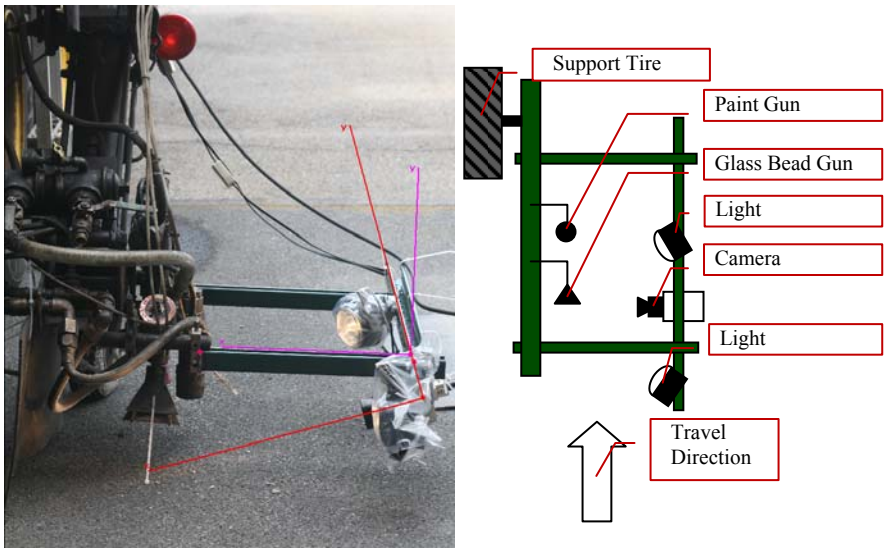

Figure 7. High-speed Camera and Lighting Setup.

The Fastcam Ultima 1024 high-speed, high-resolution digital video camera was set to record 500 frames per second at a 17.5-degree angle. The camera records monochromatic National Television System Committee images of the paint and bead application process at a 1,024 by 1,024 pixel resolution. This setup permitted the research team to "track" the application of beads with bead movements of less than 0.2 inches (5 mm) between frames. A full-featured camera control and motion analysis software package was used to control, synchronize, and operate the camera during data collection and to analyze the video images. The software permitted the selection, tracking, and full dynamic analysis of 32 moving glass beads in a video. The software calculates, for each individual bead identified in the video, the complete trajectory of absolute and relative speeds, the impact angle of the beads on the pavement marking, the bead impact speed, and the post-impact trajectory, angle, and speed. The average of each of these kinematic descriptors was computed for each of the 18 bead gun angle/truck application speeds in the experiment.

3.2.2 Sample Test Plate Evaluations

The 36 sample test plates that were prepared at the Larson Institute test track during application of the 18 experimental pavement markings, were split into two sets. One set of 18 sample test plates was used to determine the effects of accelerated trafficking on the performance of the pavement markings in a series of laboratory tests. This evaluation was intended to represent pavement marking degradation due to cumulative traffic passages on transverse pavement markings, similar to the NTPEP testing program. The second set of 18 sample test plates was used to determine the effects of weathering on the performance of the pavement markings in the same series of laboratory tests. This set of test plates was not exposed to any traffic loadings. The accelerated wear and weathering tests are described in this section of the report.

3.2.2.1 Accelerated Wear Testing

The accelerated wear tests were performed using the Model Mobile Load Simulator, 3rd scale (MMLS3). Figure 8 shows a longitudinal and end cross-sectional image of the MMLS3.

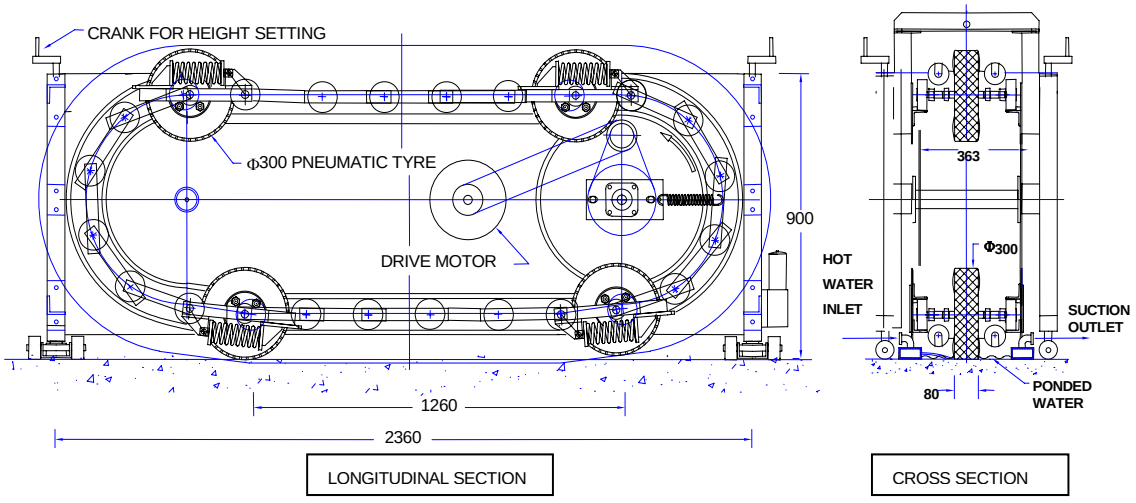

Figure 8. Cross-sectional Image of the MMLS3 Accelerated Wear Testing Machine.

The MMLS can apply up to 7,200 cycles per hour over an approximate 4 ft (1.26 m) distance, as shown in the longitudinal section of Figure 8. The 18 test plates were placed side-by-side in random order so that the loading was uniform across all plates. Based on preliminary experimental testing using the MMLS3, the research team determined that the first 6 inches (15 cm) of the MMLS3 contact area did not receive the same loading force (due to wheel bounce), so the middle 3 ft (0.9 m) were used for the evaluation. As such, only six plates (6 in x 6 plates = 3 ft) were subjected simultaneously to the MMLS loadings during experimentation. The MMLS3 was therefore used three times to apply the same number of cycles to each test plate.

A total of 1.44 million loading cycles were applied to each of the 18 sample test plates; the MMLS3 was stopped intermittently several times during the test to assess the effects of various

loading cycles on the experimental pavement markings. All testing was done under dry conditions, and the wheelpath on the MMLS3 was fixed (i.e., no wander).

After a prescribed set of loading cycles was applied to each sample test plate, two-dimensional images of the sample test plate were photographed using a Nikon D80 digital camera with a Nikkor 105 mm lens. The digital photography set also included a standard light and camera stand to ensure strictly uniform digital imaging conditions. A combination of four high-intensity ultraviolet lights and two 3000K color temperature lights were used with a normal ultraviolet-correcting lens cover. After the digital images were saved, a 1-inch square (6 cm^2) coupon was removed from each test plate for processing using a scanning electron microscope (SEM). It should be noted that digital images and a sample coupon were also secured prior to beginning the accelerated wear test to serve as a baseline condition.

The two-dimensional digital images were processed using a digital image processing software package developed by the research team for the purposes of this project. The computer code for the software program was written using Matlab®. A series of algorithms were developed by the research team to estimate the glass bead coverage in the waterborne paint applied to each sample test plate. The algorithms were developed to perform the following tasks:

- Convert the original image taken using the digital camera to a gray-scale image in accordance with National Television System Committee (NTSC) standards (1953);
- Eliminate any non-uniform illumination from the image;
- Correct the adjusted illumination image and invert it;
- Create a new binary image by thresholding the adjusted image;
- Extract each bead from the image and label them using a Watershed Reconstruction algorithm;
- Using the simplified image of detected beads, superimpose the beads on the original image (each individual bead on the image was identified using a Circular Hough transform based on the gradient field of an image);
- Analogize the beads and apply a simple artificial-intelligence voting algorithm to select beads with the highest likelihood of being a true glass bead (this algorithm enabled the software to identify debris and other particles or imperfections in the paint, and to distinguish these from the glass beads);
- Compute bead parameters, such as area, centroid, perimeter, and radius of the identified beads; and,
- Compute the area of the image covered by glass beads and compute the ratio of the beaded area with the total image.

An example of this process is shown in Figure 9. Figure 9 illustrates (from left to right) the original image of a 1-inch square (6 cm^2) coupon from the test plate, the estimation of non-uniform illumination, and the results of the Watershed Reconstruction algorithm. The bottom photograph in Figure 9 shows the results of the Hough transformation and artificial intelligence selection process. This photograph also shows each identified glass bead on the coupon and its estimated centroid, marked using a red "plus" symbol. The perimeter of the glass beads is shown in blue using the estimated radius of the sphere.

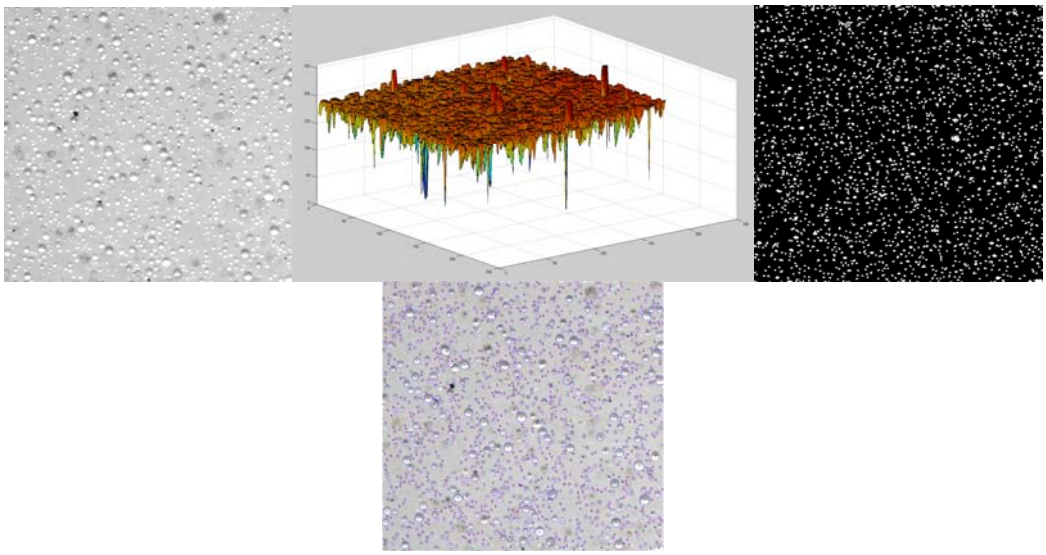

Figure 9. Example of Digital Image Processing Photographs.

More than 2,700 digital images were processed in the present study using the algorithm described above. The image-processing algorithms were capable of identifying more than 95 percent of all glass beads in each sample coupon – non-bead items were erroneously identified as glass beads in less than 0.1 percent of the cases. The glass bead radius estimation method used in the present study was found to be 97 percent accurate as result of the combined control measurement and quality-control algorithms developed.

The digital image processing analysis was used to provide data related to the proportion of the waterborne paint sample that is covered with glass beads. Additionally, the dispersion of the glass beads in the paint, based on measures of skewness and kurtosis, was computed using the digital images. Skewness is a measure of symmetry in a dataset. It can be used to determine if a distribution is the same on either side of the mean. Kurtosis is a statistical parameter used to determine the flatness of a dataset relative to the normal distribution. Low kurtosis indicates that the distribution of the beads is uniform. In this project, it was assumed that higher proportions of the glass bead coverage represented improved nighttime visibility of pavement markings. Additionally, it was assumed that lower levels of skewness and kurtosis represent improved levels of nighttime visibility when comparing the relative performance of the pavement markings to one another.

As noted previously, the SEM was used to evaluate one sample coupon from each of the 18 test plates subjected to accelerated wear. The SEM is an instrument that uses electrons rather than light to form images of a surface. In the present study, a surface of the sample coupons from the test plates was created using the SEM. The SEM has the advantage of greater depth of field, higher magnification, and greater resolution than optical imaging. The instrument used in this study was a Hitachi SEM, model S-3500N that was operated in the back-scattered electron (BSE) mode. The coupon samples were run in the variable pressure (VP) vacuum mode so that there was no need to sputter a conductive film like Au on the non-conductive surface of the sample coupons. The electron beam conditions were accelerating voltage 20 kV with a working distance (WD) of 15 mm.

The SEM was used in the present experiment to determine the dry film thickness of the experimental pavement markings applied to the sample test plates. The angle of the bead gun will not change the wet or dry film thickness of the waterborne paint, so the SEM was used to test only the dry film thickness of the three truck application speeds (12, 15, and 18 mph [19, 24, and 29 km/h]). One test coupon from three different sample test plates (three different truck speeds, all at -60 degree bead gun angle) was selected for the analysis. The SEM dry thickness analysis was performed only for the sample test plates in the baseline condition (i.e., no MMLS3 loading cycles were applied). The sample coupons were mounted in a "cold mount" system, which is a standard specimen-mounting medium, with low viscosity and room temperature curing. The specimens were cut perpendicular to the surface coating with a low-speed diamond saw to expose the coupon and coating in cross-section. These cut specimens were then polished by hand with varying size polishing media with the final polish being a 0.3 μm (1.2×10^{-5} in) diamond-on-paper finish. For the purposes of this experiment, it was assumed that greater dry film thickness represents improved opportunities for glass bead retention in the paint, resulting in improved pavement marking visibility.

In addition to the dry film thickness, the SEM was used to determine the amount of "wicking" by the glass beads in the paint. Wicking is a measure of liquid movement through a porous media; however, in the present experiment, wicking is used to determine the amount of waterborne paint buildup around a glass bead embedded in the paint. To determine this measure, one glass bead from an SEM image was analyzed. The diameter of the glass bead was noted. A horizontal and vertical axis was drawn on the glass bead shown in the image. At locations where these axes (left, top, right, and bottom) intersected the bead, the amount of wicking was measured manually from a scale on the SEM images. An example of this is shown in Figure 10.

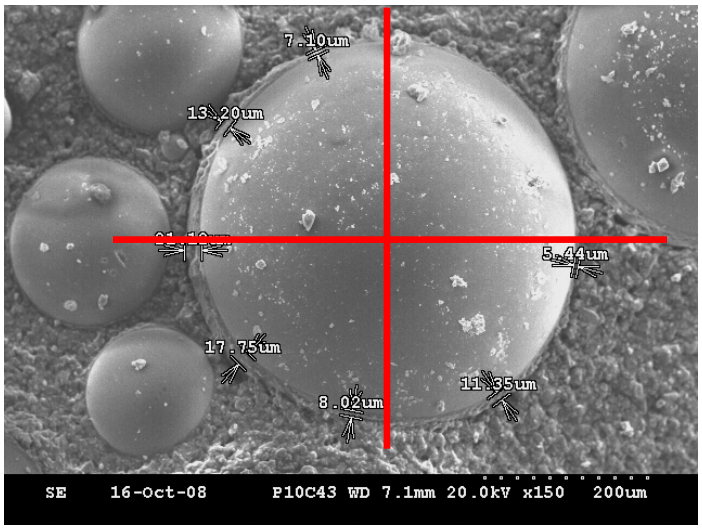

Figure 10. Example of Glass Bead Wicking in Waterborne Paint.

In Figure 10, the amount of wicking on the left, top, right, and bottom parts of the image is approximately 21.1, 7.1, 5.4, and 8.0 μm, respectively. For the purposes of this experiment, uniform wicking was assumed to produce the greatest bond strength between the glass bead and

the paint and was, therefore, considered to produce the greatest level of bead retention. Furthermore, larger amounts of wicking are representative of more paint buildup around the perimeter of the glass bead, resulting in improved bond strength between the glass bead and paint. The wicking analysis was performed for a single glass bead in each of the 18 test plates in both the baseline condition and after completing each set of MMLS3 loading cycles. If a bead in the SEM image was dislodged, the size of the bead was noted.

In summary, the accelerated wear evaluation was performed using the MMLS3. Baseline images of the 18 sample test plates were recorded and processed using two-dimensional digital image processing and an SEM. Subsequent analyses were performed after the MMLS3 was stopped during the loading process. The following performance measures were computed:

- Bead coverage, skewness, and kurtosis using digital image processing.
- Dry film thickness (baseline condition only) using the SEM.
- Glass bead wicking in paint using the SEM.

3.2.2.2 Weather Testing

The second set of 18 test plates were exposed to the weather over a period of nearly 1 year and evaluated intermittently within this time period using the digital and SEM imaging methods described in the previous section. All sample test plates were housed in an outdoor chamber at the Civil Infrastructure Testing and Evaluation Laboratory at Penn State. The test plates were positioned to receive the maximum exposure to the sun (no foliage) and precipitation. This evaluation was intended to approximate pavement marking degradation similar to that experienced by longitudinal pavement markings that are not exposed to continuous traffic passages. No dry film thickness analysis was performed using the weathered test plates. Two-dimensional and SEM images were recorded in the baseline condition (August 2008) and again in November 2008, March 2009, and June 2009.

3.2.3 Glass Bead Embedment Analysis

An analysis of glass bead embedment in the waterborne paint was performed using a combination of field and laboratory tests. In this analysis, the research team secured a sample of the glass beads from the PennDOT paint truck immediately prior to applying the 18 experimental pavement markings at the Larson Institute test track. A seize analysis was then performed on the glass beads to determine the distribution of beads. As noted in the accelerated wear test section, two-dimensional image processing was used to evaluate the glass bead coverage in the waterborne paint. A distribution of the bead size above the surface of the paint was obtained from the digital image processing analysis. This distribution was compared to the distribution of the glass beads that were used in the experimental pavement markings at the test track. The difference between the exposed glass bead distribution and the actual glass bead distribution in the paint truck was used to compute the percentage of the glass beads embedded in the paint.

For glass beads to be most effective, they should be embedded far enough into the paint surface to prevent “pop-out” during normal traffic wear. Additionally, the glass beads should not be embedded so deeply as to minimize their effectiveness in refracting incoming rays of light.

Approximately 60 percent of the bead diameter should be embedded in the waterborne paint for the bead to produce optimal visibility and retention. This is illustrated in Figure 11.

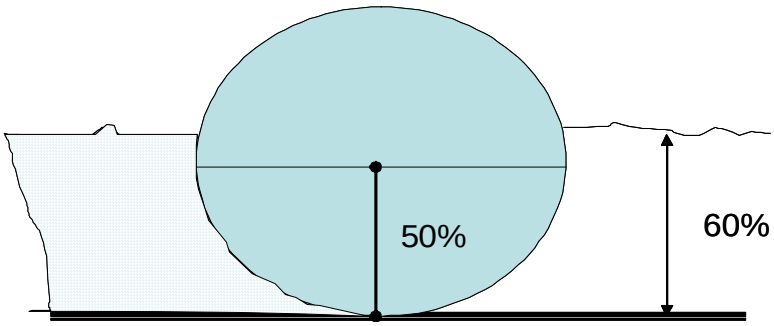

Figure 11. Idealized Glass Bead Embedment in Waterborne Paint.

Bead embedment was computed by taking the as-received glass beads and determining a particle size distribution, and then contrasting that size to the size determined by photographing the surface of the beads embedded in the paint surface. The difference between these two measurements represents the degree of embedment.

The embedment analysis was done for the baseline condition, and then again after completing various MMLS3 loading cycles. Additionally, the embedment analysis was also performed after the sample test plates were exposed to the weather for nearly 1 year.

The speed-bead gun angle combinations closest to 60 percent embedment were assumed to provide the optimal nighttime visibility in the present experiment.

3.2.4 Field Evaluations

This section of the report is separated into two subsections. The first describes the pavement marking retroreflectivity measurements that were recorded at the test track on the 18 experimental pavement markings. The second subsection describes a nighttime driving experiment that was performed to evaluate the nighttime visibility of the in-situ pavement markings.

3.2.4.1 Retroreflectivity Measurements

The retroreflectivity of each of the 18 experimental markings was measured in the direction of application by the research team using an LTL-X retroreflectometer provided by PennDOT. The LTL-X is a handheld instrument used to measure pavement marking retroreflectivity – it has a 30 meter geometry. The retroreflectometer was calibrated prior to each use. Baseline measurements were recorded by the research team approximately 1 month after application and at regular intervals thereafter for a period of nearly 1 year. The retroreflectivity measurements were taken in accordance with PennDOT's handheld retroreflectometer field measurement protocol. This field sampling protocol is shown in Figure 12 and is based on sampling sections that are 300 ft (91 m) long. All pavement markings applied at the Larson Institute test track were continuous white edge lines and 100 ft (30 m) long. As shown in Figure 11, the PennDOT

sampling plan requires that retroreflectivity measurements be taken at approximately 15-ft (5-m) intervals (or 5 paces); this sampling plan was modified for the present research. A total of 10 retroreflectivity measurements were recorded on each 100 ft (30 m) longitudinal marking.

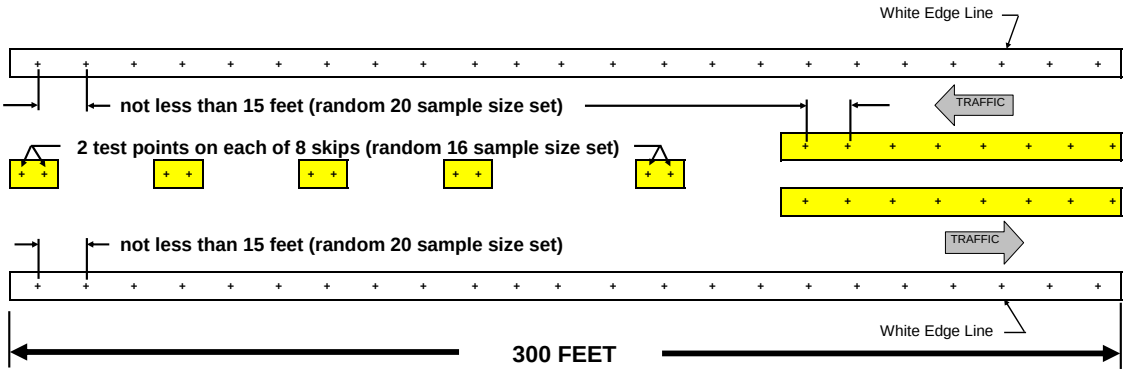

Figure 12. Retroreflectivity Sampling Plan.

The mean, standard deviation, and coefficient of variation for each pavement marking were computed after each measurement period. Higher levels of mean pavement marking retroreflectivity provide higher levels of nighttime visibility. Lower levels of the standard deviation and coefficient of variation indicate that the pavement marking application is uniform along the entire 100 ft (30 m) length.

3.2.4.2 Human Factors Evaluation

Research shows that retroreflectivity levels alone may not consistently or accurately predict the level of pavement marking luminance (i.e., brightness) a driver experiences during nighttime driving (e.g., Burns et al., 2008). This is also likely true in relation to the myriad performance measures being collected in the laboratory evaluations described previously. Changes in retroreflectivity, and for that matter, luminance, from one marking to another must be above a certain magnitude for drivers to notice a difference; this is known as the "just noticeable difference," or jnd. Studies of the jnd are concerned with determining through experimentation how perception changes as a function of changes in physical intensity.

A human factors field study was conducted to determine the jnd for pavement markings. The results of this nighttime visibility study were compared to the retroreflectivity data measured in the field. A comparison of the visibility and retroreflectivity levels that result from changes in bead gun angle and truck speed was conducted. The experimental method, research participant recruitment, and test procedures are described in this section of the report.

Method

The general methodology was a nighttime test track evaluation of the visibility of 18 pavement markings (six angles at three speeds each). Data were only collected under clear conditions with dry pavement. Data collection began at the end of civil twilight. The procedure was based on a similar procedure used by Zwahlen and Schnell (1999) where research participants were asked to

find the ends of longitudinal pavement markings that varied in pavement marking retroreflectivity.

Research Participants

Thirty-six research participants took part in the experiment. The age of the participants varied in proportion to the range of ages in the U.S. driving population (i.e., 22 percent (n = 8) between 18 and 29 years old; 30 percent (n = 10) between 30 and 44 years old; 28 percent (n = 10) between 45 and 59 years old; and 20 percent (n = 8) over 60 years old). Half of the research participants were male and the other half female. Prior to beginning the experiment, all drivers were asked to sign a consent form and to perform a visual acuity test. Subject visual acuity ranged from 20/16 to 20/40 with an average of 20/20.3. Additionally, all research participants were provided with a set of instructions prior to beginning the experiment.

Test Site

All experimentation was performed at the Larson Institute's Test Track Facility.

Procedure

The 36 research participants were asked to drive a test vehicle toward the pavement markings at approximately 10 mph (16 km/h). The vehicle was a 2004 Dodge Stratus sedan with headlamps set on low beam. An experimenter was in the passenger seat. Only one pavement marking was viewed at a time; the other 17 were covered with a black landscaping cloth that closely matched the color of the asphalt pavement (see Figure 13). When the participants were certain that they could detect the end of the marking, they alerted the experimenter. A distance measuring instrument (DMI) was used to record the detection distance. Data were collected for each of the 36 participants for each of the 18 pavement marking conditions. Data were collected during two different two periods, once within the first 3 months after pavement marking application (Phase I) and a second time near the end of the wear cycle (Phase II), approximately 6 months later, following one winter season. Four participants had to withdraw from the study before completing the second session for health or personal reasons. All experimental runs were counterbalanced in the first and second phases of the experiment to balance out order, fatigue, and practice effects.

In addition to the visibility distances, the retroreflectivity of each of the 18 test markings was measured during the first and second phases of the experiment using a Delta LTL-X portable retroreflectometer.

Figure 13. Layout of Experimental Pavement Markings with Landscaping Paper.

Analysis

The data recorded for Phase I and Phase II of the nighttime driving experiment were analyzed to determine the effect of truck application speed and bead gun angle on visibility distance. The data for Phase I and Phase II were analyzed separately and were also combined to test for differences in the visibility distances between the two separate data collection phases. The relationship between pavement marking retroreflectivity and visibility distance was also compared to determine how these measures were correlated immediately after the pavement markings were applied, and after the markings were weathered for nearly 1 year. This section of the paper describes the analyses used to assess the effects of truck application speed and bead gun angle on visibility distance, and describes how the relationship between pavement marking retroreflectivity and visibility distance was determined.

Separate Phase I and Phase II Analysis

A mixed-factor analysis of variance (ANOVA) was used to analyze the Phase I and Phase II data separately. In the case of mixed models, statistical inference for the random effects factors are not conditioned on the sample included in the study; rather, inference can be applied to the population (Keuhl, 2000; Kutner et al., 2004). It is assumed that the random factors are independent and normally distributed with mean 0 and variance σ^2. Research participants were used as a random factor in the present study as they were randomly chosen from a population of drivers in different age groups in Pennsylvania, and hence were independent. The normality assumption was tested by means of a normal probability plot of residuals and using an Anderson-Darling test. The null hypothesis in an Anderson-Darling test is that the residuals are normally distributed.

Two ANOVA models were tested using the separate Phase I and Phase II data (four total models, two for each phase). In the first model, separate main effects for the truck application speed and

the bead gun angle were included. The paint truck application speed factor consisted of three levels (12, 15, and 18 mph [19, 24, and 29 km/h]), and the bead gun angle factor consisted of six levels (-60, -40, -20, 0, 20, and 40 degrees). Both were treated as fixed factors. The interaction between paint truck application speed and bead gun angle was also included as a fixed factor in the preliminary model. Visibility distance of the pavement markings was the dependent variable. The null hypothesis for testing the equality among the means for the main effects was $\mu_1. = \mu_2. = \ldots = \mu_n.$ where $\mu_1.,\mu_2.$, etc. are the means for different factor levels. Similarly, when testing the interaction effects, the null hypothesis was that the interaction was equal to zero for all factor levels considered in the interaction.

If the bead gun angle or truck application speed fixed factors were not statistically significant in the first ANOVA, a line number fixed factor was created and consisted of 18 levels (3 bead gun angles and 6 truck application speeds). In the second ANOVA, the visibility distance remained as the dependent variable and the research participant ID remained as a random factor. The ANOVA results reported in the present study were based on the model with the highest goodness-of-fit (R^2).

If the F-statistics for the fixed effects factors were statistically significant in the mixed ANOVA (the probability of a Type I error, α, was set to 0.05), Tukey pairwise comparisons were used to test the differences in means within the factor. The null hypothesis is that the difference between means is equal to zero (i.e., $\mu_i - \mu_j = 0$).

Combined Phase I and II Analysis

Phase II of the study included the same research participants as Phase I, but was conducted approximately 6 months after the first phase was completed to evaluate the effects of weathering on the visibility distance of the pavement markings. Since the Phase I and Phase II data were collected for the same research participants subjected to the same experimental treatments, the data were analyzed as repeated measures mixed-factor ANOVA. The assumptions for the repeated measures mixed-model ANOVA include independent and normally distributed error terms with equal variance σ^2. The compound symmetry assumption -- equal correlation among repeated measures -- is a sufficient but not necessary assumption for repeated measures ANOVA. Violating this assumption cannot occur if the repeating factor has only two levels, as there is only one pairwise variance (Levine et al., 2003), which is the case in the present experiment. The normality assumption was tested using a normal probability plot of residuals and an Anderson-Darling test. Two ANOVA models were run using the combined data. In the first ANOVA, the experimental phase (2 levels), paint truck application speed (3 levels), and bead gun angle (6 levels) were the within-subject factors and considered fixed. Interaction effects were also included in the analysis. The research participant ID was the random factor. Visibility distance was the dependent variable. If the bead gun angle or truck application speed main effects were not statistically significant, a line number ID fixed-effect variable was created and included 18 levels (3 bead gun angles and 6 truck application speeds). The model used to assess the experimental results was based on the highest level of the coefficient of determination (R^2). Again, Tukey pairwise comparisons were used to test for differences in the mean visibility distance of the fixed factors, if the group-level F-statistic was statistically significant ($p \leq 0.05$).

Retroreflectivity

As noted previously, pavement marking retroreflectivity levels were measured during the Phase I and Phase II experimental runs using a handheld retroreflectometer (LTL-X) supplied by PennDOT. The retroreflectivity levels that correspond to Phase I of the nighttime driving experiment were measured approximately 3 months after the pavement markings were applied. The retroreflectivity levels that correspond to Phase II of the nighttime driving experiment were measured approximately 9 months after the pavement markings were applied. Because the experimental pavement markings were 100 ft (30 m) long, 10 retroreflectivity readings were recorded at 10-ft (3-m) intervals along the markings. The mean and standard deviation of the 10 measurements were computed.

The retroreflectivity levels recorded during the Phase I and Phase II experiment were compared to the visibility distances recorded during these same phases to determine the relationship between these two measures. Plots of the visibility distance versus retroreflectivity were constructed, and a regression function fitted to the data.

CHAPTER 4. RESULTS FROM STATIC AND DYNAMIC IMAGERY EXPERIMENTS

This chapter of the report describes the results from the static and dynamic video imagery analyses. The first section provides a discussion of the high-speed video camera analysis that provided dynamic descriptors of the glass bead application process at the Larson Institute test track. The second and third sections of this chapter describe the results from the accelerated wear and weathering laboratory experiments, including the two-dimensional image processing and scanning electron microscopy analyses. The two-dimensional image processing was used as a method to evaluate glass bead performance in the waterborne paint. The scanning electron microscopy analysis provided information concerning the waterborne paint performance. The fourth section of this chapter describes the bead embedment analysis.

4.1 High-speed Video Imagery Analysis

Several kinematic descriptors were computed during the application process of the experimental pavement markings at the test track. Each is defined as follows:

- Relative impact angle of bead (degrees)
- Bead speed in ground coordinates (mph)
- True bead speed (mph)
- Truck speed (mph)
- Impact angle (degrees)
- Bead impact angle (degrees)
- Vertical bead speed (mph)
- Relative speed of beads compared to ground at impact point (mph)
- Bead speed relative to ground (mph)
- Vertical energy (Joule)
- Horizontal energy (Joule)

Table 3 shows each of the kinematic descriptors as a function of the bead gun angle and truck application speed. For the purposes of the present study, it was assumed that the relative impact angle of the bead and true bead speed were the most relevant kinematic descriptors. A near vertical relative impact angle (90 degrees) suggests that the beads are dropping vertically into the paint, a desirable property when attempting to maximize nighttime visibility. Slower bead speeds are more desirable than higher bead speeds to eliminate the probability of beads deflecting off the paint or rolling upon impact with the paint. In the present study, the 40-degree bead gun angle generally produced the most desirable relative impact angle at the 12 and 15 mph speeds, while the 20-degree bead gun angle produced the most desirable relative impact at the 18 mph truck application speed. In the 12 and 15 mph truck application speed tests, the 40-degree bead gun angle provided the slowest true bead speed. In the 18 mph test, the 0-degree bead gun angle provided the slowest true bead speed.

Table 3. Kinematic Descriptors from High-speed Video Imagery.

Kinematic Descriptor	Speed (mph)	Bead Gun Angle (degrees)					
		-60	-40	-20	0	+20	+40
Relative impact angle of bead (degrees)	12	27.78	49.82	60.47	74.59	86.63	92.41
Bead speed in ground coordinates (mph)		5.65	3.48	2.29	1.36	0.25	-0.17
True bead speed (mph)		6.38	5.39	4.65	5.10	4.21	3.97
Truck speed (mph)		12.63	13.40	12.82	11.40	11.72	12.34
Impact angle (degrees)		26.74	19.31	20.92	20.61	18.42	21.98
Vertical bead speed (mph)		2.97	4.12	4.04	4.92	4.21	3.97
Relative bead speed compared to ground at impact point (mph)		6.98	9.92	10.52	10.04	11.47	12.51
Bead speed relative to ground (mph)		7.59	10.74	11.27	11.18	12.22	13.12
Vertical energy (Joule)		25.93	38.17	45.39	44.03	47.17	64.44
Horizontal energy (Joule)		51.46	108.94	118.74	117.07	141.63	159.65
Relative impact angle of bead (degrees)	15	29.65	51.57	46.55	80.60	83.99	92.34
Bead speed in ground coordinates (mph)		5.83	3.00	4.37	0.81	0.53	-0.12
True bead speed (mph)		6.70	4.83	6.36	4.98	5.02	2.89
Truck speed (mph)		15.46	16.51	17.35	14.42	14.39	14.48
Impact angle (degrees)		18.38	14.50	22.33	18.39	19.39	17.73
Vertical bead speed (mph)		3.32	3.78	4.62	4.91	5.00	2.88
Relative bead speed compared to ground at impact point (mph)		9.64	13.51	12.98	13.61	13.86	14.60
Bead speed relative to ground (mph)		10.19	14.03	13.78	14.47	14.74	14.88
Vertical energy (Joule)		32.75	49.25	72.12	66.06	72.10	67.45
Horizontal energy (Joule)		98.56	190.44	175.54	198.71	204.84	210.97
Relative impact angle of bead (degrees)	18	29.21	48.35	48.98	76.10	84.56	96.51
Bead speed in ground coordinates (mph)		7.66	3.75	3.78	1.28	0.95	-0.68
True bead speed (mph)		8.78	5.64	5.76	5.31	10.00	6.01
Truck speed (mph)		18.08	19.10	19.03	16.73	18.70	16.08
Impact angle (degrees)		23.00	15.71	15.55	16.98	14.51	19.90
Vertical bead speed (mph)		4.28	4.21	4.35	5.16	9.95	5.97
Relative bead speed compared to ground at impact point (mph)		10.42	15.35	15.25	15.45	17.75	16.77
Bead speed relative to ground (mph)		11.27	15.92	15.85	16.29	20.35	17.80
Vertical energy (Joule)		49.59	68.59	67.39	77.51	103.76	107.78
Horizontal energy (Joule)		116.83	243.93	242.15	253.76	401.04	297.78

4.2 Accelerated Wear Evaluation

This section is organized into two subsections. The first describes the results from the digital image processing, while the second subsection describes the results from the scanning electron microscopy.

4.2.1 Digital Image Processing

As noted in Chapter 3 of this report, a set of baseline digital images were analyzed to determine the bead coverage in all 18 sample test plates subjected to accelerated trafficking to establish a point of reference after the MMLS3 was stopped after a period of wear. For this analysis, the MMLS3 was stopped at 200,000, 300,000, 400,000, 500,000, 800,000, and after 1.2 million

cumulative cycles. Digital images were recorded after each stoppage of the MMLS3. Subjective assessments of the worn sample test plates revealed that little bead loss occurred prior to 800,000 cumulative cycles. As such, the analysis results presented in this section of the report relate only to the digital image processing analysis that occurred for the sample test plates with 800,000 and 1.2 million cumulative cycles. The results from these digital image processing results were compared to the baseline, and the percentage of bead coverage was computed. The results are shown in Table 4.

Table 4. Bead Coverage for Accelerated Wear Evaluation.

Speed (mph)	**Cycles**	**Bead Gun Angle (degrees)**						**Average**
		-60	**-40**	**-20**	**0**	**+20**	**+40**	
		Bead Coverage (%)						
12	Baseline	23.25	25.04	30.68	28.64	26.42	26.05	**26.68**
	800,000	18.84	19.04	26.24	25.00	23.29	18.00	**21.74**
	1,200,000	17.67	20.59	22.86	23.36	18.40	20.00	**20.48**
	Bead Loss[1]	*24.00*	*17.77*	*25.49*	*18.44*	*30.36*	*23.22*	***23.21***
15	Baseline	25.63	26.81	28.91	27.96	24.18	23.55	**26.17**
	800,000	24.02	21.97	26.80	28.99	23.37	23.37	**24.75**
	1,200,000	23.33	20.81	23.12	24.27	21.35	20.57	**22.24**
	Bead Loss[1]	*8.97*	*22.38*	*20.03*	*13.20*	*11.70*	*12.65*	***14.82***
18	Baseline	18.33	16.22	21.61	25.36	22.85	21.48	**20.98**
	800,000	15.72	12.76	20.93	21.18	21.77	15.68	**18.01**
	1,200,000	13.10	12.38	19.85	18.78	19.12	15.86	**16.52**
	Bead Loss[1]	*28.53*	*23.67*	*8.14*	*25.95*	*16.32*	*26.16*	***21.46***
Average		**19.99**	**19.51**	**24.56**	**24.84**	**22.31**	**20.51**	

[1] *Bead loss was computed as the percent loss in beads between 1.2 million cycles and the baseline.*

The relative bead loss shown in Table 4 was calculated as follows:

$$Bead\ Loss = \frac{\%_{Baseline} - \%_{1.2M}}{\%_{Baseline}} \times 100 \quad (1)$$

The average bead coverage was computed across each row in Table 4 to illustrate the average at each truck application speed, irrespective of the bead gun angle. Additionally, the average bead coverage was averaged over each bead gun angle, irrespective of the truck speed. The maximum bead coverage computed for the baseline condition (30.68%) was observed for the 12 mph and -20 degree speed/bead gun angle combination. After 800,000 and 1.2 million accelerated wear cycles, respectively, the 15 mph and 0 degree speed/bead gun angle combination had the greatest bead coverage (28.99% and 24.27%, respectively). The greatest relative percent bead loss occurred in the 12 mph and 20 degree speed/bead gun angle combination (30.36%). The lowest relative percent bead loss occurred in the 18 mph and -20 degree speed/bead gun angle combination (8.14%).

To further illustrate the bead coverage in each truck speed application and bead gun angle combination, Figures 14, 15, and 16 were created. Figure 14 is a contour plot for the baseline condition; Figures 15 and 16 are contour plots of bead coverage after 800,000 and 1.2 million accelerated wear cycles, respectively.

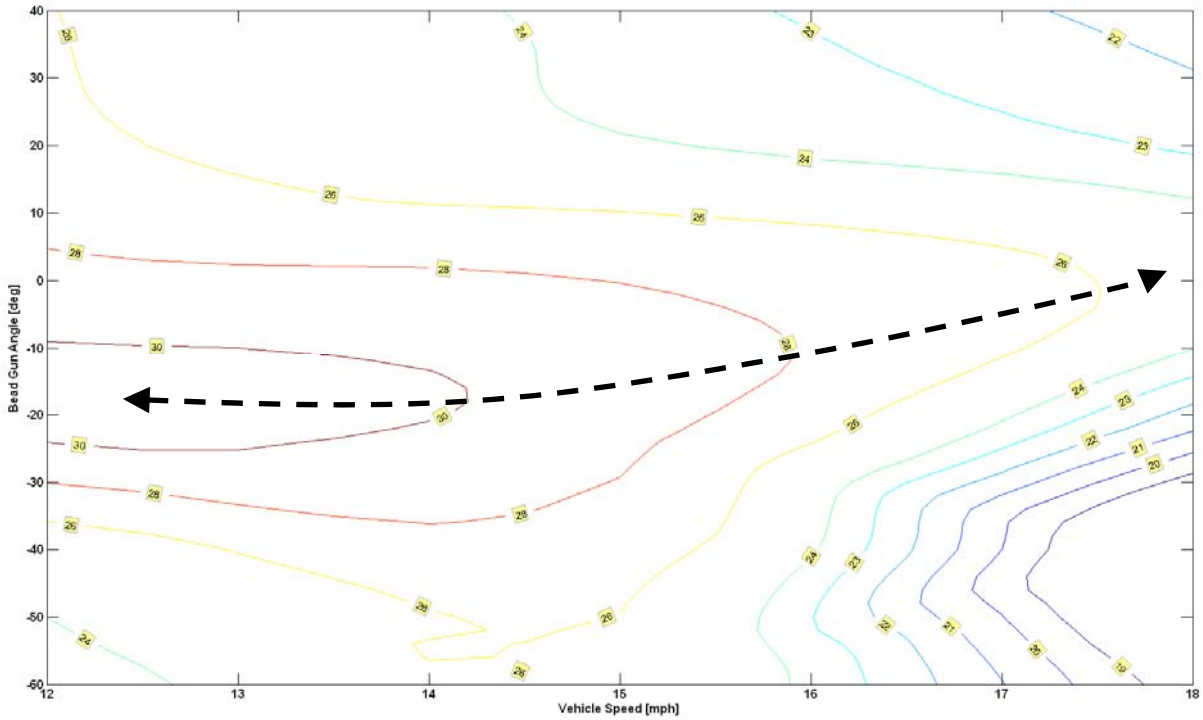

Figure 14. Contour Plot of Bead Coverage in Baseline Condition.

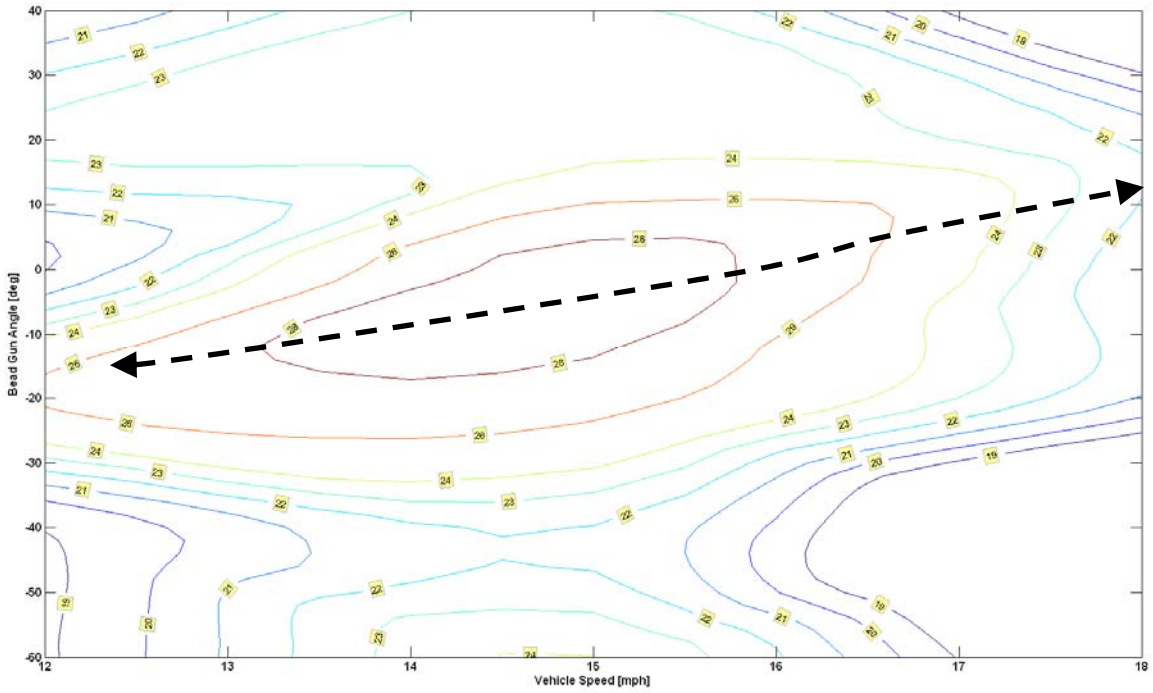

Figure 15. Contour Plot of Bead Coverage after 800,000 Accelerated Wear Cycles.

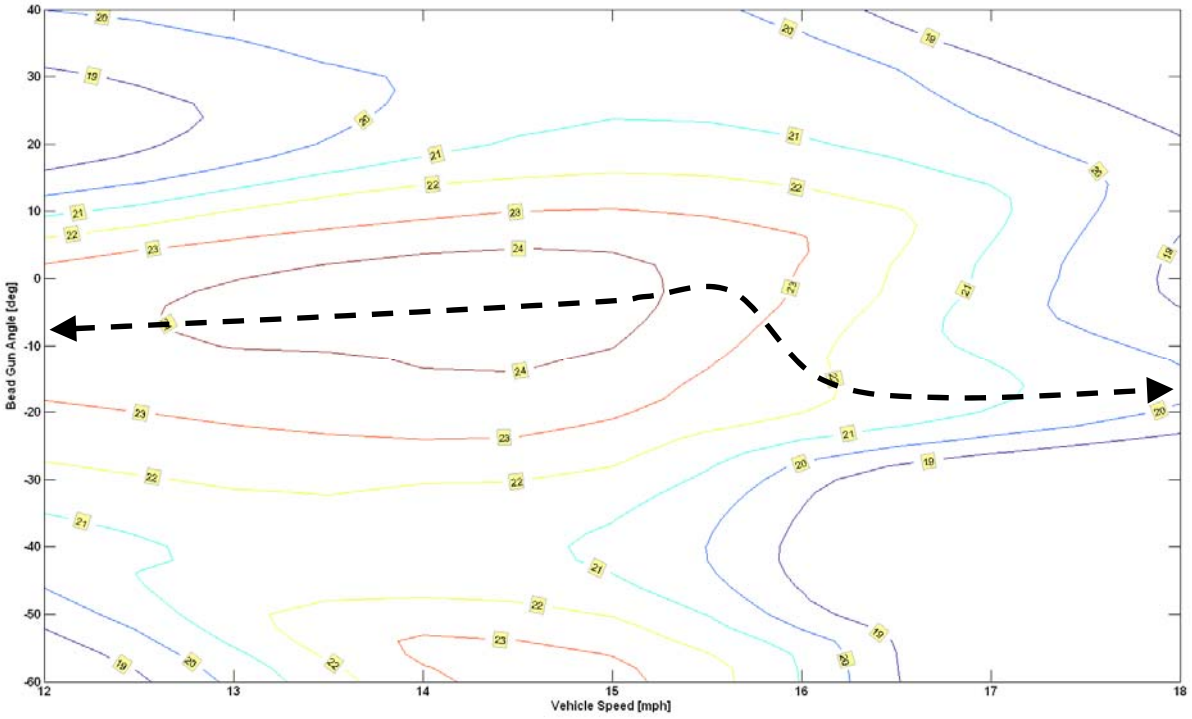

Figure 16. Contour Plot of Bead Coverage after 1.2 million Accelerated Wear Cycles.

The following general trends appear for the baseline bead coverage contour plot in Figure 14:

- The relationship between truck application speed, bead gun angle, and bead coverage is non-linear.
- Higher truck application speeds are related to lower bead coverage.
- The maximum bead coverage occurs when the bead gun angle is between -10 and -20 degrees. The bead coverage drops significantly as the bead gun angle moves from -20 to -60 degrees at all truck speeds. A similar, but less pronounced change in bead coverage occurs as the bead gun angle moves from -10 degrees to 40 degrees, where the bead coverage decreases for all truck speeds.
- The dashed trend line in Figure 13 illustrates that maximum bead coverage for the 12, 15, and 18 mph truck application speeds occurs when the bead gun angle is approximately -20, -10, and 10 degrees, respectively. This suggests that moving the bead gun forward at higher truck application speeds produces greater bead coverage in the baseline condition.

In Figure 14, the contour plot for the bead coverage after 800,000 accelerated wear cycles is similar to the baseline plot in Figure 14. The following general trends appear for the bead coverage illustrated in Figure 15:

- The relationship between truck application speed, bead gun angle, and bead coverage is slightly non-linear.
- Higher truck application speeds are related to lower bead coverage.
- The maximum bead coverage occurs when the bead gun angle is between -20 and 0 degrees. The bead coverage drops significantly as the bead gun angle moves from -20 to -60 degrees at the 12 and 18 mph truck speeds. The bead coverage decreases when the bead gun angle moves from -20 to -40 degrees at the 15 mph speed; however, the bead coverage appears to increase when the bead gun angle moves from -40 to -60 degrees. Bead coverage decreases as the bead gun angle moves from 0 to 40 degrees at all truck speeds.
- The dashed trend line in Figure 14 illustrates that maximum bead coverage for the 12, 15, and 18 mph truck application speeds occurs when the bead gun angle is approximately -10, -5, and 10 degrees, respectively. This suggests that moving the bead gun forward at higher truck application speeds produces greater bead coverage in the baseline condition.

In Figure 16, the contour plot for 1.2 million accelerated wear cycles appears similar to the baseline (Figure 13) and 800,000 accelerated wear (Figure 15) contour plots when the truck speed is 12 and 15 mph; however, a noticeable difference occurs for the 18 mph truck application speed. The maximum bead coverage appears to occur when the bead gun angle is between approximately -20 and 0 degrees. The dashed trend line in Figure 15 illustrates that maximum bead coverage for the 12, 15, and 18 mph truck application speeds occurs when the bead gun angle is approximately -10, -5, and -15 degrees, respectively.

The overall findings from accelerated wear digital image processing analysis indicate that a slow truck speed (12 mph) and a -20 degree bead gun angle produce a high level of initial bead coverage in the baseline condition. After periods of accelerated wear testing, the 15 mph truck speed, coupled with near vertical bead gun angles (-10 to 0 degrees), provides the greatest bead coverage. The 18 mph truck speed, irrespective of the bead gun angle, appears to produce the lowest bead coverage.

4.2.2 Scanning Electron Microscopy

Cross-sectional and surface morphology analyses were conducted in a laboratory setting using a Hitachi SEM. The SEM was operated in high-vacuum, back-scattered electron mode. In the cross-sectional analysis, the dry film thickness was computed, and general observations related to the glass beads and waterborne paint were noted. The cross-sectional analysis was performed using only the baseline data, prior to any accelerated trafficking applied by the MMLS3.

The surface morphology analysis was conducted using coupons from the 18 sample test plates. Images from the baseline condition were analyzed and then general observations concerning the glass beads and waterborne paint were noted after applying 500,000, 800,000, and 1.2 million cycles by the MMLS3. Additionally, an analysis of the waterborne paint "wicking" onto the glass beads was performed using the surface morphology SEM images. Approximately 10 digital images of the surface morphology of the individual coupons were recorded for each testing condition, representing in excess of 3,600 total images. The results of both the cross-sectional and surface morphology analyses are provided in this section of the report.

4.2.2.1 Cross-sectional Analysis

Three test coupons were selected from the total set for analysis by SEM in cross section, one each for the 12, 15, and 18 mph truck speeds. The primary purpose of this analysis was to assess the dry film thickness and to observe the waterborne paint. The angle of the glass bead gun will not influence the analysis results and, therefore, the different bead gun angles were not considered.

These specimens were mounted in a "cold mount" system, which is a standard specimen mounting medium with low viscosity and room temperature curing. The specimens were cut perpendicular to the surface coating with a low-speed diamond saw to expose the coupon and coating in cross-section. These cut specimens were then polished by hand with varying size polishing media, with the final polish being a 0.3 μm diamond-on-paper finish.

General observations from the cross-sectional analysis indicate that the paint coating was not uniform across the length of the specimen. The average thickness in the three test specimens examined was about 200 to 250 μm with extremes varying between 50 and 400 μm. Figure 17 is a 100-μm-thick cross-section of paint that does not contain any beads recorded for the 18 mph specimen.

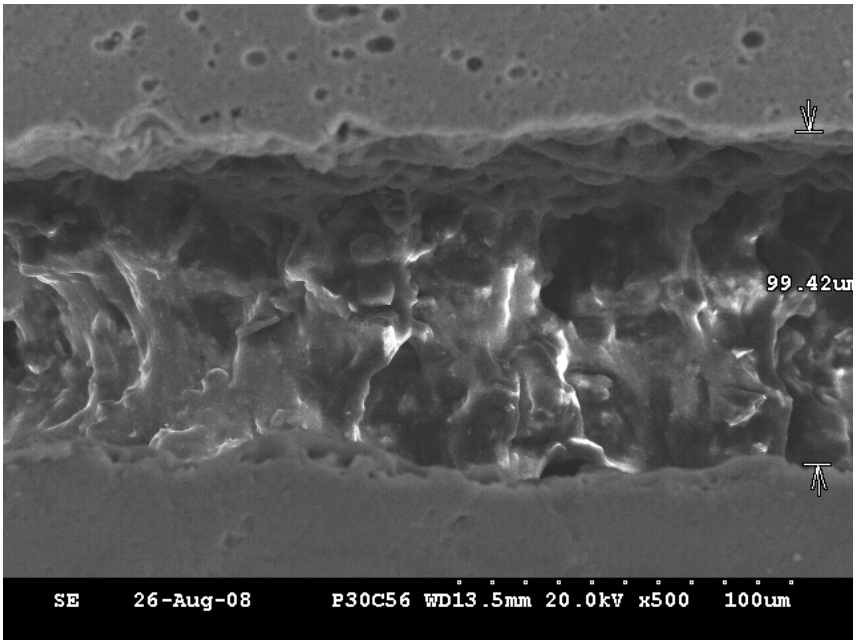

Figure 17. A 100-μm-thick Section of Paint on Aluminum Coupon Measured on the 18-mph Specimen.

In Figure 17, the aluminum coupon from the sample test plate is on top of the photograph, with the irregular surface exposed on the aluminum, the result of the sand blasting that was done to ensure good adhesion of the paint to the coupon. The mounting medium is at the bottom. The fact that both the aluminum coupon and sand blast surface be seen in the image suggests that during the polishing process some of the paint was removed, resulting in little cohesion.

Figure 18 shows a 0.5-mm glass bead in contact with the aluminum coupon and embedded about half-way into the mounting medium. The paint has not adhered strongly to either the coupon or the glass bead, and has been removed during the polishing process. Figure 19 is a lower-magnification image of a section of the painted coupon without any exposed beads.

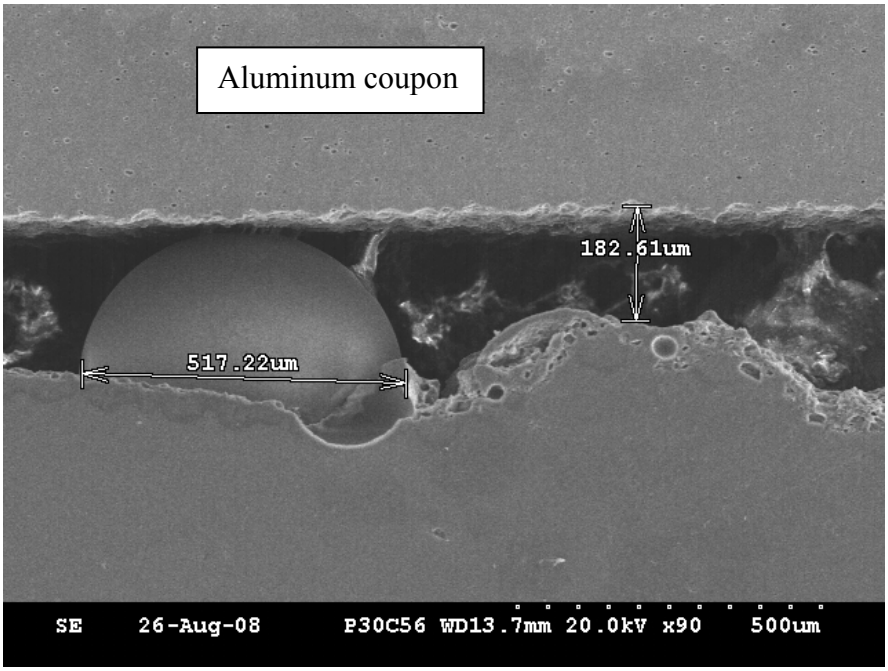

Figure 18. Cross-section with Several Exposed Glass Beads in the 18-mph Specimen.

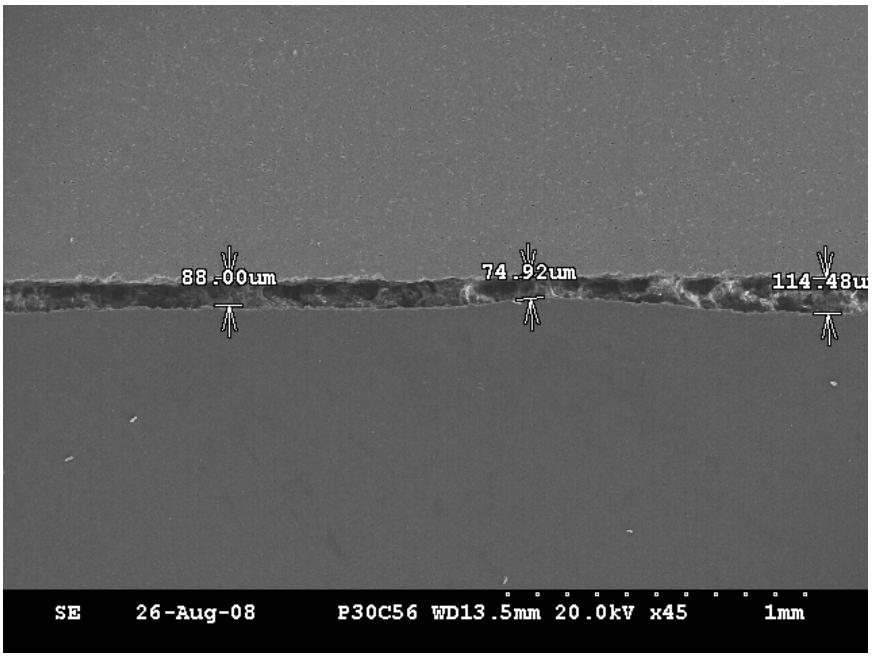

Figure 19. Low-magnification Image of the Paint in Cross-section Showing a Thickness of about 90 μm in the 18-mph Specimen.

Figure 20 dissects a glass bead resting on the aluminum substrate (coupon is on bottom of image and the mounting medium is on top). The sand blasted texture of the coupon is visible more clearly in profile in this image. The contact of the paint with the glass bead shows an embedment that is slightly over 50 percent of the diameter of the bead and the paint thickness tapers away from the bead. This is the ideal glass bead/paint configuration.

The paint in Figure 20 appears granular with little or no connective threads that were observed in Figure 17. The nature of the paint in Figure 20 is typical of what was observed throughout this study. A more careful examination of the paint shows that the granular nature observed in Figure 20 results from the mineral filler in the paint. Subsequent chemical analyses of the mineral filler suggested that it is composed of calcium carbonate, most likely derived from limestone fines. The mineral filler is euhedral with a morphology consistent with calcite. Energy dispersive x-ray mapping was conducted on the cross-section of the 18 mph specimen in order to identify the chemistry of the filler material. Figure 21 summarizes these findings. The x-ray map of the filler material shows a high calcium content, which is consistent with the other observations of grain morphology that support a composition of calcite.

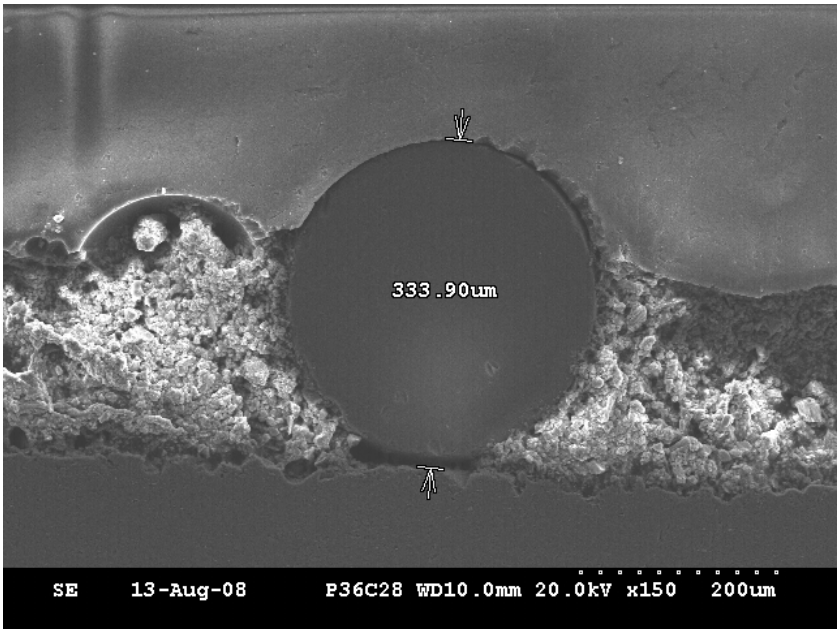

Figure 20. Cross-section through a Glass Bead in the 12-mph Specimen.
[Note: the aluminum coupon is on the bottom and the mounting medium is on top.]

Figure 22 contrasts the nature of the paint composition containing more organic components than in Figure 20, the more typical image of the paint. In Figure 21, however, two distinct mineral filler particles were observed and measured at about 20 μm. The thickness of the coating in this region was only 85 μm, which means that just four mineral filler particles supported the paint thickness.

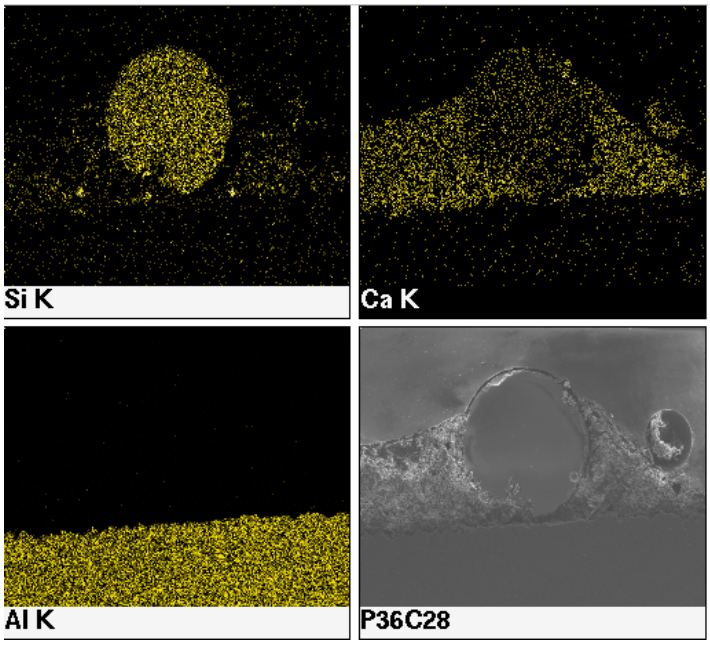

Figure 21. X-ray Map Characterization of the Cross-section of the 18-mph Specimen.
[Note: clockwise from upper left -- SiK – indicates that the glass bead is composed predominantly of silicon dioxide; CaK – shows some calcium oxide in the glass consistent with a soda-lime-glass composition and also high concentrations of calcium in the mineral filler consistent with calcite; AlK – identifies the aluminum substrate; P36C28 (18 mph truck speed/-60 degree bead gun angle) is the secondary electron SEM image of the location where the X-ray maps were obtained.]

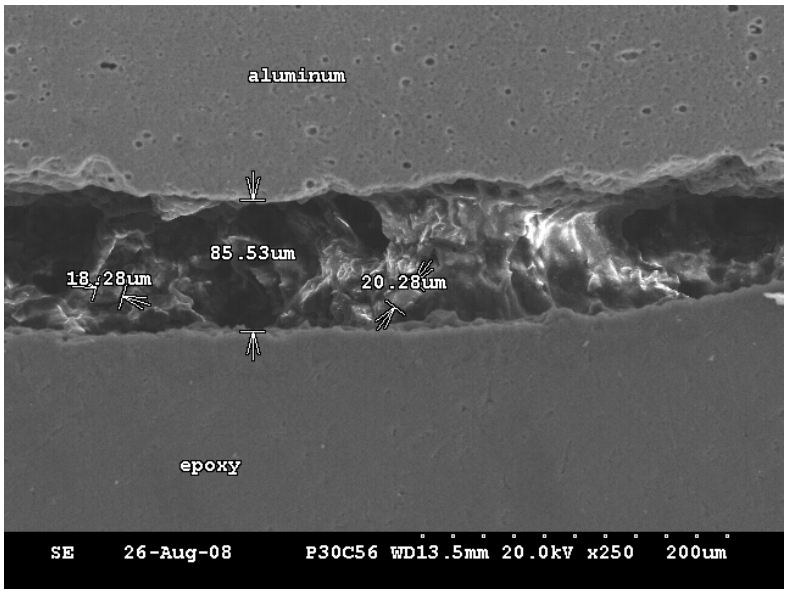

Figure 22. Details of the Size of the Mineral Fillers in an 85-µm-thick Paint Coating in the 18-mph specimen.

From these studies, it was evident that only large glass beads [greater than 300 µm] were observed to be resting on the coupon embedded in paint. Smaller particles, mostly about 200 µm

particles, were observed partially embedded in the paint at the surface, suggesting that during placement only those particles with sufficient mass and velocity rest on the coupon surface.

4.2.2.2 Surface Morphology

The first part of this subsection of the report describes the "wicking" of glass beads onto the waterborne paint, while the second part of this subsection contains general observations for the surface morphology analysis.

The image in Figure 23 shows a glass bead that was suspended in paint about 100 μm from the surface of the aluminum coupon (upper surface in this case). The paint did not adhere well to the glass bead and was removed during the polishing process. The mounting medium wet the surface of the bead and "wicked" along the glass surface.

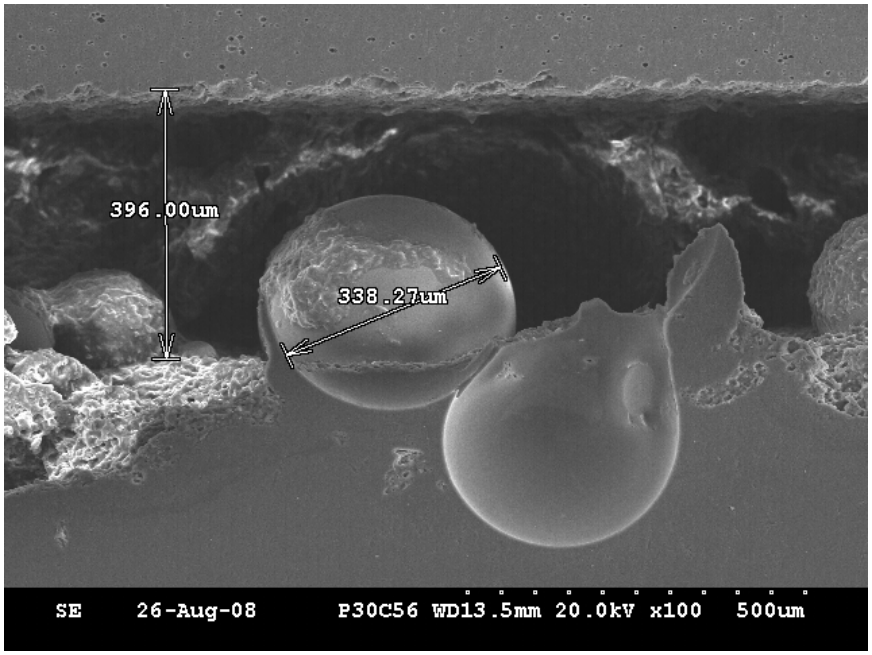

Figure 23. Cross-section Showing the "Wicking" Effect of the Mounting Medium with the Glass Beads.
[Note: the aluminum coupon is on the top in this image.]

The wetting of the glass bead surface by the mounting medium is contrasted in Figure 24 where a cross-section of a glass bead embedded in the paint is shown. In Figure 24, the granular nature of the paint does not appear to be wetting the bead. A careful examination of the image suggests that the bead is "captured" in a matrix of 20 μm particles held together by a thin coating of organic material that is sticking the mineral filler together. The mounding that is seen in cross-section can be interpreted as resulting from the impact of the bead into the paint displacing the mineral fillers around it. The rheological properties of the fresh paint would then flow around the bead and carry the mineral fillers into contact with the bead.

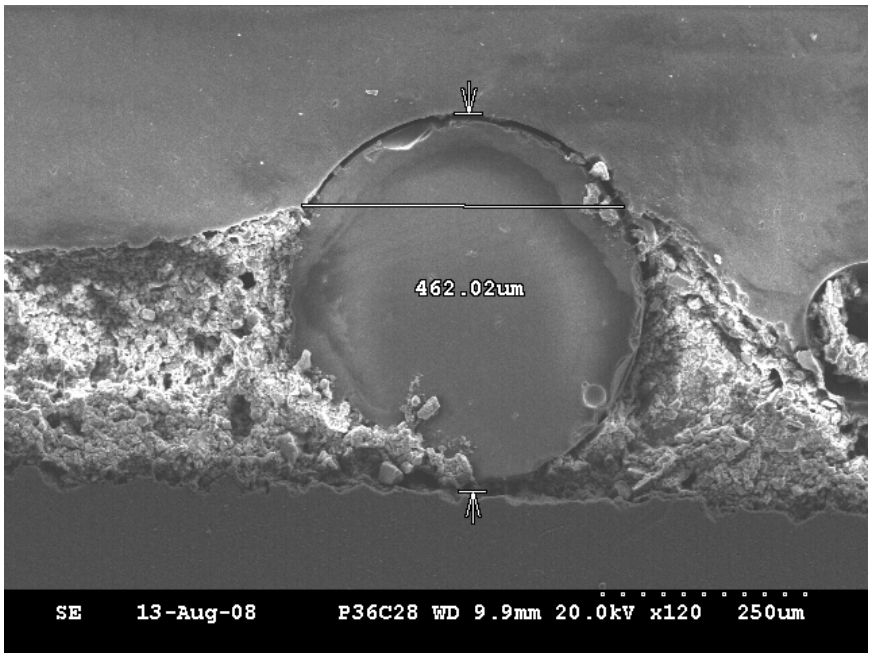

Figure 24. A Cross-section of a Glass Bead Embedded Approximately 70 percent in Paint.
[Note: aluminum coupon is on the bottom in this image]

Figure 25 is an image of the surface of a coupon with the beads exposed. What is evident in these images is that larger beads all have a "rind" (or "wicking") associated with the paint surface. The rind is, in most cases, asymmetrical in thickness. The rind is approximately 21.12, 7.10, 5.44, and 8.02 μm along the left, top, right, and bottom axes, respectively, of the glass bead shown in Figure 25. Figure 24 represents the cross section of this impact. The suggestion from these observations is that the rind results from the bead impacting into the fresh paint, displacing the mineral filler.

Appendix A contains left, top, right, and bottom axis wicking measurements from a series of baseline SEM images as a function of the truck application speed, bead gun angle, and the bead diameter exposed above the paint surface. In general, the rind size does not appear to be strongly correlated with the truck application speed or bead gun angle; rather, the rind size appears related to the bead diameter above the dry film of the paint. This apparent correlation is explored later in this report.

Based on all of the evidence provided in this section of the report, there does not appear to be strong evidence supporting a "wicking" effect in the experimental glass bead/paint systems. It is common practice for bead manufacturers to supply beads with a duplex coating that makes the surface hydrophobic to prevent clogging in the moist environment of the hopper during placement. The hydrophobic coating and the water-based paint system do not favor capillary attraction.

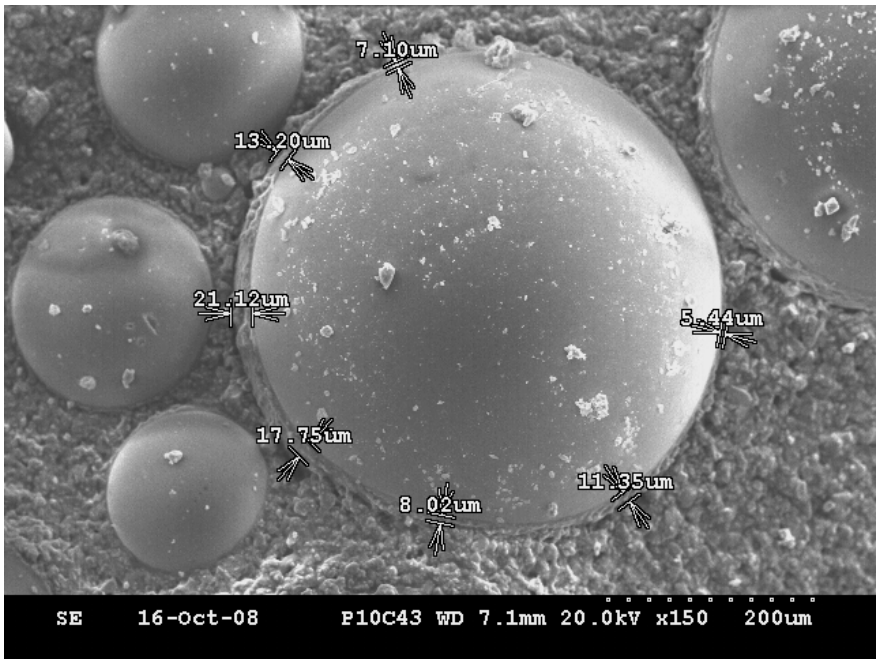

Figure 25. Surface Image of an approximately 400-μm-diameter Bead Showing an Asymmetrical Rind of Paint around the Bead.

Additional observations from the surface morphology analysis indicated that during the course of the SEM characterization, rarely were pullouts of glass beads observed. This statement stands in sharp contrast to the cross-sectional analysis that was conducted, suggesting very little in the way of adhesion of the paint to either the glass bead or the substrate in the present study.

Distress on the surface of the glass beads can be correlated to loss of retroreflectivity. The distress takes on two forms: small point abrasions, represented in the left panel in Figure 26, that are typically less than 30 μm; and larger, less common Hertican fractures, as shown in the right-hand panel of Figure 25.

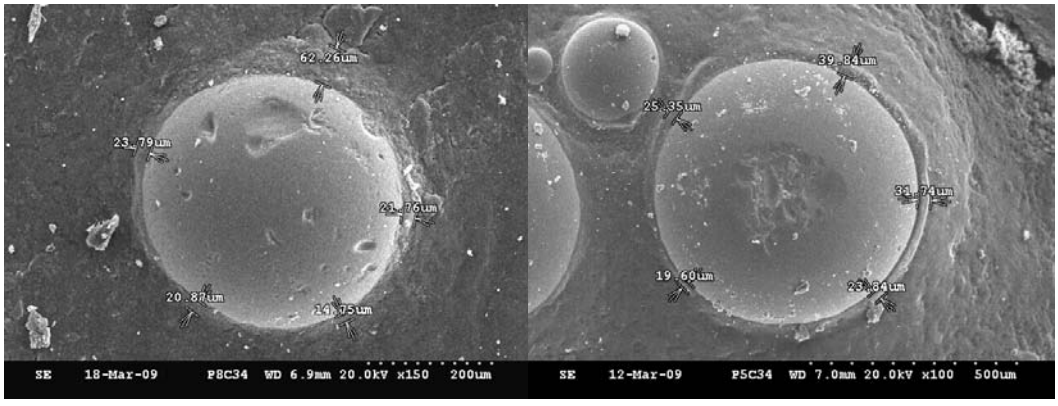

Figure 26. Two Images of Glass Beads Showing the Type of Surface Distress that was Observed at 1,200,000 Cycles.

In as-placed and low-wear beads, the incoming light that strikes the glass beads enters the sphere and through internal refraction, determined by the refractive index of the glass and the mismatch of the surrounding air, is directed back out of the bead. When the exiting "rays" of light interact with these surface distress features, the rays are scattered, effectively diffusing the intensity of the exiting light and diminishing the effectiveness of the glass bead. Figure 27 schematically illustrates this effect.

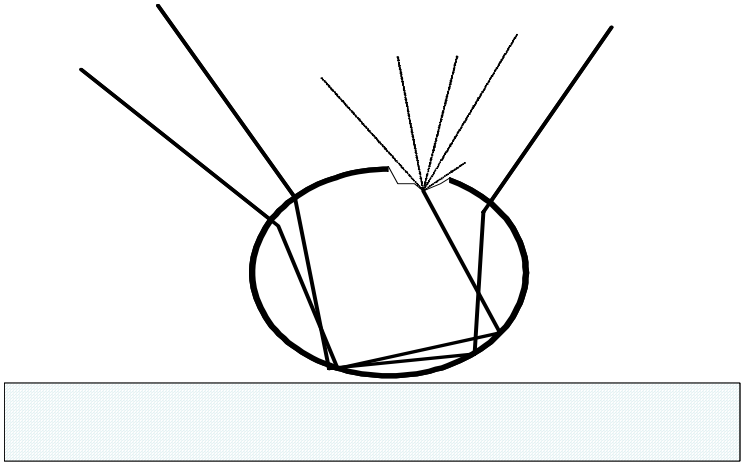

Figure 27. Schematic Illustrating the Effect of Surface Distress on Quality of Refracted Light from a Glass Bead.

Surface distress was not recognized below a threshold of 500,000 wear cycles. A contrast between the bead surface in Figure 28 (15 mph speed and +20 degree bead gun angle) and the surfaces of the images in Figure 26 is characteristic of all of the specimens studied. The onset of observable distress appeared rarely at 800,000 MMLS3 wear cycles. Distress at this stage was very uncommon, but when it was observed, it was significant.

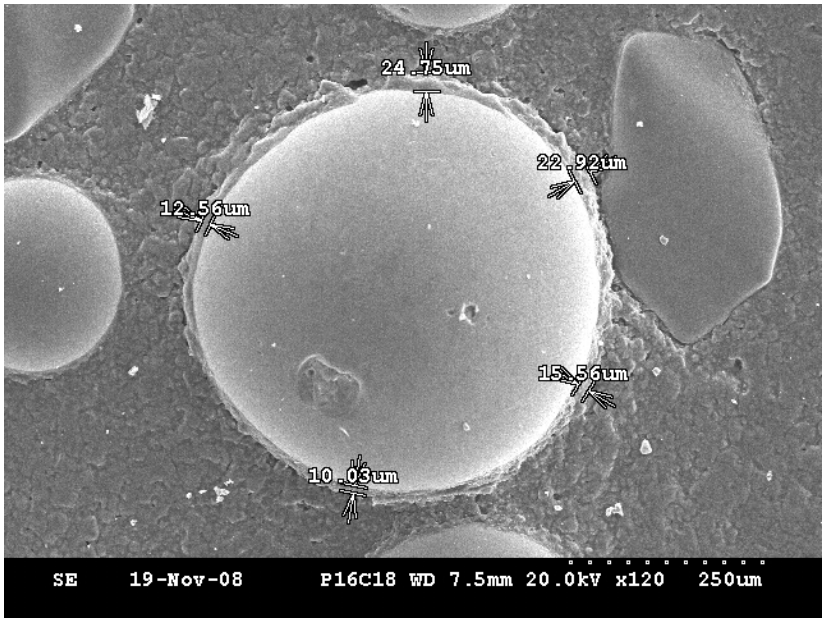

Figure 28. Surface of a Bead from the Specimen Prepared at 15 mph with a Bead Gun Angle of +20 degrees Showing a Distress-free Surface after 500,000 Wear Cycles.

At a cumulative wear level of 1,200,000 MMLS3 cycles, surface distress features characteristic of Figure 26 were commonly observed. There were, however, rare observations of beads, even at this level of wear, without observable distress, as shown in Figure 29.

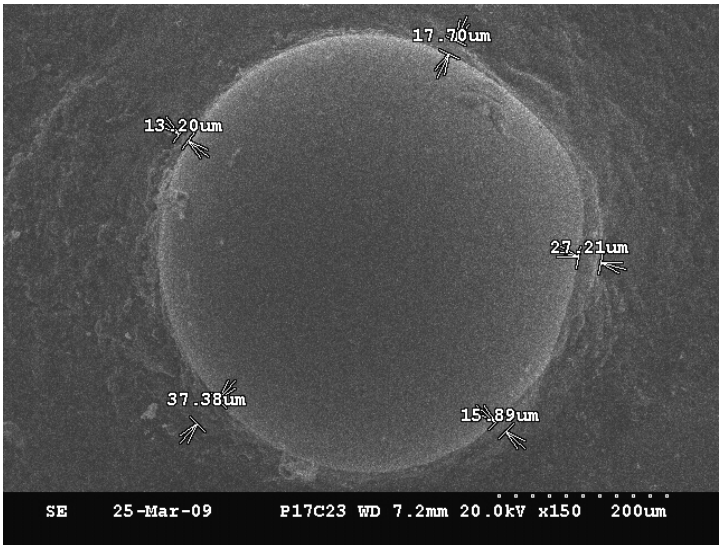

Figure 29. The Surface of a Bead Deposited at 12 mph with a Bead Gun Angle of +20 degrees after 1,200,000 Wear Cycles Showing Very Little, If Any, Distress.

A less well-defined effect of the cumulative accelerated wear studies is the impact on the waterborne paint surface. The images in Figure 30 are characteristic of this effect. The image in

the left panel is the surface of the specimen deposited at 15 mph with a bead gun angle of +20 degrees after 400,000 wear cycles, while the image in the right panel was deposited under the same conditions, but after 1,200,000 wear cycles.

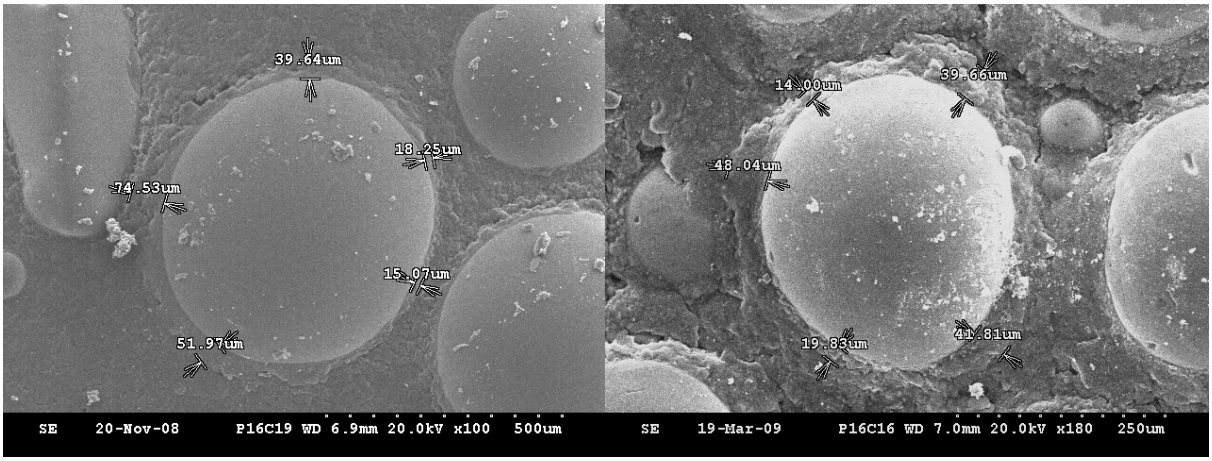

Figure 30. Contrast of the effect of wear on the surface paint for specimens deposited at 15 mph with a bead gun angle of +20 degrees: Left-hand panel after 400,000 wear cycles vs. right-hand panel after 1,200,000 wear cycles.

In Figure 30, the paint surface appears to be more friable and "flaking off" as thin lamelli. The effect was not common and no correlation to sample preparation parameters could be made.

In all of the images exposed to cumulative traffic loadings from the MMLS3, a "rind" was observed encircling the glass beads. The origin of the rind was discussed above. The rind showed directionality of impact of the glass bead and varying thicknesses. Figure 31 shows images from each of the three truck application speeds, all at a constant bead gun angle of +40 degrees, and all after 400,000 wear cycles. The sizes of the rinds observed here are reasonably consistent, but a careful examination of the 18-mph rind (Figure 31[c]) shows that in the impact direction (lower half of image), the paint did not flow back into contact with the bead as it did in the 12 and 15 mph samples. This behavior is common to most of the 18-mph specimens and, although rarely present at lower application speeds, does sometimes exist. This is shown in a collage of images for the 18 mph truck application speed in Figure 32. Figure 32(a) is the baseline image that shows paint flowing back into contact with the bead. Figures 32(b) through 32(d) are images taken after 500,000, 800,000, and 1.2 million MMLS3 cycles. In Figure 32(d), the rind without paint in contact with the glass bead is apparent in the upper right-most portion of the image. The implication of this semicircular "trench" around the bead can lead to degradation of the specimen. In actual field conditions where the pavement marking application is exposed to wet/dry cycling and to freeze/thaw cycling, both in the presence of deicing salts, trench-like openings between the paint and glass beads can allow fluids to enter, and upon freezing or the growth of salts during wet/dry cycling, can serve as a mechanism for dislodging the bead from the paint matrix, and subsequently a loss of retroreflectivity.

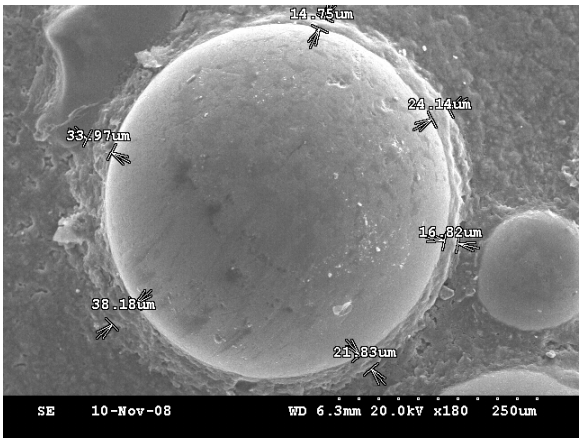

(a) 12 mph application speed.

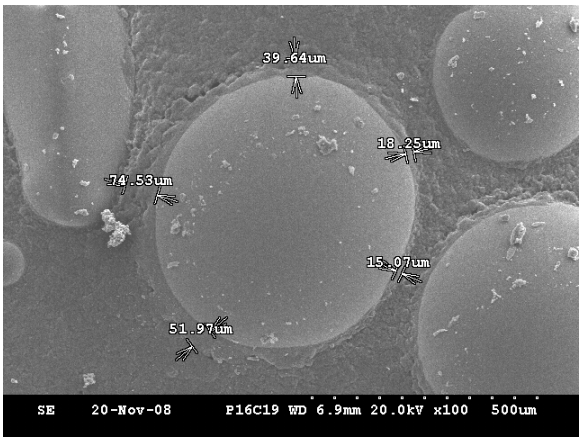

(b) 15 mph application speed.

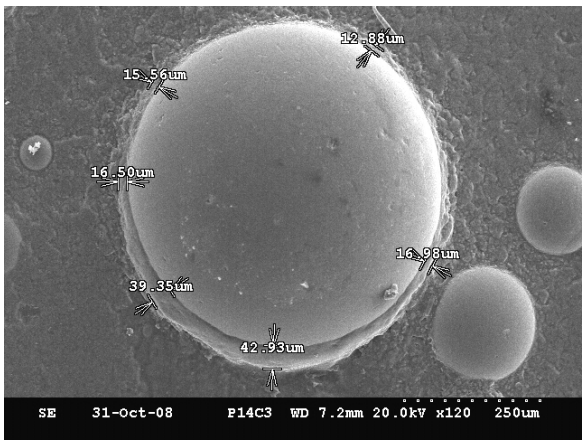

(c) 18 mph application speed.

Figure 31. Images of Beads Placed at 12, 15, and 18 mph at a +40-degree Bead Gun Angle Exposed to 400,000 Wear Cycles.

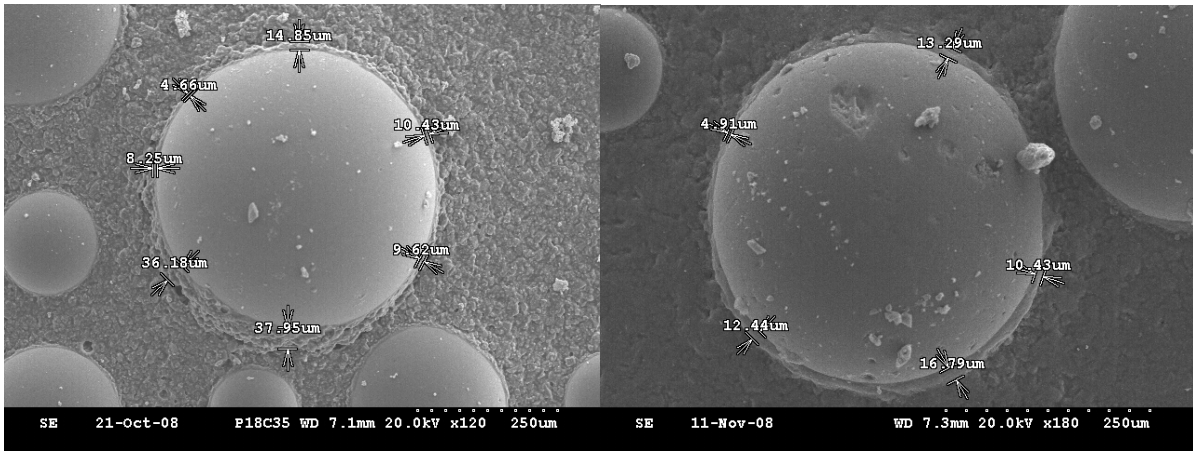

(a) Baseline condition (no MMLS3 cycles). *(b) 500,000 MMLS3 cycles.*

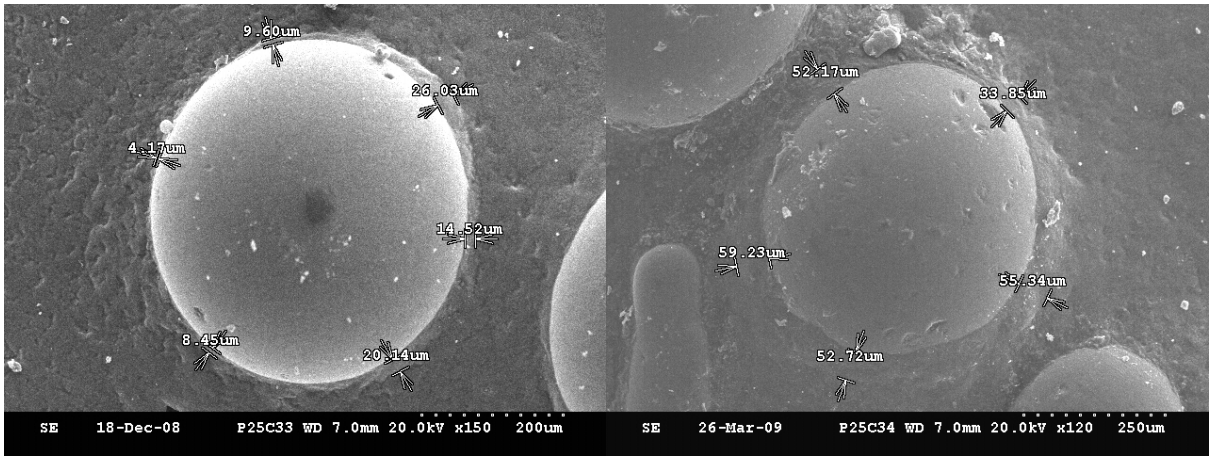

(c) 800,000 MMLS3 cycles. *(d) 1,200,000 MMLS3 cycles.*

Figure 32. Images of Beads Placed at 18 mph at a +40-degree Bead Gun Angle Exposed To Various Accelerated Wear Cycles.

Appendix B provides a collage of photos from the baseline SEM surface morphology from the 18-mph truck speed and -40-degree bead gun angle. A second collage of photos from the 18-mph speed and -40-degree bead gun angle are also contained in Appendix B, illustrating the effects of 1.2 million MMLS3 cycles. Figure B-2 illustrates the glass bead surface distress and paint flaking off as thin lamelli around the glass beads after 1.2 million accelerated traffic loads. Figure B-1 illustrates the baseline condition where the glass beads do not appear to be distressed and the paint around the beads is not flaking off.

4.3 Weathering Evaluation

This section is organized into two subsections. The first describes the results from the digital image processing, while the second subsection describes the results from the scanning electron microscopy. It is important to note that the second set of 18 test plates was used in the

weathering evaluation – these test plates were housed in an outdoor laboratory and were not trafficked.

4.3.1 Digital Image Processing

Like the accelerated wear evaluation described in section 4.2 of this report, baseline digital images were analyzed to determine the bead coverage in all 18 sample test plates prior to weathering. These data were used to establish a point of reference after weathering the sample test plates for a period of 1 year. The sample test plates were photographed in November 2008, March 2009, and June 2009, 1 year after the experimental pavement markings were applied at the Larson Institute test track. Because the digital image processing analysis is focused on the glass bead coverage on the sample test plates, and because subjective assessments of the weathered samples did not show any signs of bead loss, only the weathered images from June 2009 were analyzed. The bead coverage for the baseline and June 2009 weathered digital image processing analysis is shown in Table 5.

Table 5. Bead Coverage for Weathering Evaluation.

Speed (mph)	**Weathering Duration**	**Bead Gun Angle (degrees)**						**Average**
		-60	**-40**	**-20**	**0**	**+20**	**+40**	
		Bead Coverage (%)						
12	Baseline	23.25	25.04	30.68	28.64	26.42	26.05	**26.68**
	One year	20.31	21.35	23.10	19.41	21.33	20.00	**20.92**
	Bead Loss[1]	*12.65*	*14.74*	*24.71*	*32.23*	*19.27*	*23.22*	***21.13***
15	Baseline	25.63	26.81	28.91	27.96	24.18	23.55	**26.17**
	One year	19.32	21.23	21.67	23.07	20.03	19.81	**20.86**
	Bead Loss[1]	*24.62*	*20.81*	*25.04*	*17.49*	*17.16*	*15.88*	***20.17***
18	Baseline	18.33	16.22	21.61	25.36	22.85	21.48	**20.98**
	One year	14.68	11.36	19.03	17.43	16.86	14.25	**15.60**
	Bead Loss[1]	*19.91*	*29.96*	*11.94*	*31.27*	*26.21*	*33.66*	***25.49***
Average		**20.25**	**20.34**	**24.17**	**23.65**	**21.95**	**20.86**	**21.87**

[1] *Bead loss was computed as the percent loss in beads between 1 year of weathering and the baseline.*

The relative bead loss shown in Table 5 was calculated using Equation (1). The average bead coverage was computed across each row in Table 5 to illustrate the average at each truck application speed, irrespective of the bead gun angle. Additionally, the average bead coverage was averaged over each bead gun angle, irrespective of the truck speed. The results indicate that the greatest bead coverage occurred in the 12-mph truck speed, followed by the 15-mph truck speed, irrespective of the bead gun angle. The -20-degree bead gun angle produced the greatest bead coverage over the 1-year weathering period, followed by the 0-degree bead gun angle, irrespective of the truck application speed. The greatest bead coverage after 1 year of weathering was found in the 12-mph speed and -20-degree bead gun angle (23.10 percent), followed by the 15-mph speed and 0-degree bead gun angle (23.07 percent).

The contour plot of the baseline condition shown in Figure 14 illustrates the bead coverage prior to weathering. A contour plot showing the bead coverage as a function of the bead gun angle and truck application speed, after 1 year of weathering, is shown in Figure 33. The dashed line in Figure 33 shows the maximum bead coverage as a function of the truck application speed and

the bead gun angle. At the lowest speed (12 mph), the maximum bead coverage occurs when the bead gun angle is -20 degrees. At the 15-mph truck application speed, the maximum bead coverage occurs when the bead gun angle is approximately -5 degrees. The maximum bead coverage occurs at the 18-mph truck application speed when the bead gun angle is approximately -20 degrees.

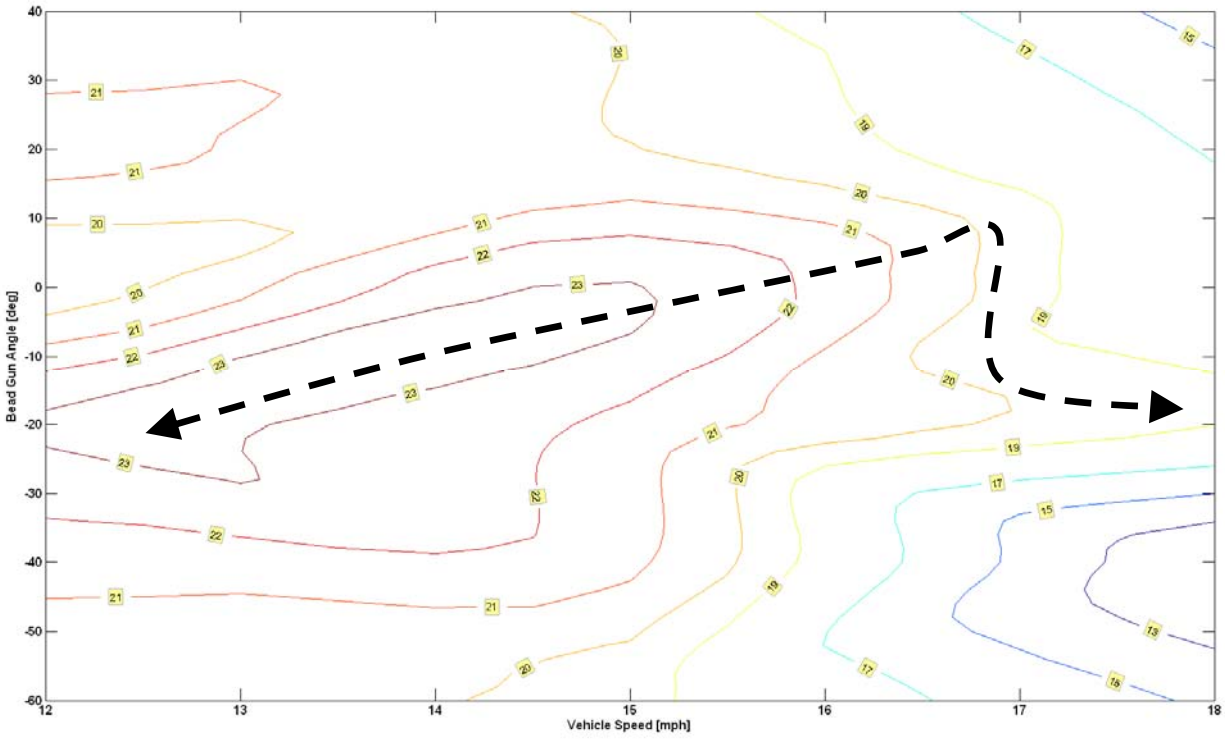

Figure 33. Contour Plot of Bead Coverage after 1 Year of Weathering.

The overall findings from the bead coverage analysis for the weathered test plates suggest that slower truck application speeds, combined with a -20-degree bead gun angle, produce the greatest bead coverage in the sample test plates after 1 year of weathering. This finding appears to be consistent with the baseline digital image processing results. For a 15-mph truck application speed, a near-vertical bead gun angle appears to produce the maximum bead coverage after 1 year of weathering. This is also generally consistent with the baseline condition, where an approximate -15-degree bead gun angle was shown to produce the greatest bead coverage. At an 18-mph truck application speed, the digital image processing results appear to support a bead gun angle between 0 and -20 degrees.

4.3.2 Scanning Electron Microscopy

A surface morphology analysis was conducted in a laboratory setting using the Hitachi SEM. The analysis was conducted using coupons from the 18 sample test plates exposed to the weather.

Images from the baseline condition were analyzed and then general observations concerning the glass beads and waterborne paint were noted after the plates were weathered for 5, 9, and 12 months. The nature of this study examined the durability of the paint rather than the glass beads. A careful observation of the paint surface from all of the specimens examined indicates that a water-soluble component of the paint has been removed, resulting in the formation of tiny pits, 5 to 20 μm in diameter, that penetrate into the paint layer and expose the mineral filler in the paint, as shown in Figure 34.

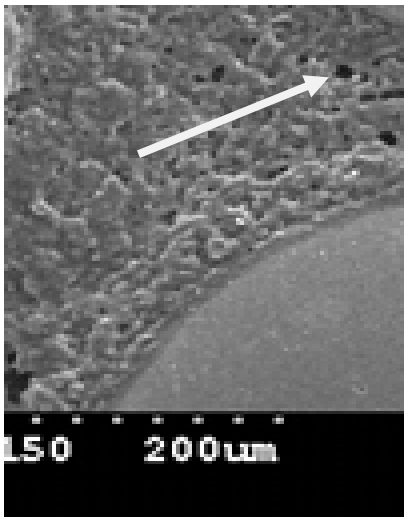

Figure 34. Enlargement of a Segment of Paint from the Right-hand Panel of Figure 31, Showing Leached-out Pitting.

All of the weathered paint surfaces look granular in contrast to the smooth surfaces from the baseline specimens, as shown in Figure 35. A weak trend can be seen in the weathering specimens where the granular nature of the paint appears to become more pronounced with prolonged exposure. There does not appear to be any specific correlation between the placement parameters and the observed degradation of the paint.

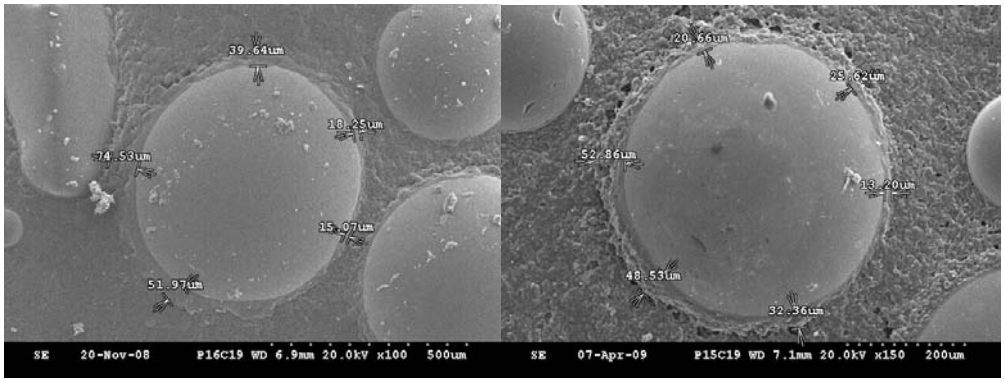

Figure 35. Baseline and weathered samples of 15 mph application speed at a bead gun angle of +40 degrees showing the effects of weathering on the paint substrate.

Of more interest is the behavior of the rind associated with some specimens. The right-hand panel of Figure 35 illustrates the observation. The outer circumference of the rind appears to leach away preferentially to the embedding paint. The result of this differential dissolution is a more porous cavity around the glass bead. As water continues to penetrate this low-porosity region assocated with the bead, and with repeated freeze/thaw cycling, the probability of glass beads popping out of the paint increases. Figure 36 illustrates this concept throughout the weathering process. The baseline condition (before weathering) is shown in Figure 36(a). Figures 36(b), 36(c), and 36(d) are associated with 5, 9, and 12 months of weather exposure, respectively. After 5 months of weather exposure, the rind becomes more apparent around the glass bead (Figure 36(c)). The rind in Figure 35(d), which was recorded after 12 months of weather exposure, is very apparent and considerably larger than the rind in the other images shown in Figure 36 (see bottom portion of the image).

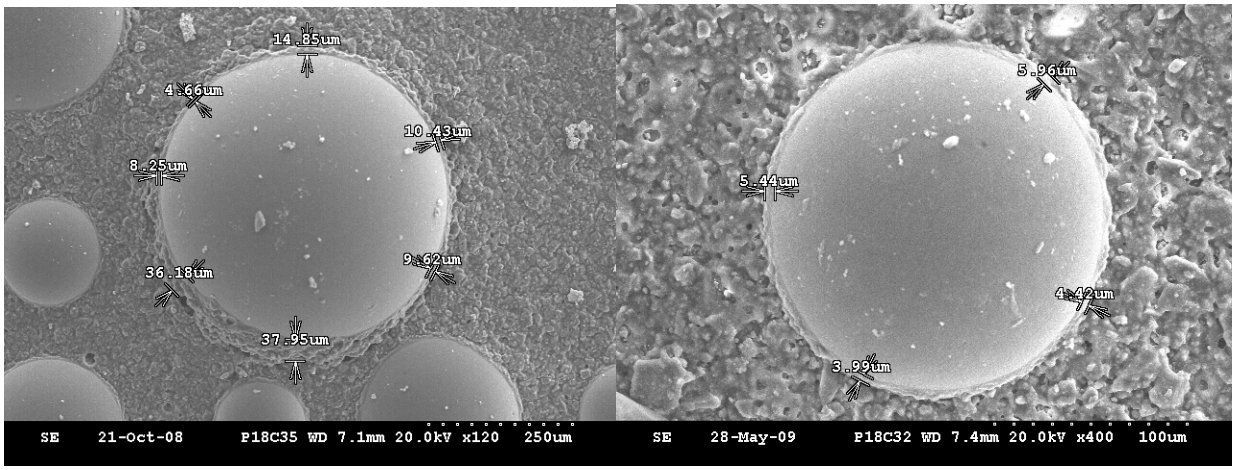

(a) Baseline Condition. *(b) Five Months of Weathering.*

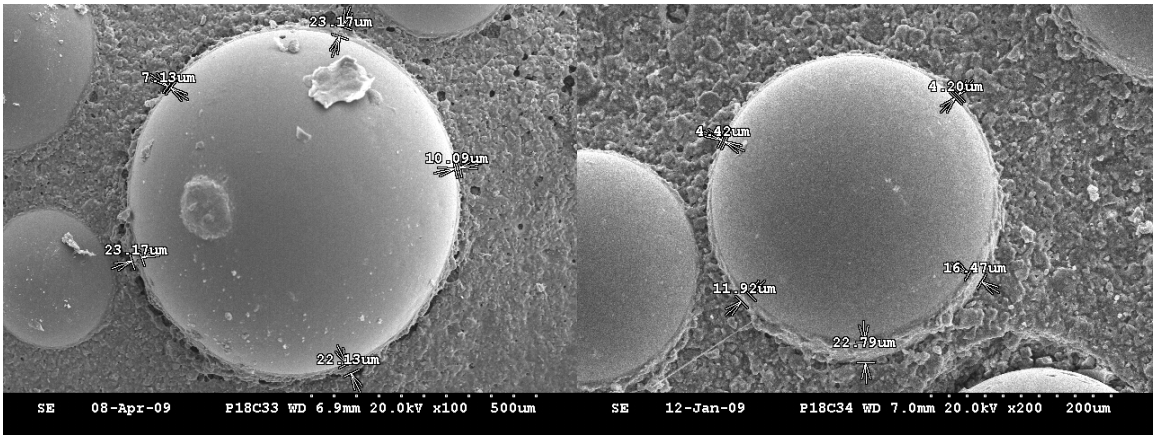

(c) Nine Months of Weathering. *(d) Twelve Months of Weathering.*

Figure 36. Baseline and Weathered Samples Applied at a 12-mph Speed and +40-degree Bead Gun Angle.

Appendix C contains a collage of SEM images for the 18-mph truck speed and -40-degree bead gun angle after 1 year of weathering. These images illustrate many of the issues described in this section of the report, namely the loss of water-soluble components from the paint and leaching away the rind around the glass beads, after 1 year of weathering.

4.4 Glass Bead Embedment

A sieve analysis was used to determine the distribution of glass beads in the PennDOT paint truck prior to dispensing the beads on the experimental pavement markings at the test track. The glass bead distribution is shown in Table 6. PennDOT glass bead size distribution specifications are provided in section 2.1 of this report. The as-received glass beads met the specification. To compute the embedment, the digital image processing results were used.

Table 6. As-received Glass Bead Size Distribution.

Glass Bead Size (μm)	Percent (%)	Cumulative Percent (%)
76.32		
	0.03	
88.91		0.03
	0.09	
103.58		0.12
	0.25	
120.67		0.37
	0.60	
140.58		0.97
	1.32	
163.77		2.29
	2.67	
190.80		4.96
	5.00	
222.28		9.96
	8.59	
258.95		18.55
	12.77	
301.68		31.32
	15.87	
351.46		47.19
	17.15	
409.45		64.34
	14.49	
477.01		78.83
	11.00	
555.71		89.83
	7.06	
647.41		96.89
	3.11	
754.23		100.00
	0.00	
878.67		

Figure 37 is a graphical representation of the data shown in Table 6, expressed as a volume percentage versus the particle size (in microns).

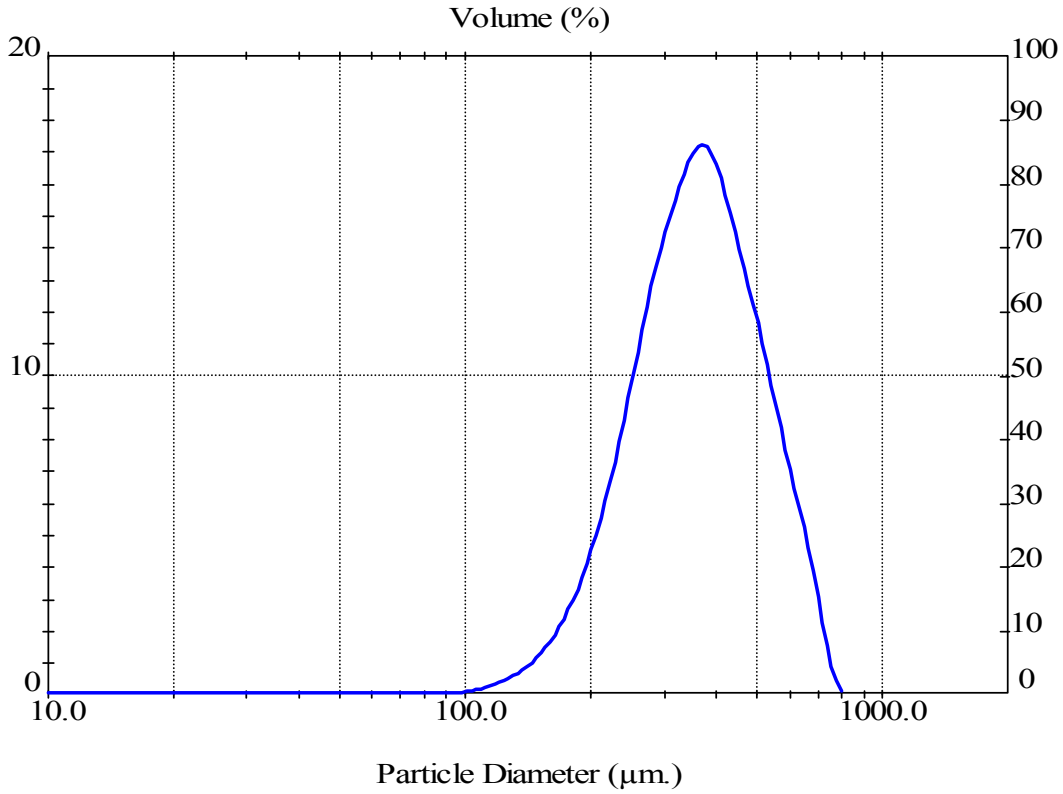

Figure 37. Size Distribution of the Glass Beads Expressed as Volume Percentage.

The distribution of the glass bead particle diameter, as observed in the baseline digital images, is shown in Figure 38. A small but distinct skew in the distribution can be observed. This skew can be attributed to the glass bead embedment in the waterborne paint. As such, the observed diameter of the glass beads is skewed because of embedment, which in turn alters the observable bead diameter. The difference in the observed distribution of the diameter of glass beads, compared to the original true measured glass bead diameter distribution, was used in a statistical calculation to compute the average glass bead embedment in the waterborne paint. The overall bead diameter distributions for the baseline, worn, and weathered surfaces are shown in Figure 39.

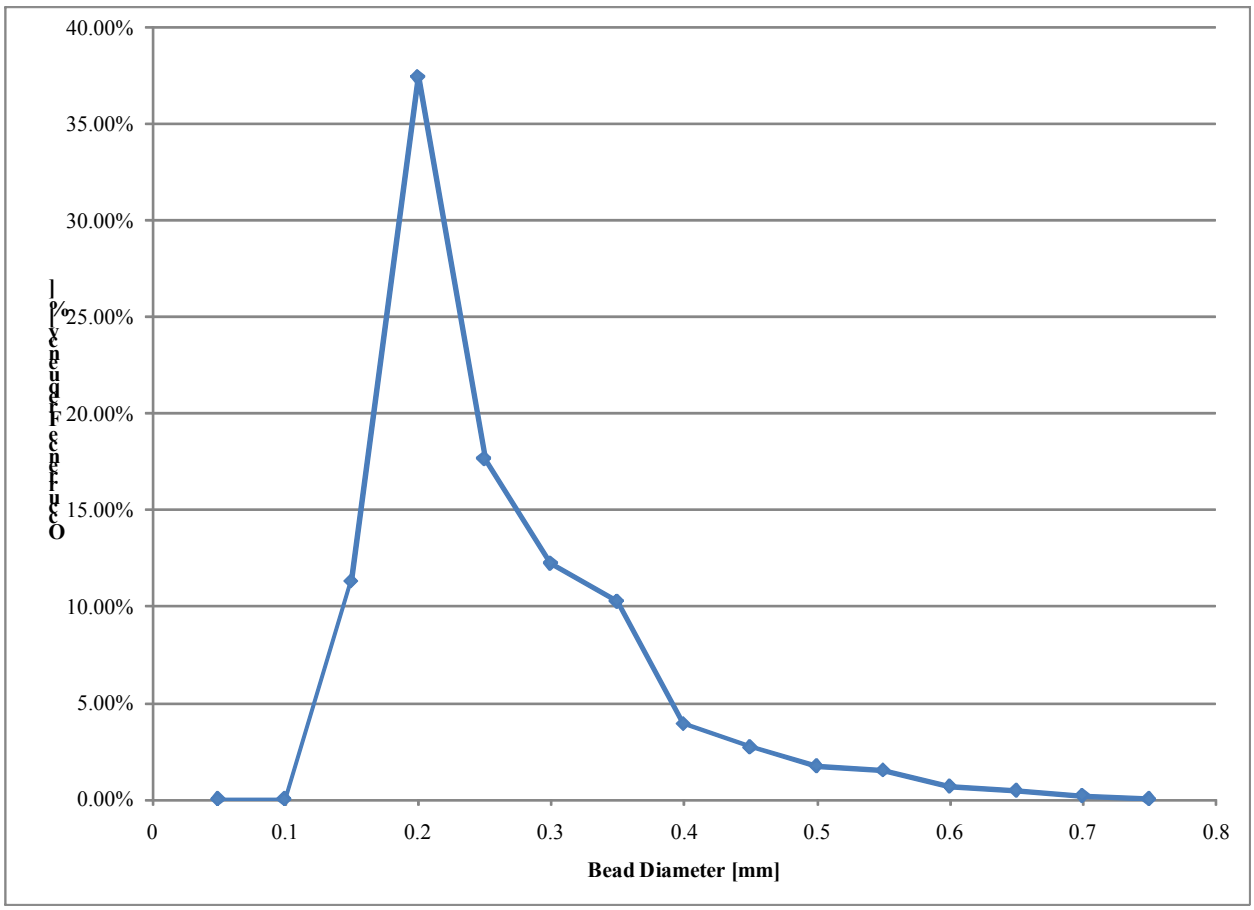

Figure 38. Bead Diameter Distribution in Baseline Photographs.

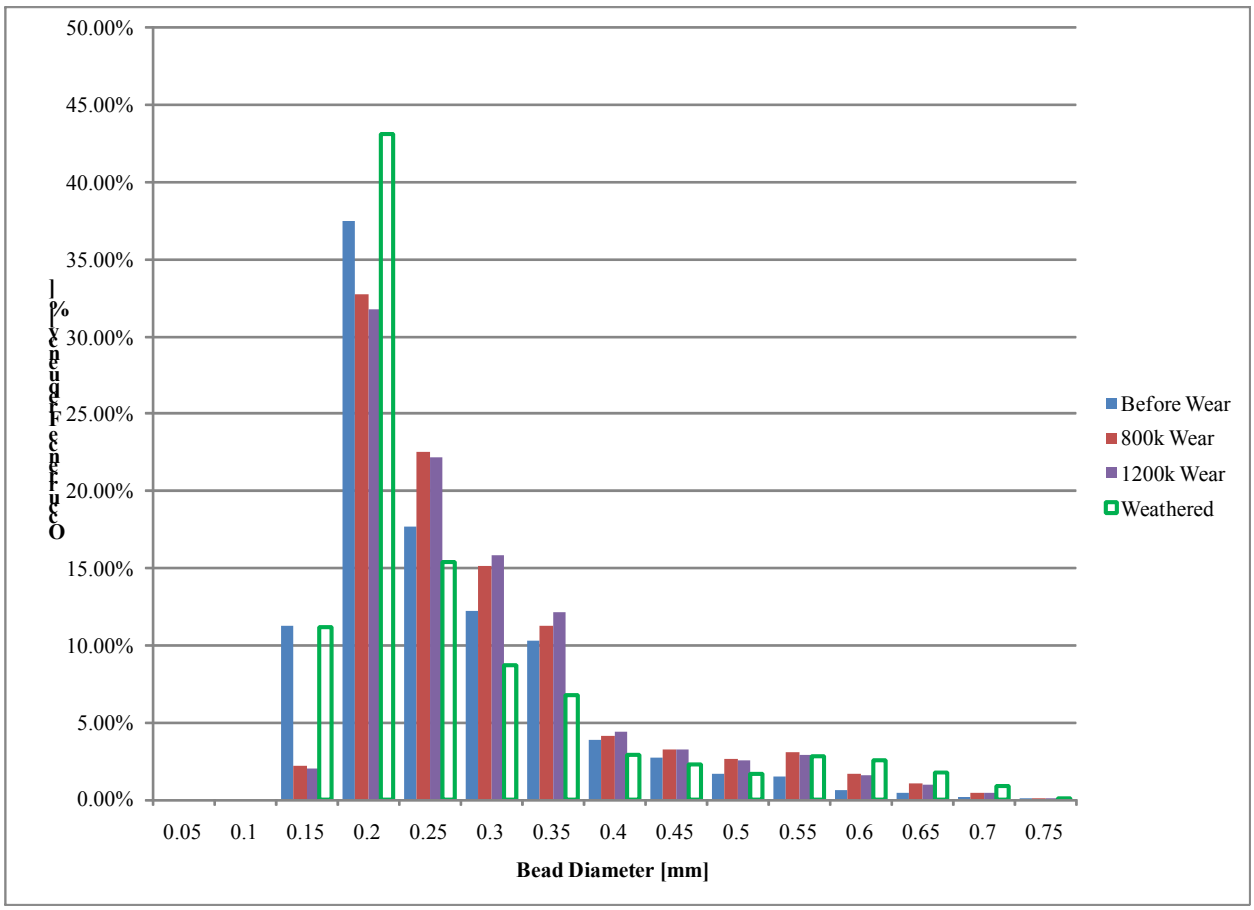

Figure 39. Diameter of Glass Beads in Baseline, Wear, and Weathered Conditions.

The measured distribution of the diameter of glass beads detected from the image-processing analysis in the baseline condition, as well as during two accelerated-wear periods, and in the weathered condition, is shown in Figure 40. As shown in Figure 40, the frequency distribution of larger glass beads in the waterborne paint increases as more accelerated traffic loads are applied to the samples, and after 1 year of weathering, relative to the baseline condition. This finding suggests that small glass beads are "popping out" of the waterborne paint after being exposed to traffic loads and weather.

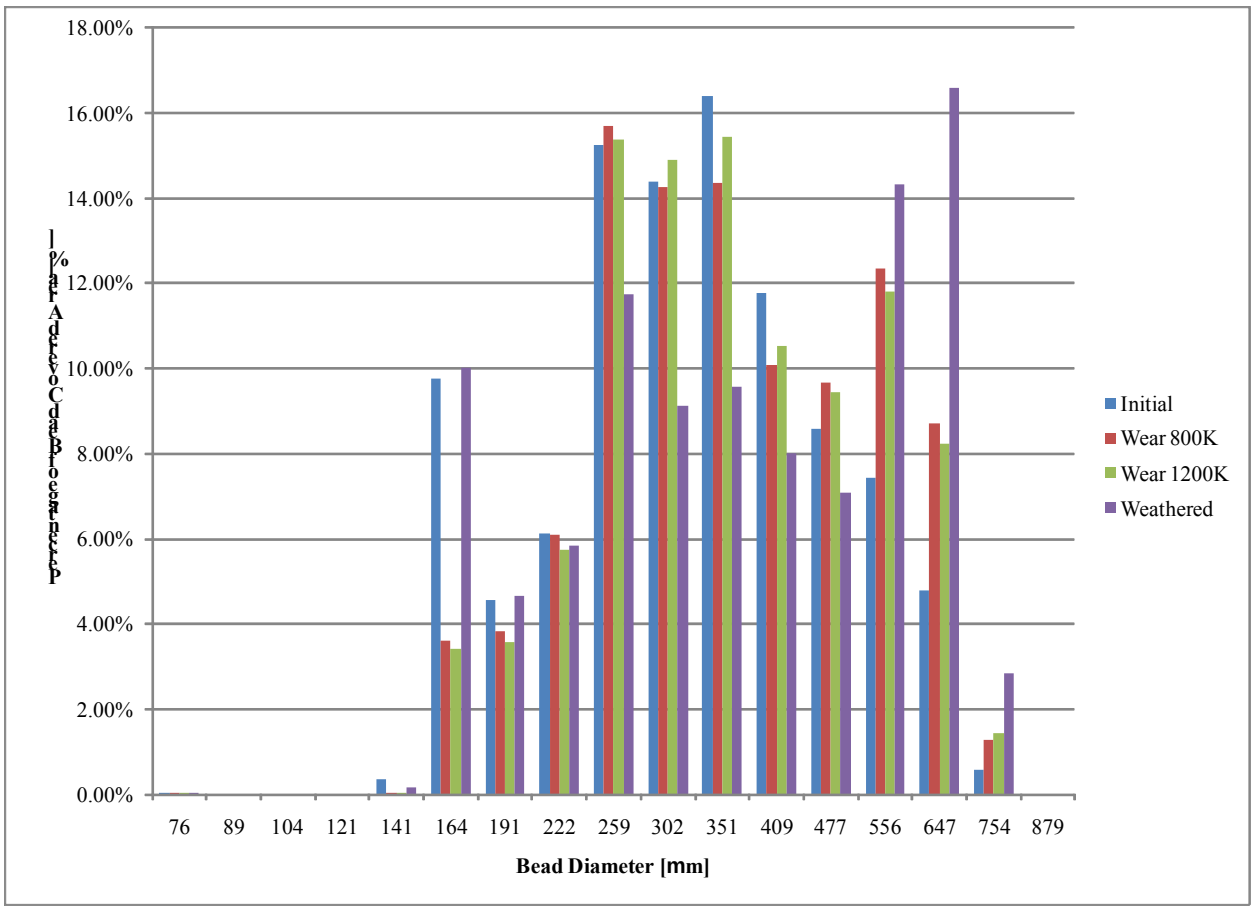

Figure 40. Bead Diameter Frequency Distribution in Baseline, Wear, and Weathered Conditions.

In Figure 40, there is a clear difference between the bead diameter distributions resulting from accelerated wear and weathering. The weathered samples show a much higher frequency of large beads in the waterborne paint when compared to the baseline and accelerated-wear samples.

Figure 41 depicts the bead coverage (percent) as a function of the observed bead diameter. Little variation exists in bead coverage for each bead gun angle and truck speed application.

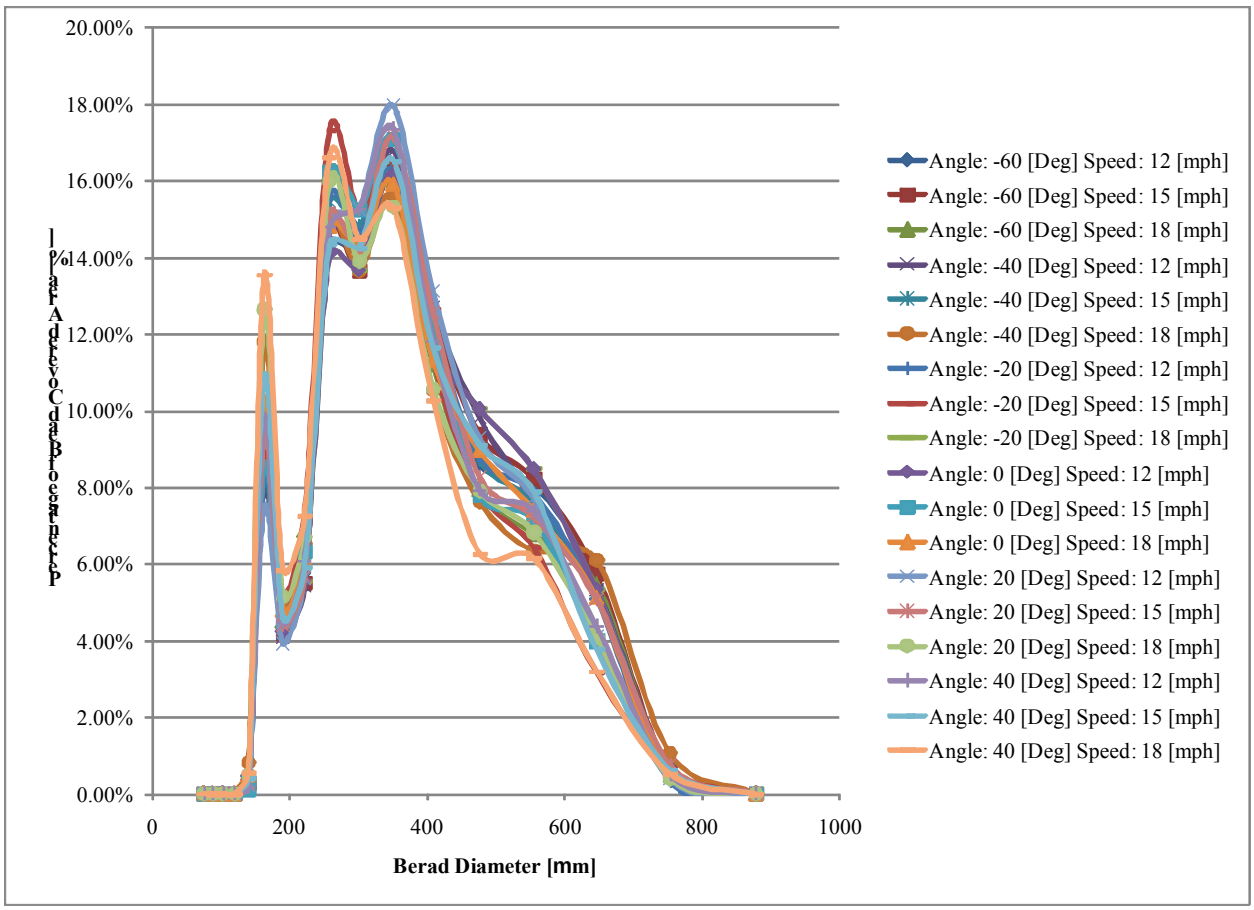

Figure 41. Distribution of Bead Coverage as a Function of Bead Diameter.

As a result of the limited variability in bead coverage among the various bead gun angles and truck application speeds, the bead embedment calculations are performed using the average bead diameter distributions among the bead gun angle/truck speed combinations. The average bead embedment for the different wear and weather cycles was calculated and averaged over all bead gun angle/truck speed combinations. The result is shown in Figure 42. As shown in Figure 42, the average bead embedment was approximately 55 percent in the baseline condition. After 800,000 and 1.2 million MMLS3 accelerated wear cycles, the average embedment was approximately 48 percent. After a 1-year weathering period, the average embedment was approximately 43 percent. As such, weathering appeared to increase the probability of bead loss moreso than accelerated trafficking in the present study. The average embedment in the baseline condition was near the optimal 60 percent.

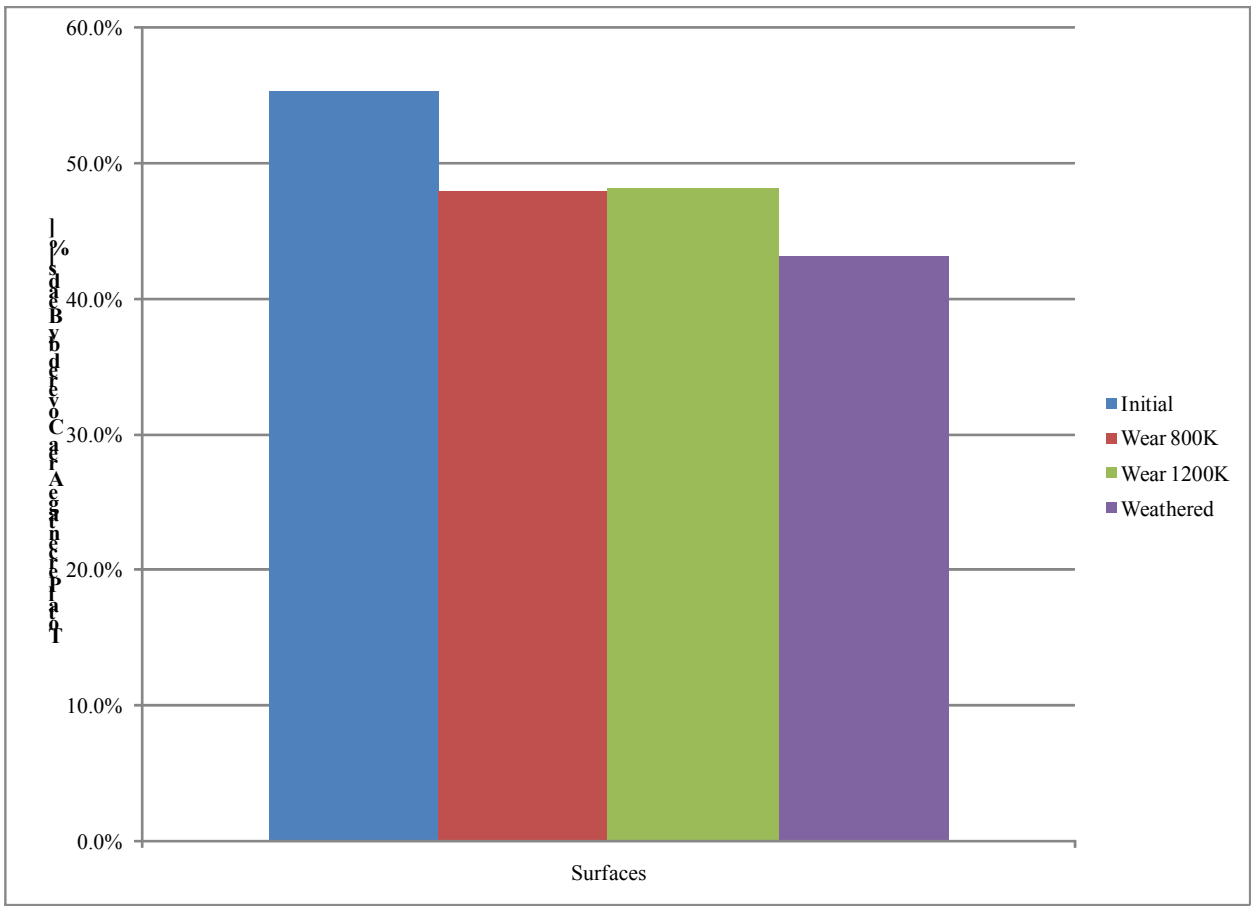

Figure 42. Average Bead Embedment Over All Truck Speed/Bead Gun Angle Combinations in Baseline, Wear, and Weathered Conditions.

Figure 43 shows the average bead embedment in the baseline condition, after two accelerated trafficking periods, and after 1 year of weathering as a function of the truck speed. It appears that increasing the truck application speed results in slightly higher average bead embedment levels when compared to lower truck application speeds. Again, weathering appears to have a more pronounced effect on average bead embedment than accelerated trafficking. Figure 44 shows the average bead embedment as a function of the bead gun angle. Weathering appears to have a more profound effect on average bead embedment than 800,000 or 1.2 million traffic loading cycles.

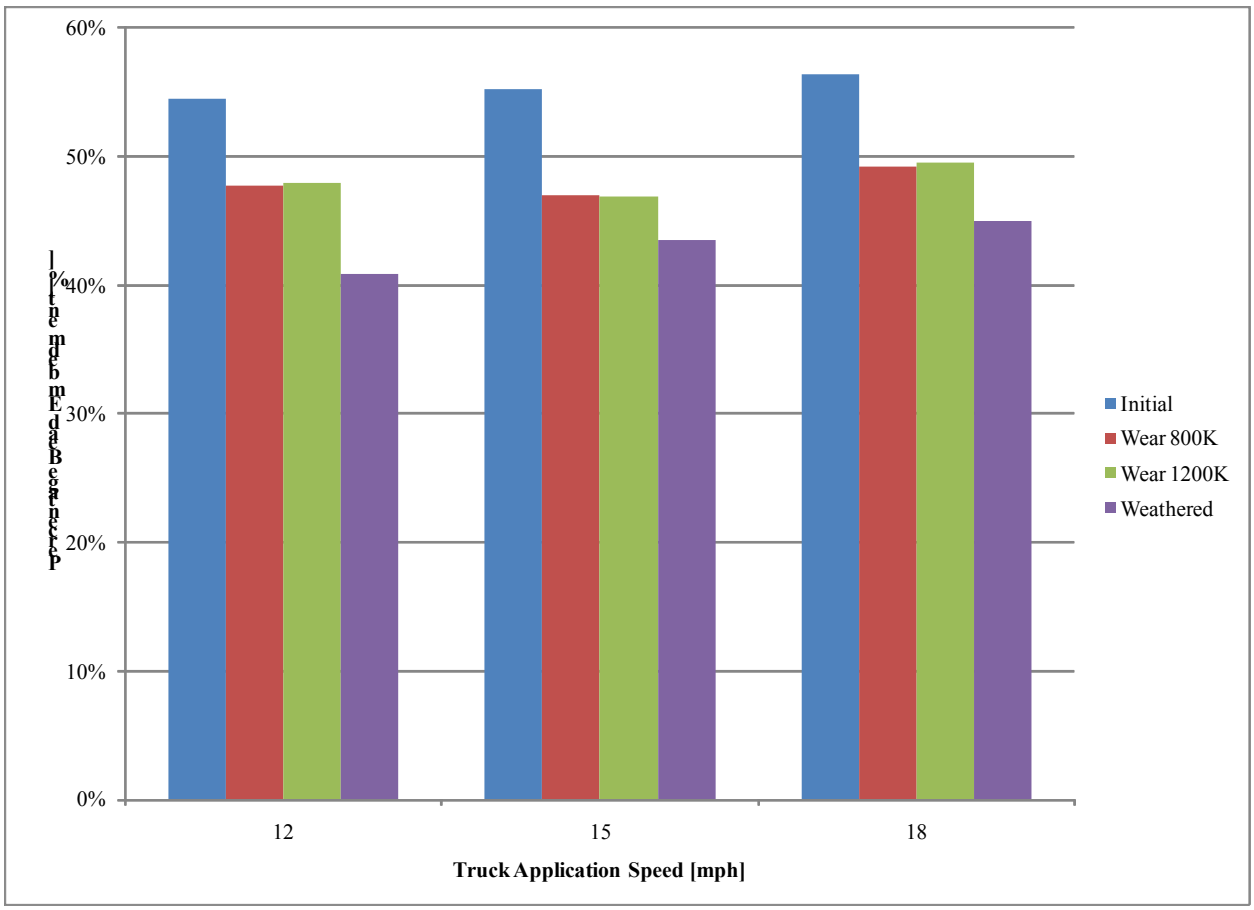

Figure 43. Average Bead Embedment for Baseline, Wear, and Weathered Conditions as a Function of Truck Application Speed.

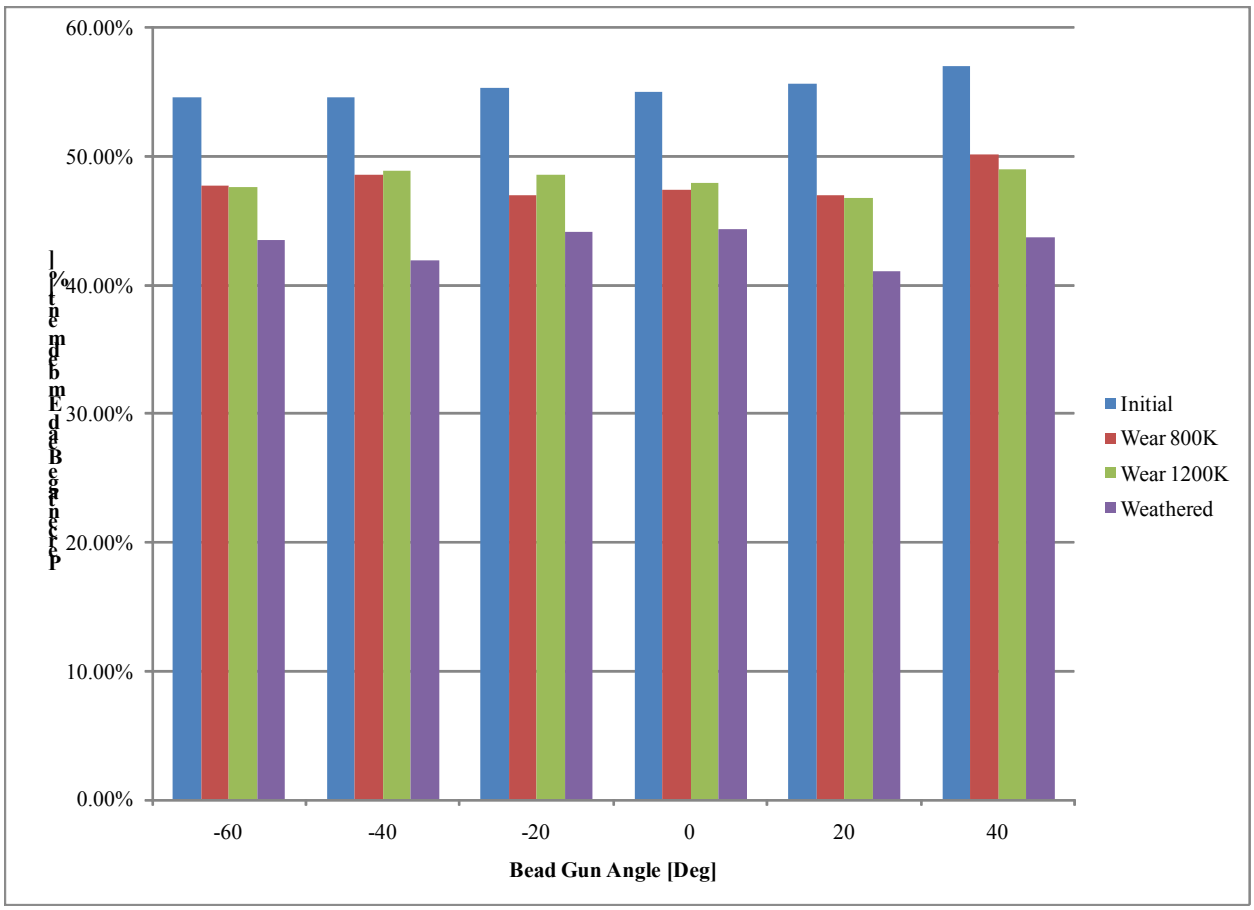

Figure 44. Average Bead Embedment for Baseline, Wear, and Weathered Conditions as a Function of Bead Gun Angle.

4.5 Summary of Laboratory Testing

A series of laboratory tests were run to determine the truck application speed/bead gun angle combination(s) that produce favorable conditions for pavement marking visibility. These included high-speed video imagery analysis of the glass beads as they were applied to the experimental pavement markings at the Larson Institute test track; a series of accelerated-wear and weathering evaluations using two sets of 18-sample test plates that were prepared during the application of the experimental pavement markings at the test track; and bead-embedment calculations. The accelerated-wear tests were performed at the MMLS3, which applied cyclic traffic loadings representative of transverse pavement markings. The accelerated-wear and weathering evaluations were completed using digital image processing and SEM imaging.

The performance metrics considered in the laboratory tests included the following:

- Kinematic bead descriptors (trajectory and speed);
- Glass bead coverage (digital image processing)
- Dry film thickness of the waterborne paint (SEM);

- Wicking of glass beads onto waterborne paint (SEM); and
- Glass bead embedment in the paint (sieve analysis and digital image processing).

The accelerated wear evaluations permitted an evaluation of glass bead adhesion with the waterborne paint. The weathering evaluation permitted an evaluation of the waterborne paint performance. For the purposes of this chapter of the report, it was hypothesized that a low-speed, vertical drop of the glass beads onto the waterborne paint would provide the greatest levels of nighttime visibility of the pavement markings. It was also hypothesized that greater levels of glass bead coverage in the waterborne paint would provide higher levels of nighttime visibility of the pavement markings. Thicker dry-film thickness of the pavement markings was hypothesized to provide higher probabilities of glass bead adhesion of the waterborne paint. Greater wicking of the glass beads onto the waterborne paint was hypothesized to produce the greatest bond strength between the beads and paint, resulting in improved durability of the pavement markings. The optimal glass bead embedment into the waterborne paint was assumed to be 60 percent – values less than this level were assumed to increase the probability of bead pop-out after a period of weathering or cumulative traffic passages.

The results of the laboratory evaluations suggest the following:

- The 12- and 15-mph truck application speeds, combined with the 40-degree bead gun angle, appear to produce the desirable properties of a slow-speed, vertical drop of glass beads onto the waterborne paint. In the 18-mph test, a 20-degree bead gun angle produced the most vertical drop angle, while the 0-degree bead gun angle produced the lowest bead speed. The optimal speed/bead gun angle combination with respect to the bead impact angle and speed was the 15 mph/40 degree combination.
- The 12 mph/-20 degree truck speed/bead gun angle combination produced the greatest bead coverage in the baseline condition and after a 1-year weathering period. The 15 mph/0 degree truck speed/bead gun angle combination produced the greatest bead coverage after 1.2 million MMLS3 traffic loads were applied to the pavement marking samples.
- The cross-sectional analysis in the SEM indicated that the dry-film thickness varied considerable across all truck application speeds, and that many mineral fillers were present in the waterborne paint with few connective threads.
- The SEM surface morphology analysis indicated that little “wicking” of the paint to the glass beads occurred in any speed/bead gun angle combinations.
- Few glass bead “pop-outs” were observed after 1.2 million accelerated traffic loads were applied to the sample test plates. However, significant surface distress occurred on the glass beads after 1.2 million cycles. The effect of the surface distress is a resultant loss of nighttime visibility.
- In the 18-mph truck speed tests, considerable paint was observed leaching away from the glass beads after 1.2 million traffic loading cycles. The resultant effect of this phenomenon is an increased probability of bead loss.
- The SEM weathering surface morphology analysis revealed that the waterborne traffic paint becomes more granular after a period of 1 year, increasing the probability of bead loss.

- The baseline condition revealed that the glass beads were approximately 55 percent embedded in the waterborne paint. This was a near-optimal level. After applying 1.2 million MMLS3 traffic loads, the embedment was approximately 48 percent. After a 1-year weathering period, the embedment was approximately 43 percent. Higher truck application speeds were associated with greater embedment levels in the present experiment.

CHAPTER 5. FIELD EVALUATION RESULTS

This chapter of the report is divided into two sections. The first describes the results of the nighttime end detection distance (herein referred to as visibility distance) study, and the second section summarizes the retroreflectivity measurements.

5.1 Nighttime Visibility Experiment

This section describes the nighttime visibility experiment results. The experimental procedure was described in Chapter 3 of this report. The minimum, maximum, mean, and standard deviation of visibility distances from experimental Phases I and II are shown in Table 7. The discussion that follows is organized into separate sections for Phases I and II, and a section where the results from Phases I and II were combined.

Table 7. Visibility Distance Summary Statistics.

PM[1] Line #	Speed (mph)	Bead Gun Angle[2] (degrees)	Visibility Distance: Phase I (feet)				Visibility Distance: Phase II (feet)			
			Min.	Max.	Mean	Std. Dev.	Min.	Max.	Mean	Std. Dev.
1	18	-60	107	265	197.2	34.3	94	285	183.9	45.2
2	15	-60	114	371	210.4	47.6	92	271	196.1	43.7
3	12	-60	101	366	206.8	46.0	85	284	197.6	45.1
4	12	-40	81	294	208.0	46.9	96	310	192.2	46.9
5	15	-40	81	309	208.6	45.6	89	284	187.0	47.3
6	18	-40	61	304	204.8	47.2	72	265	188.0	46.3
7	18	-20	102	302	219.6	55.0	98	299	197.7	51.9
8	15	-20	100	369	244.8	63.8	88	332	212.8	53.2
9	12	-20	96	334	233.4	55.7	76	289	203.3	55.3
10	18	0	86	390	229.0	62.6	79	324	204.0	59.1
11	15	0	112	393	228.0	62.1	113	306	199.1	53.0
12	12	0	116	407	218.4	60.1	116	284	200.5	46.4
13	12	20	126	316	235.3	54.1	119	328	216.3	52.9
14	15	20	99	325	228.9	55.4	79	314	206.1	58.2
15	18	20	105	396	245.0	69.9	87	330	219.8	58.6
16	18	40	101	369	240.8	67.1	78	344	220.2	62.8
17	15	40	105	384	235.2	66.6	57	338	212.3	57.0
18	12	40	108	418	240.2	57.3	90	311	210.0	53.2

[1] PM stands for Pavement Marking

[2] Bead gun angles were measured with respect to a vertical axis. As such, a -60 degree angle corresponds to a bead gun angle that is 60 degrees behind a vertical axis relative to the pavement surface. A -60 degree angle is pointed opposite the direction of the pavement marking application.

5.1.1 Phase I Analysis

The average nighttime visibility distances recorded for the research participants in Phase I of the experiment are shown in Figure 45. Figure 45 indicates that the -60 and -40 degree bead gun angles are associated with low nighttime visibility distances when compared to the other four bead gun angles, irrespective of the speed of application.

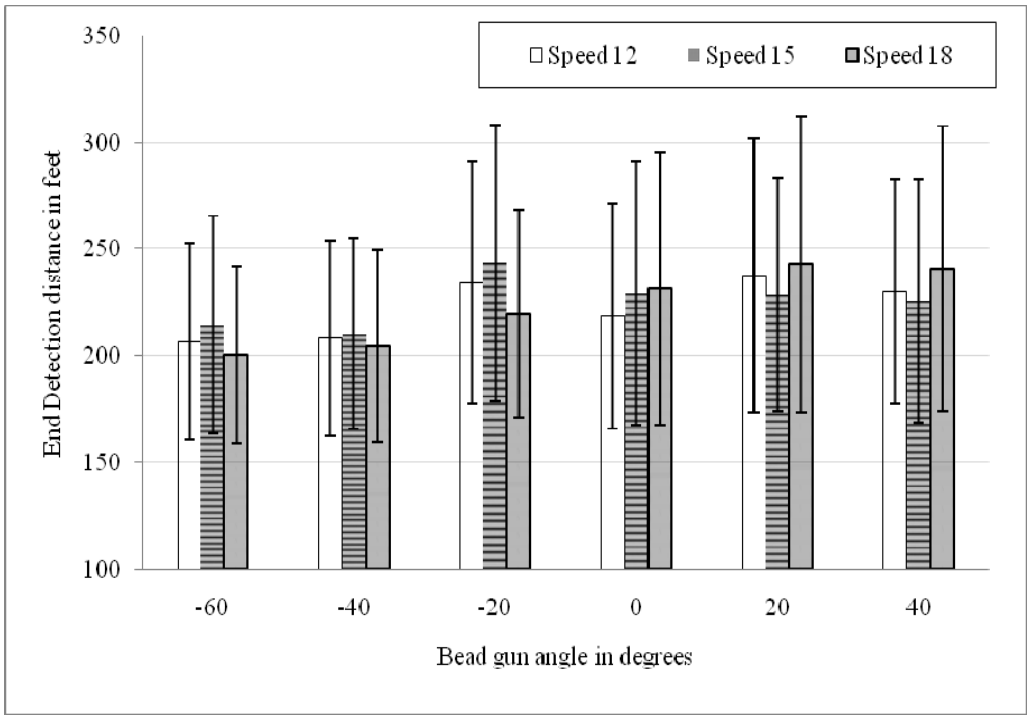

Figure 45. Phase I Visibility Distances.

Preliminary analysis revealed that the truck application speed was not statistically significant ($F(2,591) = 0.74$, $p = 0.48$) in Phase I of the nighttime driving experiment. The bead gun angle and speed/bead gun angle interaction were statistically significant ($F(5,591) = 32.43$, $p < 0.001$ for the bead gun angle, and $F(10,291) = 2.90$, $p=0.001$ for the speed/bead gun angle interaction). The research participant ID random effect was also found to be statistically significant ($F(35,591) =54.92$, $p<0.001$). Since the interaction term was found to be statistically significant, a second ANOVA was carried out using line number (18 levels) as an independent variable. Table 8 shows the results of this ANOVA for Phase I using line number and research participant ID as independent variables.

Table 8 shows that participant ID and line number were statistically significant ($F(35,591) = 54.92$, $p < 0.001$ for participant ID, and $F(17,591) = 11.32$, $p < 0.001$ for pavement marking line number). The adjusted R^2 for the model was 76.18 percent, indicating that approximately 76 percent of the variability in the nighttime visibility distance during the Phase I experiment was explained by the factors included in the model. The partial η^2 for the pavement marking line number was 0.24, which indicates that 24 percent of the variance in the fitted model is accounted

for by the line number – the remaining variability (76 percent) in the fitted model is explained by the participant ID.

As the data were collected from different participants and the order in which the experimental treatments were presented to the research participants was not the same, the observations were considered independent. A residuals versus order plot of the data indicates that serial correlation is not present in the data. The normal probability plot and the Anderson-Darling statistic (A = 0.57; p = 0.14) confirmed that the data in Phase I were normally distributed. A plot of the standardized residuals versus fitted values indicated constant variance among the data. Each of the residuals plots is shown in Figure 46. Collectively, these plots indicate that all ANOVA assumptions were met.

Tukey pairwise comparisons showed that the line numbers corresponding to treatments 8 (15mph/-20 degrees), 13 (12 mph/20 degrees), 15 (18 mph/20 degrees), 16 (18mph/40 degrees), 17 (15 mph/40 degrees), and 18 (12 mph/40 degrees) were significantly different from the other treatments during Phase I of the experiment, but were not significantly different from each other. The range in visibility distance for these six markings was 235 to 245 ft (72 to 75 m).

Table 8. Analysis of Variance Results for Phase I Experiment.

Source	**DF**	**Seq SS**	**Adj SS**	**Adj MS**	**F**	**P**	**Partial η^2**
Subject ID	35	1502157	1506841	43053	54.92	<0.001	0.76
Line number	17	150847	150847	8873	11.32	<0.001	0.24
Error	591	463314	463314	784			
Total	643	2116317					
Anderson-Darling test statistic (A) = 0.57, p = 0.14							
$R^2 = 0.762$							

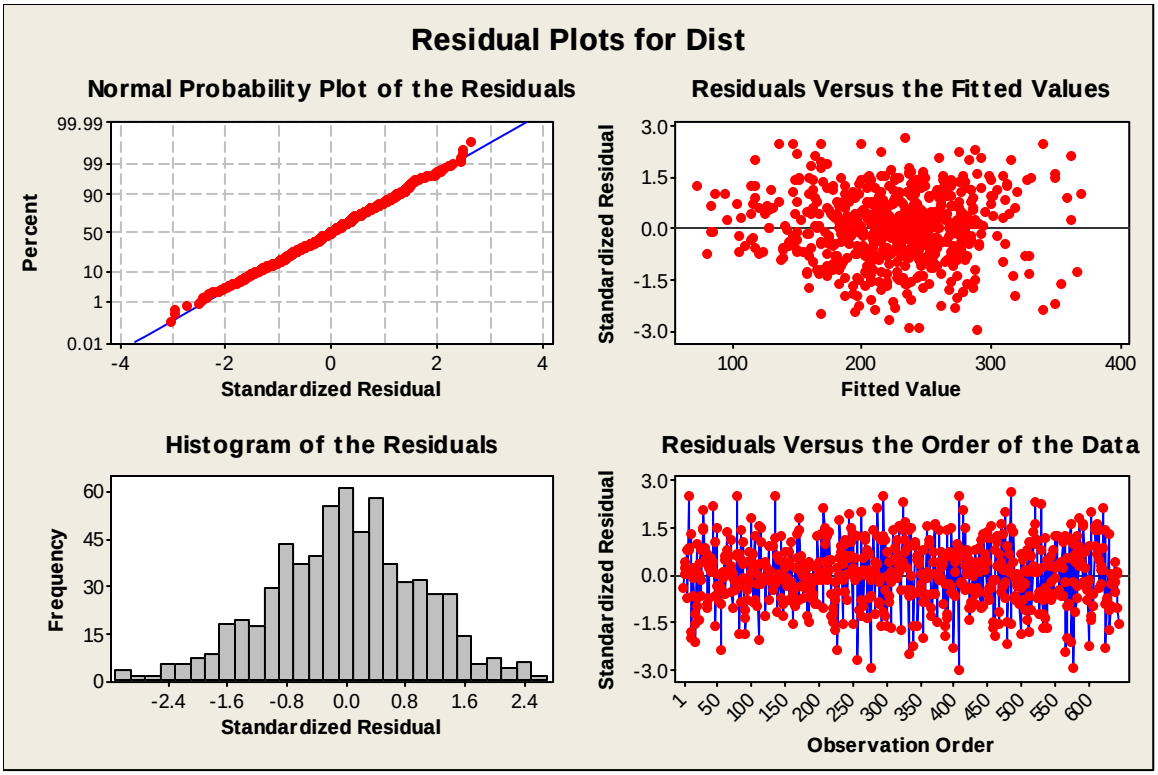

Figure 46. Residual Plots for Phase I Analysis.

5.1.2 Phase II Analysis

The average nighttime visibility distances recorded for the participants in Phase II of the study are shown in Figure 47. The bead gun angle/speed combinations that appear to produce the shortest visibility distances are 12 mph/0 degrees, 12 mph/-40 degrees, 15 mph/-40 degrees, 15 mph/-60 degrees, and 18 mph/-60 degrees – most of these distances correspond to the backward-facing bead gun angles.

The truck application speed was not statistically significant ($F(2,516) = 0.11$, $p = 0.89$) in the preliminary ANOVA model when entered in the model as a fixed factors at three levels. The bead gun angle and speed/bead gun angle interaction were statistically significant ($F(5,516) = 18.71$, $p < 0.001$ for the bead gun angle factor, and $F(10,516) = 2.55$, $p = 0.005$ for the speed/bead gun angle interaction) in the preliminary ANOVA model using the Phase II data. The research participant ID random effect was also found to be statistically significant ($F(31,516) = 61.94$, $p < 0.001$). A second ANOVA was carried out using line number (18 levels) as an independent variable. Table 9 shows the results of this ANOVA model for Phase II using line number and research participant ID as independent variables. The line number ID was a fixed factor, while the research participant ID was a random factor.

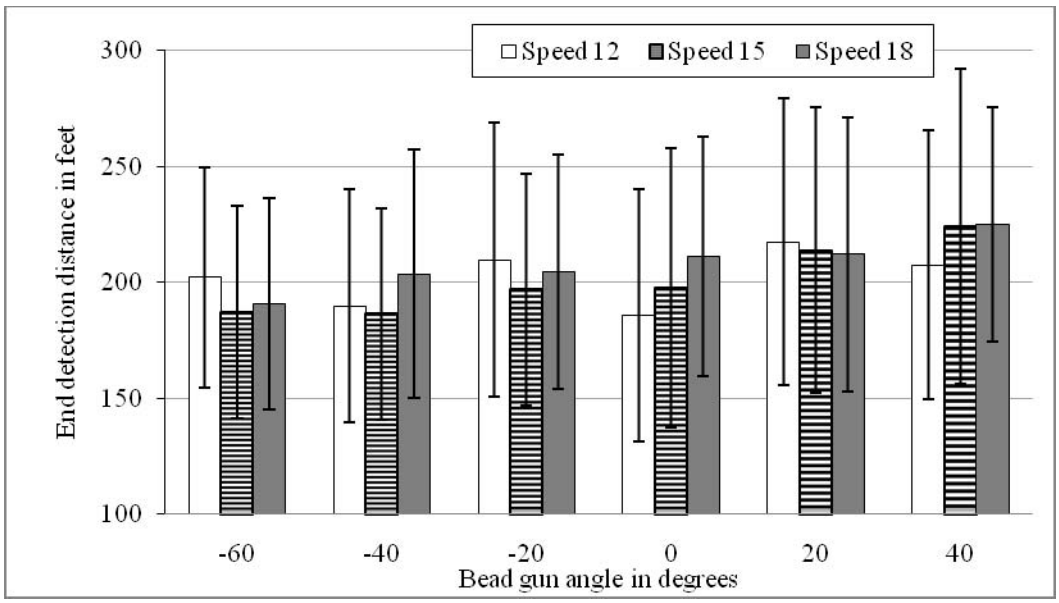

Figure 47. Phase II Visibility Distances.

Table 9. Analysis of Variance Results for Phase II Experiment.

Source	DF	Seq SS	Adj SS	Adj MS	F	P	Partial η^2
Subject ID	31	1154730	1161084	37454	61.94	<0.001	0.79
Line number	17	71517	71517	4207	6.96	<0.001	0.19
Error	516	312031	312031	605			
Total	564	1538278					
Anderson-Darling test statistic (A) = 0.47, p = 0.25							
$R^2 = 0.778$							

Table 9 shows that participant ID and line number were statistically significant ($F(31,516) = 61.94$, $p < 0.001$ for the participant ID factor, and $F(17,516) = 6.96$, $p < 0.001$ for the line number factor). The adjusted R^2 for the model was 77.83 percent, indicating that approximately 78 percent of the variability in the nighttime visibility distance during the Phase II experiment was explained by the research participant random effect and the pavement marking line number fixed effect. Partial η^2 values are also shown in Table 9. The line number factor explains approximately 19 percent of the variability in the fitted model.

A normal probability plot of residuals and the Anderson-Darling statistic (A) = 0.47 (p = 0.25) confirmed that the Phase II experimental data met the normality assumption. The constant variance (homoskedasticity) assumption was confirmed based on a standardized residual versus fitted values plot. No serial correlation was observed in the data as shown in the residuals versus order plot of the data. All residuals plots for the Phase II data are shown in Figure 48. Collectively, the residuals plots indicate that all ANOVA assumptions were met for the Phase II analysis.

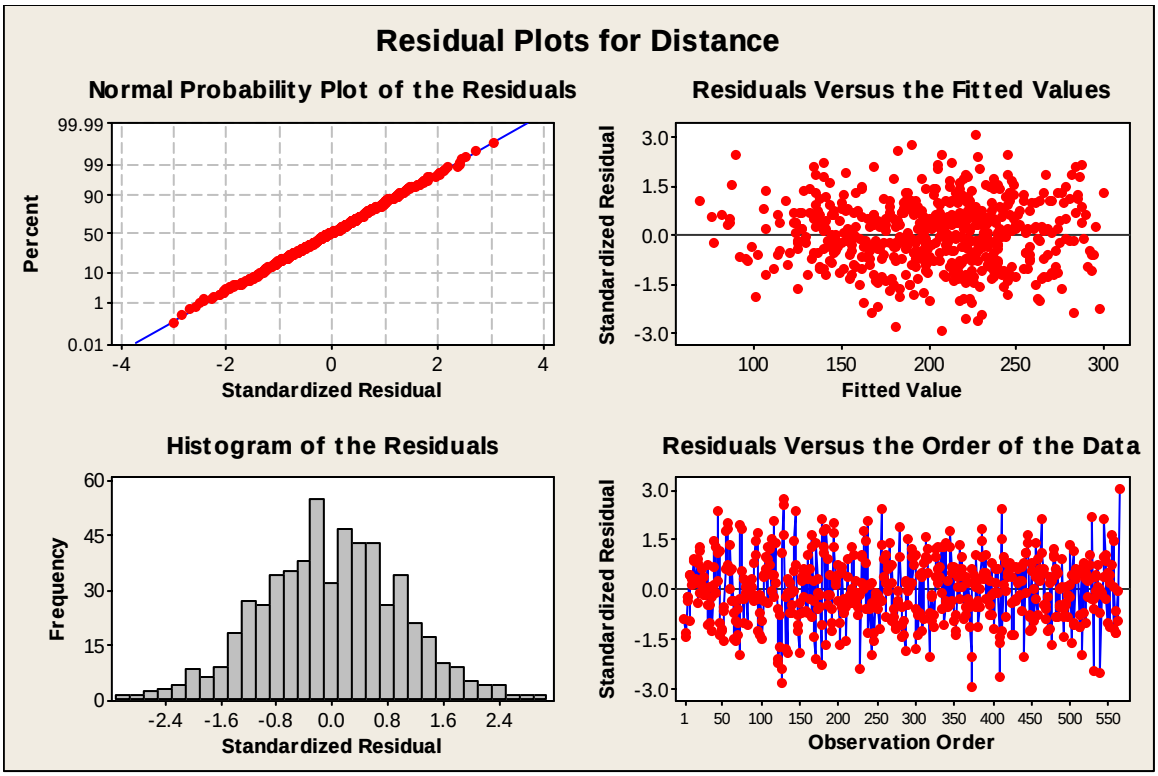

Figure 48. Residuals Plots for Phase II Experimental Data.

Tukey pairwise comparisons showed that the line numbers corresponding to treatments 8 (15mph/-20 degrees), 13 (12 mph/20 degrees), 15 (18 mph/20 degrees), 16 (18mph/40 degrees), 17 (15 mph/40 degrees), and 18 (12 mph/40 degrees) were significantly different from the other treatments during Phase II of the experiment, but were not significantly different from each other. The range in visibility distance for these six pavement markings was 210 to 220 ft (64 to 67 m).

When comparing the Phase I and Phase II results, it appears that the same six treatments offer the longest visibility distance for new pavement markings and pavement markings that are weathered. Of these six treatments, five had forward-facing bead gun angles, suggesting that a forward-facing bead gun angle produces longer visibility distances when compared to backward- and vertical-facing bead gun angles. A possible explanation for this is that when the markings are applied, the glass beads "plow" into the waterborne paint when the bead gun is pointed in the direction of the pavement marking application. The side of the bead that is exposed to traffic is not covered in paint and produces a high level of initial nighttime visibility. Because the beads are applied at a forward angle, the beads are embedded deep into the waterborne paint. As such, bead retention is likely high for this bead gun angle. As a result, the visibility distance for the weathered pavement markings remains high. It should also be noted that of the five forward-facing bead gun angles that produced longest visibility distance, four were applied at 12 mph (19 km/h) and 18 mph (29 km/h).

5.1.3 Combined Phase I and II Data

The assumptions of repeated-measures ANOVA were evaluated using the combined Phase I and II visibility distance data. The Anderson-Darling test statistic (A) was 0.65 (p = 0.08), indicating that the assumption of normally distributed residuals was met. The absence of heteroskedasticity was confirmed using a standardized residual versus fitted values plot. No serial correlation was observed in the data based on the residuals versus order plot. Each of the residuals plots is shown in Figure 49. Collectively, the residuals plots indicate that the ANOVA assumptions were met when combining the Phase I and II data.

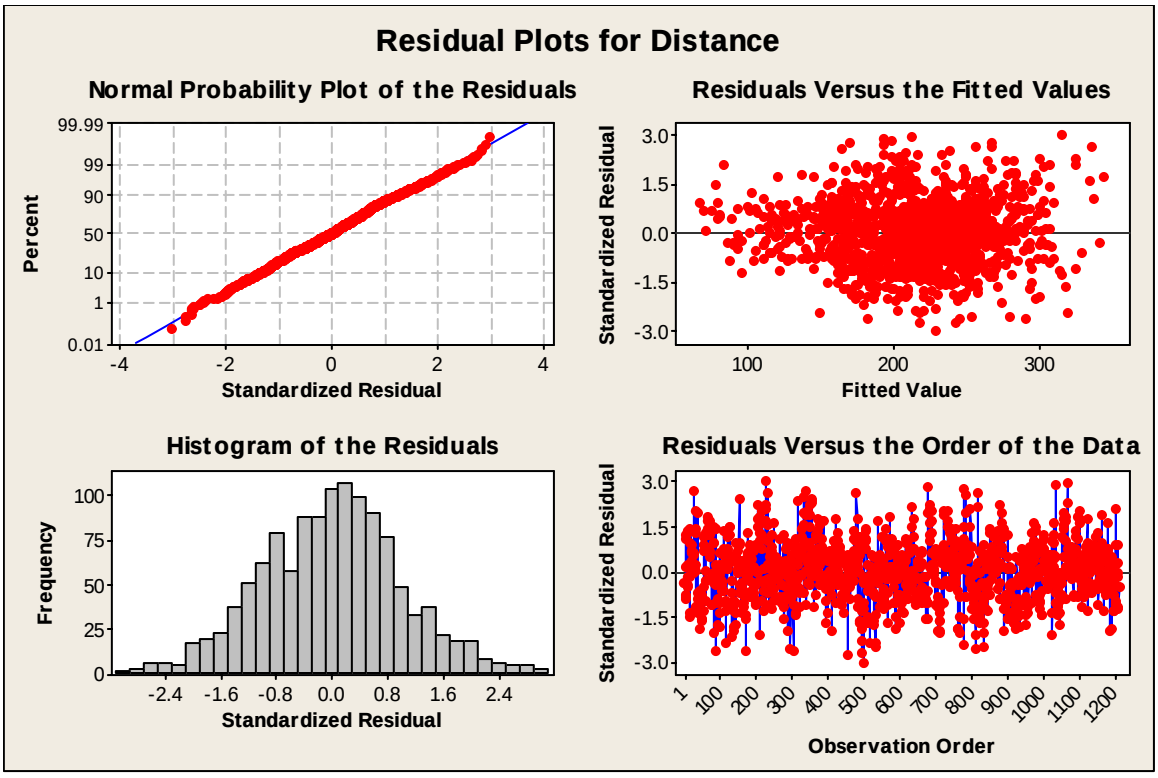

Figure 49. Residuals Plots for Combined Phase I and Phase II Experimental Data.

A preliminary ANOVA model showed that the truck application speed main effect (F [2, 1163] = 0.15, p = 0.85), a phase-speed interaction (F [2, 1163] = 0.5, p = 0.61) and a phase-bead gun angle interaction (F [5, 1163] = 1.65, p = 0.15) were not statistically significant when separate factors for the truck application speed, bead gun angle, and the experimental phase were used as independent variables in the model. The participant ID and bead gun angle main effects were statistically significant (F [35, 1163] = 67.43, p< 0.001 for participant ID, and F [5, 1163] = 34.4, p<0.001 for bead gun angle). A second ANOVA model was run using the research participant ID as a random effect, and fixed effects for the phase and line number ID. The results of this model are provided in Table 2. A phase-line number interaction was also included in the model to determine if weathering the pavement markings had a significant effect on the visibility distance.

Table 10 shows that the experimental phase, participant ID, and the line number (18 levels) were statistically significant (F [1, 1143] = 124.6, p< 0.001 for phase; F [35, 1143] = 68.48, p < 0.001

for participant ID; and, F [17, 1143] = 12.21, $p < 0.001$ for line number). The interaction between phase and line number was not statistically significant (F [17, 1143] = 0.78, p = 0.72). The adjusted R^2 for the model was 68.9 percent. Partial η^2 values for the independent variables and interaction term are also shown in Table 10. The line number ID explains approximately 16 percent of the variability in the fitted model. Based on the combined data analysis results shown in Table 10, it appears that the visibility distance differs among phases, among research participants, and the 18 pavement markings.

Table 10. Analysis of Variance for Combined Phase I and Phase II Experimental Data.

Source	**DF**	**Seq SS**	**Adj SS**	**Adj MS**	**F**	**P**	**Partial η^2**
Phase	1	142257	123314	123314	124.6	<0.001	0.11
Subject ID	35	2363994	2372091	67774	68.48	<0.001	0.68
Line number	17	210320	205461	12086	12.21	<0.001	0.16
Phase*Line number	17	13093	13093	770	0.78	0.72	0.01
Error	1143	1131219	1131219	990			
Total	1213	3860883					
Anderson-Darling test statistic (A) = 0.65, p = 0.08							
$R^2 = 0.689$							

Tukey pairwise comparisons showed that the line numbers corresponding to treatments 8 (15mph/-20 degrees), 13 (12mph/20degrees), 15 (18 mph/20 degrees), 16 (18 mph/40 degrees), 17 (15 mph/40 degrees), and 18 (12 mph/40 degrees) were significantly different from the other treatments, but were not significantly different from each other. The mean visibility distance in Phase I was 224 feet [68.3m], and the mean visibility distance in Phase II was 202 ft [61.6m], indicating that nearly 1 year of weathering did affect the visibility distance. It is again worth noting that the same six pavement marking treatments that provided the longest visibility distances when combining the data from both phases of the nighttime driving experiment, were the same as those when analyzing the data separately for the two phases of the experiment.

5.2 Retoreflectivity

A total of 10 retroreflectivity readings were recorded periodically on each of the 18 pavement markings applied at the Larson Institute test track. All of the recorded data are provided in Appendix B of this report. The mean, standard deviation, and coefficient of variation for each set of retroreflectivity measurements are shown in Table 11, organized by the truck application speed and bead gun angle.

Table 11. Retroreflectivity Data for 18 Experimental Pavement Markings.

Speed (mph)	Angle (degrees)	Baseline (30 days)			Reading #2 (90 days)			Reading #3 (150 days)			Reading #4 (225 days)			Reading #5 (315 days)			Reading #6 (380 days)			Reading #6 (Reverse – 380 days)		
		Mean	SD	CV	Mean	SD	CV	Mean	SD	CV	Mean	SD	CV	Mean	SD	CV	Mean	SD	CV	Mean	SD	CV
18	-60	244	8.7	0.04	295	15.6	0.05	262	32.3	0.12	163	26.5	0.16	204	30.7	0.15	185	11.0	0.06	142	12.6	0.09
15		238	13.5	0.06	271	14.4	0.05	251	13.5	0.05	182	24.5	0.14	213	28.0	0.13	206	21.0	0.10	149	17.8	0.12
12		283	21.1	0.07	320	18.1	0.06	289	35.0	0.12	176	14.1	0.08	218	22.8	0.10	200	31.9	0.16	146	26.3	0.18
18	-40	286	20.4	0.07	304	22.9	0.08	315	19.6	0.06	167	32.5	0.19	210	24.0	0.11	225	27.9	0.12	163	22.0	0.14
15		277	18.9	0.07	292	15.0	0.05	278	17.1	0.06	207	33.5	0.16	233	42.6	0.18	228	30.8	0.13	182	29.4	0.16
12		297	14.5	0.05	311	22.4	0.07	303	20.9	0.07	210	27.9	0.13	250	25.6	0.10	244	26.7	0.11	185	22.0	0.12
18	-20	252	28.7	0.11	274	29.6	0.11	280	19.8	0.07	175	31.6	0.18	217	13.0	0.06	218	12.1	0.06	150	15.1	0.10
15		284	16.3	0.06	299	14.1	0.05	316	18.3	0.06	235	16.6	0.07	248	23.5	0.09	252	15.9	0.06	191	11.0	0.06
12		293	11.1	0.04	315	21.7	0.07	326	15.0	0.05	237	20.7	0.09	272	26.7	0.10	254	28.7	0.11	201	29.3	0.15
18	0	285	18.3	0.06	334	12.2	0.04	319	21.5	0.07	228	15.0	0.07	227	28.5	0.13	230	22.7	0.10	193	34.6	0.18
15		268	17.2	0.06	305	18.5	0.06	283	17.6	0.06	228	27.4	0.12	246	26.5	0.11	221	29.1	0.13	198	33.0	0.17
12		245	16.9	0.07	289	6.1	0.02	268	28.7	0.11	182	20.5	0.11	214	18.2	0.08	215	18.3	0.09	172	21.6	0.13
18	20	279	13.2	0.05	295	21.3	0.07	277	25.1	0.09	241	20.7	0.09	254	28.2	0.11	236	16.6	0.07	175	17.8	0.10
15		268	31.6	0.12	301	33.3	0.11	283	52.9	0.19	209	43.5	0.21	244	26.3	0.11	226	22.2	0.10	176	28.8	0.16
12		267	6.7	0.03	310	7.5	0.02	292	27.4	0.09	200	34.3	0.17	247	42.2	0.17	228	38.4	0.17	206	40.8	0.20
18	40	269	15.8	0.06	289	19.3	0.07	280	25.9	0.09	241	18.2	0.08	243	15.0	0.06	237	32.3	0.14	188	23.8	0.13
15		268	9.9	0.04	301	12.0	0.04	295	19.7	0.07	235	17.4	0.07	250	30.0	0.12	247	20.0	0.08	209	23.9	0.11
12		247	8.7	0.04	275	8.2	0.03	279	12.5	0.04	248	22.7	0.09	257	19.6	0.08	252	42.4	0.17	210	35.9	0.17

Notes:
All baseline retroreflectivity readings were recorded on July 30, 2008
Reading #2 was recorded on October 1, 2008
Reading #3 was recorded on December 3, 2008
Reading #4 was recorded on February 17, 2009
Reading #5 was recorded on May 20, 2009
Reading #6 was recorded on July 16, 2009

The following observations and trends related to pavement marking retroreflectivity are noteworthy:

- Not all experimental pavement markings have retroreflectivity levels that exceed the average minimum level for newly applied markings. The minimum level for white pavement markings is 250 mcd/m^2/lux. The markings applied at a speed/bead gun angle combination of 18 mph/-60 degrees, 15 mph/-60 degrees, 12 mph/0 degrees, and 12 mph/40 degrees all have retroreflectivity levels nominally less than 250 mcd/m^2/lux in the baseline condition. It is worth noting that after a period of 90 days, all of these markings had retroreflectivity levels exceeding 250 mcd/m^2/lux.
- Retroreflectivity levels for all 18 pavement markings increased between 30 and 90 days. The relative percent increase ranged from approximately 5.3 percent (15 mph/-20 degrees) to approximately 20.9 percent (18 mph/-60 degrees).
- Retroreflectivity levels for all 18 pavement markings decreased between 150 and 225 days. The range was approximately -11.1 percent (12 mph/40 degrees) to -47.0 percent (18 mph/-40 degrees). The retroreflectivity decrease between 150 and 225 days occurred during the winter months.
- Retroreflectivity levels for all but one of 18 pavement markings (18 mph/0 degrees) increased between 225 and 315 days. For most of the pavement markings, the increase in retroreflectivity exceeded 15 percent, including a 47 percent increase for the 12 mph/20 degree speed/bead gun angle combination. The increase in retroreflectivity after a period of winter weathering is likely attributable to the pavement markings being "cleaned" by rain and melting snow.
- After 1 year of bus wear and weathering, the retroreflectivity levels remained above 200 mcd/m2/lux, except for the 18 mph/-60 degree speed/bead gun angle combination, which was 185 mcd/m^2/lux.
- Retroreflectivity levels were higher when taking readings in the direction of the pavement marking application after a period of 1 year (reading #6) when compared to retroreflectivity levels measured opposite the direction of application (reverse reading #6). This difference ranged from approximately 9.6 percent (12 mph/20 degrees) to approximately 31.2 percent (18 mph/-20 degrees).

The baseline and reading #6 retroreflectivity levels are included in Table 12, along with the percent retroreflectivity loss over the 1-year period. Additionally, the mean retroreflectivity level for each speed/bead gun angle combination was computed, irrespective of the age, and is shown in Table 12. Finally, the mean retroreflectivity level across all bead gun angles, irrespective of the speed, was computed and is also shown in Table 12.

Table 12. Retroreflectivity Loss and Other Performance Metrics.

Speed (mph)	Angle (degrees)	Baseline Mean (30 days) (mcd/m^2/lux)	Reading #6 Mean (380 days) (mcd/m^2/lux)	Percent Loss in Retroreflectivity (%)	Mean Retroreflectivity Across Rows from Table 11 (mcd/m^2/lux)	Mean Retroreflectivity for Each Bead Gun Angle (mcd/m^2/lux)
18	-60	244	185	24.2	225.5	233.3
15		238	206	13.4	226.8	
12		283	200	29.3	247.7	
18	-40	286	225	21.3	251.2	257.8
15		277	228	17.7	252.5	
12		297	244	17.8	269.2	
18	-20	252	218	13.5	236	263.7
15		284	252	11.3	272.3	
12		293	254	13.3	282.8	
18	0	285	230	19.3	270.5	254.8
15		268	221	17.5	258.5	
12		245	215	12.2	235.5	
18	20	279	236	15.4	263.7	258.7
15		268	226	15.7	255.2	
12		267	228	14.6	257.3	
18	40	269	237	11.9	259.8	261.8
15		268	247	7.8	266.0	
12		247	252	-2.0	259.7	

Note: The shaded cells in Table 12 represent the maximum within each speed/bead gun angle combination.

Noteworthy observations from Table 12 are as follows:

- When the bead gun angle is pointed opposite the direction of travel (i.e., -20, -40, and -60 degrees), the 12-mph truck speed provides the highest level of initial retroreflectivity in all cases, and the highest level of retroreflectivity in two of three cases after a period of one year (-20 and -40 degree bead gun angles). These same trends occurred when averaging the retroreflectivity across the entire study period (rows in Table 11).
- When the bead gun angle is pointed vertically or in the direction of travel (i.e., 0, 20, and 40 degrees), the 18-mph truck speed provides the highest level of initial retroreflectivity in all cases, and the highest level of retroreflectivity in two of three cases after a period of 1 year (0 and 20 degrees). These same trends were generally observed when averaging the retroreflectivity across the entire study period (rows in Table 11), except when the bead gun was angled 40 degrees forward.
- The relative percent retroreflectivity loss occurred in the 18-mph speeds in four of the six bead gun angle settings (-40, -20, 0, and 40 degrees). For the -60 degree bead gun angle, the 12-mph speed resulted in the greatest retroreflectivity loss. For the 40 degree bead gun angle case, the 15-mph speed resulting in the greatest retroreflectivity loss.
- There does not appear to be a significant difference between the mean retroreflectivity levels for the -40, -20, 0, 20, and 40 degree bead gun angles. The -60 degree bead gun angle appears to produce retroreflectivity levels that are significantly lower than the other bead gun angles.

- The highest retroreflectivity levels, averaged over the entire study period, occurred for the 12 mph/-20 degree, 18 mph/0 degree, and 12 mph/-40 degree speed/bead gun angle combinations.
- Although not shown in Table 12, the average retroreflectivity, average over each bead gun angle for the entire study period, was 258.7, 255.2, and 251.1 for the 12-mph, 15-mph, and 18-mph truck application speeds, respectively.

5.3 Summary of Field Evaluation Studies

The field evaluation studies conducted in the present experiment were designed to evaluate the performance of the pavement markings over time based on quantifiable visibility metrics (i.e., retroreflectivity and end detection distance). Retroreflectivity measurements were recorded using a handheld retoreflectometer while the end detection or visibility distance was measured in a nighttime driving experiment. In the nighttime driving experiment, the 15 mph/-20 degree, 12 mph/20 degree, 18 mph/20 degree, 12 mph/40 degree, 15 mph/40 degree, and 18 mph/40 degree truck application speed/bead gun angles provided the longest nighttime visibility distances. This finding was consistent when considering the Phase I and Phase II data separately or collectively. From the human factors experiment, it appears that drivers can detect the end of the pavement marking at longer distances when the bead gun is pointed forward (in the direction of travel) as opposed to a vertical or backward-facing bead gun angle, while varying the truck application speed does not appear to offer similar advantages.

The highest retroreflectivity levels, when averaged over the entire study period, were observed for the 12 mph/-40 degree, 12 mph/-20 degree, 15 mph/-20 degree, 18 mph/0 degree, 18 mph/20 degree, and 15 mph/40 degree truck application speed/bead gun angle combinations. While three of these speed/bead gun angle combinations corroborate with the visibility distance findings (15 mph/-20 degrees, 18 mph/20 degrees, and 15 mph/40 degrees), the retroreflectivity measurements appear to generally suggest that when the bead gun angle is pointed opposite the direction of application, better retroreflectivity can be obtained by painting at slower speeds. When the bead gun angle is vertical (perpendicular to the pavement surface) or pointed in the same direction as the application, it appears that higher retroreflectivity levels can be obtained by painting at faster speeds. The notable exception to this is for the 40 degree bead gun angle, where the retroreflectivity levels were nearly unchanged over the entire study period for all truck application speeds.

CHAPTER 6. PUTTING IT ALL TOGETHER

The primary purpose of this chapter is to determine the optimal truck application speed and bead gun angle that produces the greatest nighttime visibility for drivers in Pennsylvania. Provided that pavement marking retroreflectivity is the principal means of assessing nighttime visibility of pavement markings, the discussion and analyses presented in this chapter of the report focus on developing correlations between the various performance metrics computed in the present study and retoreflectivity. Prior to doing so, however, an assessment of the optimal truck speed application/bead gun angle is made based on the results of the laboratory and field evaluations described in Chapters 4 and 5 of this report.

6.1 Assessment of Optimal Speed/Bead Gun Angle based on Laboratory and Field Evaluations

The following performance metrics were used to assess the effects of varying truck application speeds and bead gun angles on pavement marking visibility:

- Relative impact angle of the glass beads and the true bead speed in the high-speed video imagery analysis of the 18 experimental pavement markings at the Larson Institute test track. It was assumed that a low-speed, vertical drop was related to better nighttime visibility of the pavement markings.
- Two-dimensional image processing was used to evaluate bead coverage on the sample test plates. Two sets of 18-sample test plates were created at the test track, each set representing the 18 different speed/bead gun angle combinations. The first set of sample test plates was used in accelerated-wear testing. The second set of sample test plates was used to evaluate the effects of weathering on the pavement markings. It was hypothesized that higher proportions of the waterborne paint covered in glass beads would result in better visibility.
- A scanning electron microscope was used to evaluate the surface morphology of the sample test plates. In the accelerated-wear test, it was assumed that less glass bead surface damage would result in better pavement marking visibility. It was also assumed that a greater and more uniform rind around the glass beads in the waterborne paint would lead to improved bonding between the beads and the paint, resulting in more durable pavement markings. In the weathering evaluation, it was assumed that less flaking of the paint around the glass beads would relate to lower probabilities of bead "pop-out," subsequently resulting in higher levels of pavement marking visibility over time.
- Bead embedment was computed for the baseline, weathered, and accelerated-wear conditions based on the size distribution of as-received glass beads and the size distribution of glass beads in the digital image-processing results. It was assumed for the purpose of this study that the optimal embedment was 60 to 65 percent.
- Pavement marking end detection distance was measured in a nighttime driving experiment on the 18 markings applied at the test track. Longer end detection distances were assumed to provide improved nighttime visibility of the pavement markings.

The high-speed video imagery analysis revealed that the 40 degree bead gun angle provided the lowest bead speed and a near vertical impact angle in the 12- and 15-mph truck speed application tests. In the 18-mph truck application speed tests, the 0 and 20 degree bead gun angles provided the lowest bead speed and most vertical bead impact angle, respectively. The optimal combination appeared to occur in the 15 mph/40 degree speed/bead gun angle combination.

Based on the accelerated-wear laboratory evaluations, the following assessments can be made:

- The 12-mph truck speed and -20 degree bead gun angle provided the greatest bead coverage in the baseline condition, and also provided a high-level of bead coverage relative to other truck speed/bead gun angle combinations after applying 1.2 million traffic loading cycles. However, the 15-mph speed and 0 degree bead gun provided the highest level of bead coverage after 1.2 million cycles. As such, it appears from a subjective assessment of the bead coverage analysis that a 12-mph speed and -20 degree bead gun angle produce maximum bead coverage for newly applied pavement markings, but a 15-mph speed and 0 degree bead gun angle provide better long-term bead coverage when the pavement markings are exposed to accelerated trafficking.
- The SEM surface morphology analysis indicated that bead loss was rarely observed after applying 1.2 million cycles using the MMLS3. However, accelerated trafficking did produce significant surface distress on the beads after 1.2 million loading cycles. Surface distress was observed frequently for all truck speed/bead angle combinations.
- A "rind" or "trench" around the glass beads was commonly observed in the 18-mph truck speed samples. This "trench" grew in size as the number of MMLS3 loadings increased. The "trench" around the glass bead can lead to an increased probability of bead loss in the waterborne paint, and subsequent loss of visibility over time.

Based on the weathering evaluations, the following assessments can be made:

- The 12-mph truck speed and -20 degree bead gun angle provided the greatest bead coverage in the baseline condition, and after a 1-year weathering period. It should be noted, however, that the 15-mph speed and 0 degree bead gun angle combination did produce similar bead coverage levels in the baseline and after 1 year of weathering. The percentage of bead loss over a 1-year period was lower for the 15 mph/0 degree truck speed/bead gun angle combination when compared to the 12 mph/-20 degree truck speed/bead gun angle combination.
- The weathering process appears to contribute to the loss of water-soluble components in the waterborne traffic paint. Although this effect does not appear to be more strongly correlated with any particular truck application speed or bead gun angle combination, it does indicate that 1 year of weathering may increase the probability of bead loss in the waterborne paint.

An approximate 55 percent embedment was attained in the baseline condition when aggregated across all truck speed/bead gun angle combinations. Little variability in embedment existed among the various bead gun angles. After applying 1.2 million accelerated traffic loads to the sample specimens, the embedment was reduced to approximately 48 percent, suggesting that traffic does increase the probability of bead loss. After 1 year of weathering, the embedment was

approximately 43 percent, suggesting that ultraviolet rays, freeze/thaw cycles, and other weather effects increase the probability of bead loss. Higher truck application speeds generally resulted in greater embedment levels.

The accelerated-wear and weathering evaluations appear to favor slower truck application speeds (12 or 15 mph) and vertical (0 degrees) or slightly backward-facing bead gun angles (-20 degrees). This finding was not validated in the nighttime driving experiment. In both the first and second phases of the nighttime driving experiment, the statistical analysis of end detection distance indicates that the following truck application speed/bead gun angle combinations provide the greatest visibility distance: 15 mph/-20 degrees, 12 mph/20 degrees, 18 mph/20 degrees, 12 mph/40 degrees, 15 mph/40 degrees, and 18 mph/40 degrees. This visibility analysis suggests that forward-facing bead gun angles (20 or 40 degrees) produce the greatest pavement marking end detection distance; however, no truck application speed effects were found.

The retroreflectivity data collected on the 18 experimental pavement markings did generally validate the accelerated wear and weathering laboratory evaluations. When aggregated over the 1-year data collection period, the 12-mph truck application speed and -20 degree bead gun angle produced the highest retroreflectivity levels.

Collectively, the laboratory and field evaluations generally appear to converge on a 12-mph truck application and -20 degree bead gun angle as the combination offering the most favorable nighttime visibility in the present study. The combination produced a high-level of initial retroreflectivity as well as high retroreflectivity levels 1 year after application. This same truck speed/bead gun angle combination provided nighttime end detection distances that were only 5 to 8 percent lower than the maximum end detection distances measured in the nighttime driving experiment. The digital image processing analysis validated that the 12 mph/-20 degree truck speed/bead gun angle combination produced the greatest bead coverage on the sample test plates in the baseline condition and after 1 year of weathering. After applying 1.2 million MMLS3 cycles, the digital image processing results showed that maximum bead coverage occurred in the 15 mph/0 degree truck speed/bead gun angle combination; however, the bead coverage for the 12 mph/-20 degree truck speed/bead gun angle combination was only 6 percent lower. Table 13 ranks each truck speed/bead gun angle combination for each laboratory and field evaluation, and sums the ratings across each row. The lowest aggregate rating is the speed/bead gun angle combination that provides the best pavement marking visibility in the present study. Based on the relative ranking, the 12 mph/-20 degree bead gun angle has the lowest composite score, suggesting this speed/bead gun angle performed the best across all laboratory and field evaluations. The 15 mph/-20 degree speed/bead gun angle produced the next best relative ranking, followed by the 12 mph/20 degree, 12 mph/40 degree, and 15 mph/20 degree truck speed/bead gun angle combinations. The highest relative ranks occurred in the 18 mph/-60 degree, 12 mph/-60 degree, and 18 mph/-40 degree truck speed/bead gun angle combinations.

Table 13. Composite Rating of Speed/Bead Gun Angle Combinations.

Speed (mph)	Angle (degrees)	Visibility Distance (feet)		Retroreflectivity		Bead Coverage			Embedment			Impact Angle	Bead Speed	Sum	Rank*
		Phase I	Phase II	Baseline	One year	Baseline	Wear	Weathering	Baseline	Wear	Weathering				
18	-60	18	18	17	18	17	17	16	1	1	1	17	17	158	18
15		13	14	18	16	8	3	12	2	3	2	16	16	123	15
12		16	13	6	17	13	15	7	3	2	3	18	15	128	17
18	-40	15	15	3	12	18	18	18	1	1	1	14	11	127	16
15		14	17	8	9	5	6	6	2	3	2	11	5	88	9
12		17	16	1	5	10	7	4	3	2	3	12	10	90	11
18	-20	11	12	14	14	15	11	13	1	1	1	13	12	118	14
15		2	4	5	2	2	4	3	2	3	2	15	14	58	2
12		7	9	2	1	1	5	1	3	2	3	10	4	48	1
18	0	8	8	4	8	9	13	14	1	1	1	8	9	84	8
15		10	11	10	13	4	1	2	2	3	2	7	6	71	6
12		12	10	16	15	3	2	11	3	2	3	9	7	93	13
18	20	5	3	7	7	14	12	15	1	1	1	4	18	88	9
15		9	7	10	11	11	5	8	2	3	2	5	8	81	7
12		1	2	13	9	6	14	5	3	2	3	3	3	64	3
18	40	3	1	9	6	16	16	17	1	1	1	6	13	90	11
15		6	5	10	4	12	8	10	2	3	2	1	1	64	3
12		4	6	15	2	7	9	9	3	2	3	2	2	64	3

* Rank is a relative measure based on the summation of the ranks across each row.

6.2 Statistical Correlations between Experimental Measures

This section of the report explores the statistical correlation between the various quantitative measures collected in the laboratory and field evaluations. The Pearson correlation coefficient was used to determine the correlation, and is computed as follows (Gujarati, 2003):

$$r = \frac{\sum x_i y_i}{\sqrt{\left(\sum x_i^2\right)\left(\sum y_i^2\right)}} \quad (2)$$

where: r = coefficient of correlation;

$x_i = (X_i - \overline{X})$ = deviation of observed value from sample 1 from mean value of sample 1;

$y_i = (Y_i - \overline{Y})$ = deviation of observed value from sample 2 from mean value of sample 2;

The coefficient of correlation measures the linear association between two variables. Scatter plots for the pairs of data collected and computed in the present study were generally linear. The coefficient of correlation (r) can be either negative or positive and ranges from -1 to +1. A positive value of r indicates that the association is positive (i.e., a change in one variable is associated with a positive change or increase in the other variable). Values near zero do not necessarily imply that there is no association between two variables; rather, it could suggest that the association is nonlinear. The linear correlations for each of the variables that were collected or computed in the present study are shown in Table 14.

Based on the results shown in Table 14, the following variable pairs were correlated in the present study:

- Truck speed and bead coverage: All bead coverage measures were negatively correlated with the truck speed, indicating that as the truck application speed increases, the bead coverage increases. In the baseline and weathered bead coverage evaluations, the 12 mph truck application speed provided the greatest bead coverage percentage, irrespective of the bead gun angle, while the 18 mph truck application speed provided the lowest bead coverage. In the wear study, the 15 mph truck application speed provided the greatest bead coverage, followed by the 12 mph truck application speed. In all bead coverage analyses, the 18 mph truck application speed provided the lowest level of bead coverage.
- Bead gun angle and retroreflectivity: Each of the retroreflectivity measurements included in the correlation analysis (baseline condition, measurement after 1 year of wear and weathering, and the aggregate retroreflectivity over a 1-year period) was positively correlated with bead gun angle. This suggests that increasing the bead gun angle is associated with an increase in retroreflectivity. In the case of bead gun angle and retroreflectivity, however, there is a non-linear relationship as shown in Figure 50. In Figure 50, a polynomial curve is fit to the data and shows that the highest level of retroreflectivity occurs when the bead gun angle is between 0 and 20 degrees.
- Bead gun angle and detection distance: Both the phase I (baseline) and phase II (1-year) end detection distances are positively associated with the bead gun angle. As the bead gun angle increases, the end detection distance increases.

- Retroreflectivity and detection distance: All retroreflectivity measures are positively correlated with all end detection distances, indicating that as the retroreflectivity increases the end detection distance increases. When considering all of the retroreflectivity data collected in the present study as well as all of the end detection distances for each phase of the nighttime driving experiment, the relationship between these variables follows a logarithmic function as shown in Figure 51. In Figure 51, the relationship between retroreflectivity and end detection distance (visibility) is flat in the right-hand portion of the graphic. These data were collected during phase I of the nighttime driving experiment when the retroreflectivity levels were relatively high (range of 270 to 320 mcd/m^2/lux). The left-hand portion of the figure is more linear and corresponds to data collected during phase II of the nighttime driving experiment when the range in retroreflectivity was between 204 and 272 mcd/m^2/lux. This finding suggests that there may be a threshold value of retroreflectivity, given PennDOT's current pavement marking specifications, which does not produce significantly different pavement marking retroreflectivity levels.
- Aggregate retroreflectivity and baseline bead coverage: The aggregate retroreflectivity was computed for each truck application speed/bead gun angle over the entire study period and a positive correlation was found between this measure and the baseline bead coverage. The correlation coefficient was positive and statistically significant, indicating that as the bead coverage increases, the retroreflectivity increases. The highest level of aggregate retroreflectivity and baseline bead coverage was measured for the 12 mph/-20 degree speed/bead gun angle combination.
- Baseline bead coverage and baseline detection distance: A positive correlation exists between the bead coverage and detection distance prior to any significant wear or wreathing of the experimental pavement markings. This indicates that as the bead coverage increases the end detection distance increases. The 12 mph speed and -20 degree bead gun angle combination provided the highest bead coverage in the baseline condition and the 15 mph/-20 degree speed/bead gun angle combination provided the highest end detection distance in the first phase of the driving experiment. The baseline retroreflectivity for the 12 mph/-20 degree and 15 mph/-20 degree speed/bead gun angle combinations were 293 and 284 mcd/m^2/lux, respectively. Similarly, the baseline bead coverage for the 12 mph/-20 degree and 15 mph/-20 degree speed/bead gun angle combinations were 30.68 and 28.91 percent, respectively. For both performance measures, the relative percent difference between these speed/bead gun angle combinations was less than 6 percent.
- As expected, the truck speed and bead gun angles are highly correlated with the bead impact angle and true bead speed. The correlation coefficients are positive in both cases indicating that as the speed or bead gun angle increases, the bead speed and bead impact angles increase.
- The aggregate retroreflectivity was positively correlated with the bead impact angle. This suggests that increasing the bead impact angle increases the pavement marking retroreflectivity. This finding appears to validate the hypothesis that near vertical bead impact angles produce the greatest nighttime visibility as measured using retroreflectivity. This same association was found between the bead impact angle and end detection distance in the nighttime driving experiment, suggesting that 12 and 15 mph truck speeds,

coupled with 40 degree bead gun angles, produce a near vertical bead drop and maximize retroreflectivity and end detection distance.

- The bead coverage after 1 year of weathering was negatively correlated with the true bead speed. Slower bead speeds produce higher levels of bead coverage.
- The bead coverage measures are all negatively correlated with the embedment measures. This suggests that as the bead coverage increases, the embedment decreases. This finding should be interpreted with some care because the range in embedment levels is nominal.
- The true bead speed is positively correlated with the embedment, suggesting that as the bead speed increases, the embedment increases. This finding should be interpreted with some care because the range in embedment levels is nominal.

Table 14. Correlations between Truck Application Speed and Performance Measures.

Pearson Correlation (p-value)	Truck Speed	Bead Gun Angle	Baseline Retro	Retro (One year)	Aggregate Retro	Baseline Detection Distance	Detection Distance (One year)	Baseline Bead Coverage	Wear Bead Coverage	Weathered Bead Coverage	Average Rind Size	Bead Impact Angle	Bead Speed	Initial Embed	Wear Embed
Bead Gun Angle															
Baseline Retro	-0.067 (0.793)	-0.069 (0.785)													
Retro (One year)	-0.230 (0.358)	0.573 (0.013)	0.489 (0.039)												
Aggregate Retro	-0.201 (0.423)	0.435 (0.071)	0.781 (<0.001)	0.859 (<0.001)											
Baseline Detection Distance	-0.026 (0.918)	0.825 (<0.001)	0.128 (0.614)	0.715 (0.001)	0.630 (0.005)										
Detection Distance (One year)	-0.040 (0.875)	0.815 (<0.001)	0.069 (0.785)	0.559 (0.016)	0.492 (0.038)	0.931 (<0.001)									
Baseline Bead Coverage	-0.652 (0.003)	0.165 (0.513)	0.103 (0.684)	0.431 (0.074)	0.417 (0.085)	0.413 (0.088)	0.265 (0.288)								
Wear Bead Coverage	-0.494 (0.037)	0.136 (0.589)	-0.060 (0.812)	0.332 (0.208)	0.225 (0.369)	0.339 (0.168)	0.193 (0.442)	0.875 (<0.001)							
Weathered Bead Coverage	-0.711 (0.001)	0.041 (0.872)	0.124 (0.624)	0.312 (0.208)	0.338 (0.171)	0.241 (0.336)	0.114 (0.652)	0.862 (<0.001)	0.834 (<0.001)						
Average Rind Size	0.394 (0.105)	0.203 (0.420)	0.196 (0.435)	0.242 (0.334)	0.230 (0.358)	0.157 (0.535)	0.088 (0.727)	-0.153 (0.544)	0.009 (0.970)	-0.137 (0.589)					
Bead Impact Angle	-0.024 (0.925)	0.973 (<0.001)	-0.003 (0.991)	0.549 (0.018)	0.461 (0.054)	0.755 (<0.001)	0.734 (0.001)	0.199 (0.429)	0.146 (0.563)	0.053 (0.833)	0.188 (0.455)				
Bead Speed	0.499 (0.035)	-0.366 (0.135)	-0.069 (0.785)	-0.443 (0.066)	-0.327 (0.185)	-0.164 (0.515)	-0.078 (0.758)	-0.388 (0.112)	-0.325 (0.188)	-0.433 (0.073)	-0.279 (0.262)	-0.392 (0.107)			
Baseline Embedment	1.00 (N/A)	0.000 (1.00)	-0.067 (0.793)	-0.230 (0.358)	-0.201 (0.423)	-0.026 (0.918)	-0.040 (0.875)	-0.652 (0.003)	-0.494 (0.037)	-0.711 (0.001)	0.394 (0.105)	-0.024 (0.925)	0.499 (0.035)		
Wear Embedment	0.500 (0.035)	0.000 (1.00)	0.047 (0.853)	-0.182 (0.470)	-0.109 (0.667)	-0.090 (0.723)	0.001 (0.996)	-0.594 (0.009)	-0.713 (0.001)	-0.703 (0.001)	-0.158 (0.532)	-0.003 (0.991)	0.454 (0.059)	0.500 (0.035)	
Weather Embedment	1.00 (N/A)	0.000 (1.00)	-0.067 (0.793)	-0.230 (0.358)	-0.201 (0.423)	-0.026 (0.918)	-0.040 (0.875)	-0.652 (0.003)	-0.494 (0.037)	-0.711 (0.001)	0.394 (0.105)	-0.024 (0.925)	0.499 (0.035)	1.00 (N/A)	0.500 (0.035)
Shaded cells indicate that the correlation coefficient is statistically significant at the 90 percent confidence level.															

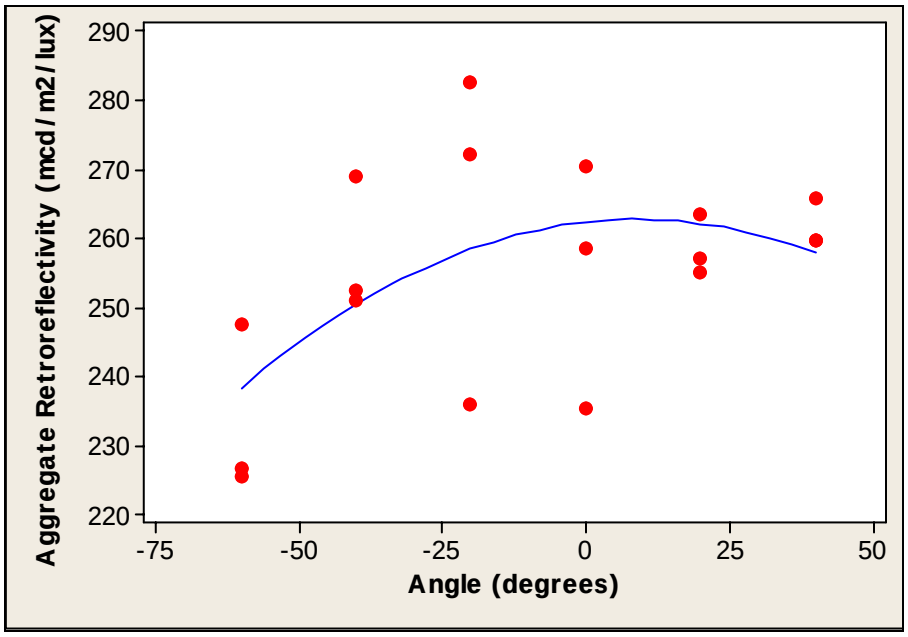

Figure 50. Relationship between Bead Gun Angle and Aggregate Retroreflectivity.

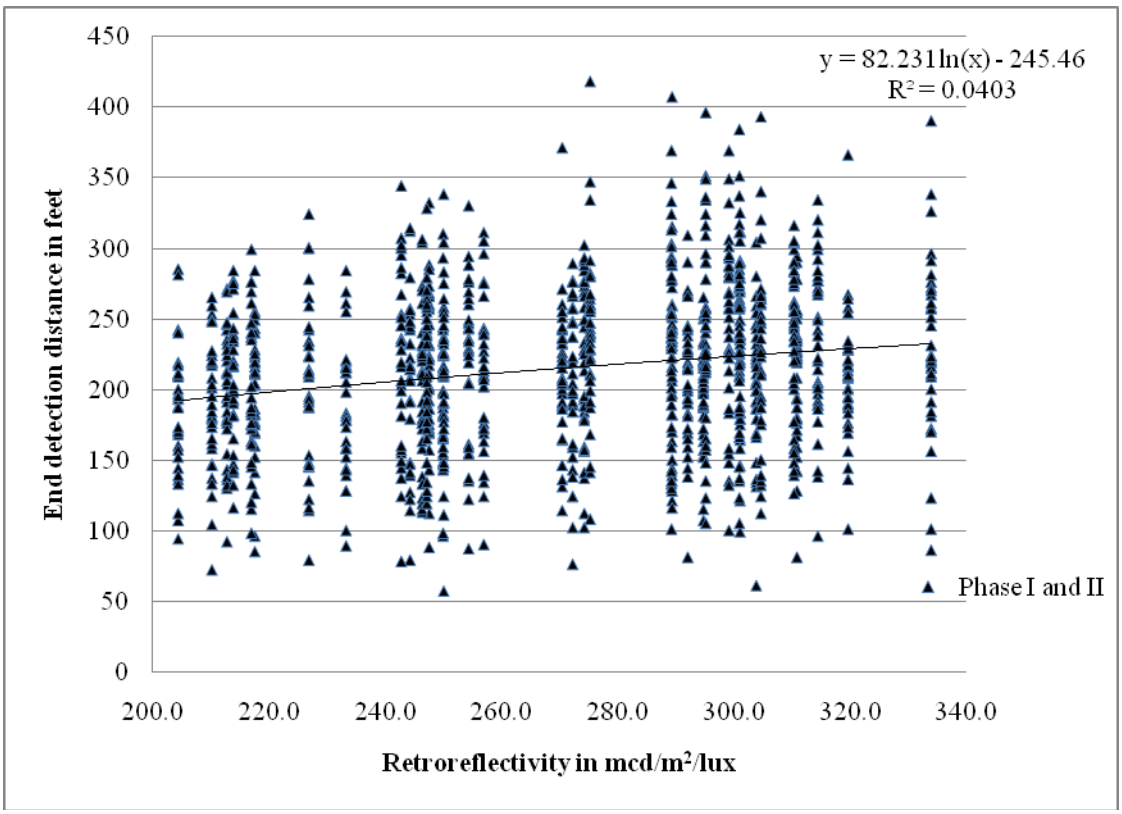

Figure 51. Relationship beteween Retroreflectivity and Visibility.

CHAPTER 7. CONCLUSIONS

The present study was undertaken to determine the optimal truck application speed and bead gun angle combinations that could be used by PennDOT to maximize nighttime visibility of waterborne pavement markings. Based on the laboratory and field experiments, there are several methodological findings of note. First, computing the bead coverage using digital image processing appears to provide a reasonable method to predict retroreflectivity, particularly over a 1-year period. Secondly, the use of high-speed video imagery to compute glass bead kinematics appears to provide a reasonable method to predict retroreflectivity over a 1-year period. Finally, there appears to be a strong correlation between end detection distance measured in a nighttime driving experiment and pavement marking retroreflectivity.

Ranking the relative performance of each bead gun angle/truck application speed across each of the laboratory and field evaluations undertaken in the present study appears to suggest that a 12 mph/-20 degree bead gun angle provides the optimal speed/bead gun angle combination. A 15 mph/-20 degree speed/bead gun angle combination also produces a high relative ranking compared to other speed/bead gun angle combinations. The 18-mph truck application speed, irrespective of the bead gun angle, appeared to produce a near-optimal embedment; however, this speed did not perform favorably relative to the 12- and 15-mph truck application speeds in the laboratory and field evaluations. Although the embedment range was quite narrow in the present study, this finding suggests that embedment does not adequately predict pavement marking performance.

REFERENCES

Aktan, F. and T. Schnell. Performance Evaluation of Pavement Markings Under Dry, Wet, and Rainy Conditions in the Field. *Transportation Research Record: Journal of the Transportation Research Board, No. 1877*, Transportation Research Board of the National Academies, Washington, D. C., 2004, pp. 38-49.

Baker, T. E. and T. Ferragut. *Feasibility Study: European Accelerated Pavement Marking System Testers and Potential Application to American Transportation Programs.* FHWA/AASHTO International Exchange Program, Superior Materials Scan Implementation, January 2005.

Burns, D.M., T. P. Hedblom, and T. W. Miller. Modern Pavement Marking Systems: The Relationship between Optics and Nighttime Visibility. *Transportation Research Record: Journal of the Transportation Research Board, No. 2056*, Transportation Research Board of the National Academies, Washington, D. C., 2008, pp. 43-51.

Choubane, B., S. Gokhale, and J. Fletcher. Feasibility of Accelerated Pavement Testing to Evaluate Long-term Performance of Raised Pavement Markings. *Transportation Research Record: Journal of the Transportation Research Board, No. 1948*, Transportation Research Board of the National Academies, Washington, D. C., 2006, pp. 108-113.

Mizera, C., O. Smadi, N. Hawkins, and W. Zitterich. Pavement Marking Application: A Bead Gun Evaluation Study using a High-speed Camera. Paper No. 09-2450, *Proceedings of the 88th Annual Meeting of the Transportation Research Board*, Washington, DC, January 2009.

Donnell, E. T., G. R. Chehab, X. Tang, and D. Schall. Exploratory Analysis of Accelerated Wear Testing to Evaluate Performance of Pavement Markings. *Transportation Research Record: Journal of the Transportation Research Board*, Transportation Research Board of the National Academies, Washington, DC, 2009 (in press).

Edwards, C. J., S. Binder, T.A. Dingus, R.B. Gibbons, and J.M. Hankey. *Enhanced Night Visibility Series, Vol. VIII: Phase II – Study 6: Detection of Pavement Markings During Nighttime Driving in Clear Weather.* Report No. FHWA-HRT-04-139, Federal Highway Administration, McLean, VA, December 2005.

Ferragut, T., M. Ruiz, and T. Baker. *Accelerated Testing of Traffic Markings Wear Simulator Feasibility Study: Visit to AETEC Wear Simulator Facility, Madrid, Spain.* Draft Report, International Scan Technology Exchange Program, July 2005.

Finley, M.D., P.J. Carlson, N.D. Trout, and D.L. Jasek. *Sign and Pavement Marking Visibility from the Perspective of Commercial Vehicle Drivers.* Report No. FHWA/TX-03/4269-1, Texas Transportation Institute, College Station, TX, 2002, 124 pp.

Gibbons, R.B. and J. Hankey. *Wet Night Visibility of Pavement Markings: Dynamic Experiment.* Transportation Research Record: Journal of the Transportation Research Board, No. 2015, Transportation Research Board of the National Academies, Washington, D. C., 2007, pp. 73-80.

Gibbons, R.B. *Pavement Marking Visibility Requirements during Wet Night Conditions.* Report No. VTRC 07-CR7, Virginia Transportation Research Council, Charlottesville, Virginia, 2006, 61 pp.

Gujarati, D. N. *Basic Econometrics* (4th edition). McGraw-Hill/Irwin, New York, NY, 2003.

Keppler, R. *Tests for Road Marking Systems in Germany*. Federal Highway Research Institute, Bergisch Gladbach, Germany, June 2003.

Kuehl. R. O. *Design of Experiments: Statistical Principles of Research Design and Analysis (2nd edition)*. Duxbury Press, 2000.

Kutner. M. H., C. J. Nachtsheim, J. Neter, and W. Li. *Applied Linear Statistical Models (5th edition)*. McGraw Hill, 2004.

Levine. G, M. C. Page, S. L. Braver, and D. P. MacKinnon. *Levine's Guide to SPSS for Analysis of Variance (2nd edition)*. Lawrence Erlbaum Associates Publishers, 2003.

National Television System Committee. Report and Reports of Panel No. 11, 11-A, and 12-19, Petition for Adoption of Transmission Standards for Color Television. Library of Congress, Washington, DC, 1953.

O'Brien, J. Embedment and Retroreflectivity of Drop-on Glass Spheres in Thermoplastic Markings. *Transportation Research Record: Journal of the Transportation Research Board, No. 1230*, Transportation Research Board of the National Academies, Washington, D. C., 1989, pp. 37-44.

Pennsylvania Department of Transportation. *Highway Construction Specifications: Publication 408*, Harrisburg, PA, 2007.

Rich, M. J., R. E. Maki, and J. Morena. Development of a Pavement Marking Management System: Measurement of Glass Sphere Loading in Retroreflective Pavement Paints. *Transportation Research Record: Journal of the Transportation Research Board, No. 1794*, Transportation Research Board of the National Academies, Washington, D. C., 2002, pp. 49-54.

Zwahlen, H. T. and T. Schnell. Visibility of New Pavement Markings at Night Under Low-Beam Illumination. *Transportation Research Record: Journal of the Transportation Research Board, No. 1495*, Transportation Research Board of the National Academies, Washington, D. C., 1995, pp. 117-127.

Zwahlen, H. T. and T. Schnell. Visibility of New Dashed Yellow and White Center Stripes as Function of Material Retroreflectivity. *Transportation Research Record: Journal of the Transportation Research Board, No. 1553*, Transportation Research Board of the National Academies, Washington, D. C., 1996, pp. 73-80.

Zwahlen, H. T. and T. Schnell. Visibility of New Centerline and Edge Line Pavement Markings. *Transportation Research Record: Journal of the Transportation Research Board, No. 1605*, Transportation Research Board of the National Academies, Washington, D. C., 1997, pp. 49-61.

Zwahlen, H.T. and T. Schnell. Visibility of Road Markings as a Function of Age, Retroreflectivity Under Low-Beam and High-Beam Illumination At Night. *Transportation Research Record: Journal of the Transportation Research Board, No. 1692*, Transportation Research Board of the National Academies, Washington, DC, 1999, pp. 152-163.

APPENDIX A
GLASS BEAD WICKING CALCULATIONS

Table A-1. Glass Bead Wicking Analysis.

Truck Application Speed [mph]	Bead Gun Angle [degrees]	Bead Diameter [μm]	Wicking along Axes				Mean [μm]	'True' Bead Diameter [μm]
			Left [μm]	Top [μm]	Right [μm]	Bottom [μm]		
12	+40	321	14	5	9	16		421
		722	23	23	10	22		946
		171	5	6	4	4		224
		435	34	15	17	22		570
		482	0	15	16	33		631
		642	57	32	21	40		841
		505	20	18	27	16		662
	Mean	*468*	*22*	*16*	*15*	*22*	*19*	*613*
	Std. Dev.	*186*	*19*	*9*	*8*	*12*	*4*	*243*
12	+20	438	8	15	0	0		530
		489	22	15	18	27		592
		476	15	21	6	13		576
		411	9	7	14	0		497
		657	10	38	12	10		795
		607	37	31	15	28		734
		400	24	62	22	15		484
	Mean	*497*	*18*	*27*	*12*	*13*	*18*	*601*
	Std. Dev.	*99*	*11*	*19*	*7*	*11*	*7*	*119*
12	0	293	17	9	14	16		381
		278	4	12	20	16		361
		607	37	31	15	30		789
		400	24	62	22	15		520
		480	17	15	16	10		624
		305	11	10	7	20		397
	Mean	*352*	*17*	*23*	*14*	*17*	*18*	*456*
	Std. Dev.	*163*	*11*	*19*	*6*	*7*	*3*	*214*
12	-20	224	6	10	8	10		267
		319	12	6	5	13		380
		257	5	10	6	6		306
		595	12	18	0	7		708
		591	40	20	13	18		703
		457	14	13	0	28		544
		525	34	30	40	28		625
	Mean	*424*	*18*	*15*	*10*	*16*	*15*	*505*
	Std. Dev.	*157*	*14*	*8*	*14*	*9*	*3*	*186*
12	-40	450	28	11	26	26		594
		500	12	30	15	9		660
		388	7	6	40	13		512
		534	26	15	13	22		705
		387	14	14	7	13		511
		279	20	19	30	25		368
		625	34	67	58	30		825
	Mean	*452*	*20*	*23*	*27*	*20*	*23*	*596*
	Std. Dev.	*113*	*10*	*21*	*18*	*8*	*3*	*150*

Table A-1. Glass Bead Wicking Analysis (con't).

Truck Application Speed [mph]	Bead Gun Angle [degrees]	Bead Diameter [μm]	Wicking along Axes				Mean [μm]	'True' Bead Diameter [μm]
			Left [μm]	Top [μm]	Right [μm]	Bottom [μm]		
12	-60	289	14	6	8	16		379
		418	14	13	16	13		548
		282	16	18	11	15		369
		534	10	9	17	31		700
		557	30	30	25	81		730
		487	29	15	16	14		638
	Mean	*429*	*17*	*15*	*15*	*26*	*18*	*562*
	Std. Dev.	*110*	*9*	*8*	*5*	*25*	*5*	*144*
15	40	372	16	11	6	21		450
		436	53	21	13	32		528
		467	11	29	16	17		565
		569	52	40	17	40		688
		511	13	25	16	11		618
		454	27	32	21	30		549
		328	49	25	40	30		397
	Mean	*448*	*32*	*26*	*18*	*26*	*26*	*542*
	Std. Dev.	*81*	*19*	*9*	*11*	*10*	*5*	*98*
15	20	548	9	25	12	27		652
		256	15	16	6	5		305
		350	14	9	22	23		417
		395	9	24	6	6		470
		464	20	70	30	80		552
		619	34	15	31	30		737
	Mean	*388*	*17*	*24*	*17*	*26*	*21*	*461*
	Std. Dev.	*182*	*9*	*21*	*11*	*26*	*5*	*216*
15	0	450	12	5	5	15		540
		286	9	9	15	32		343
		343	12	10	13	10		412
		418	13	20	13	15		502
		733	70	100	72	130		880
		697	13	16	16	26		836
	Mean	*444*	*20*	*26*	*21*	*36*	*26*	*533*
	Std. Dev.	*205*	*22*	*33*	*23*	*42*	*8*	*247*
15	-20	629	12	38	59	18		818
		583	23	31	17	34		758
		297	6	8	10	5		386
		358	20	19	14	19		465
		559	16	27	19	18		727
		700	30	44	33	31		910
		614	70	48	33	21		798
	Mean	*534*	*25*	*31*	*26*	*21*	*26*	*695*
	Std. Dev.	*149*	*21*	*14*	*17*	*10*	*4*	*194*
15	-40	460	15	13	9	11		603
		363	10	11	6	12		476
		363	20	12	8	12		476
		336	23	10	17	20		440
		619	35	24	28	31		811
		432	55	14	76	43		566
		410	20	10	7	20		537
	Mean	*426*	*25*	*13*	*22*	*21*	*20*	*558*
	Std. Dev.	*96*	*15*	*5*	*25*	*12*	*5*	*125*

Table A-1. Glass Bead Wicking Analysis (con't).

Truck Application Speed [mph]	Bead Gun Angle [degrees]	Bead Diameter [μm]	Wicking along Axes				Mean [μm]	'True' Bead Diameter [μm]
			Left [μm]	Top [μm]	Right [μm]	Bottom [μm]		
15	-60	571	40	19	28	26		679
		457	15	48	13	10		544
		267	23	18	8	11		318
		500	40	40	28	16		595
		350	34	9	5	18		417
		512	12	10	10	24		609
		395	16	10	10	11		470
	Mean	*436*	*26*	*22*	*14.6*	*16.6*	*20*	*519*
	Std. Dev.	*105*	*12*	*16*	*9*	*6*	*5*	*125*
18	40	342	6	29	28	37		458
		490	20	21	20	21		657
		550	25	10	15	17		737
		571	17	13	17	43		765
		583	17	70	53	46		781
		600	18	13	21	30		804
		357	23	21	29	18		478
	Mean	*499*	*18*	*25*	*26*	*30*	*25*	*669*
	Std. Dev.	*108*	*6*	*21*	*13*	*12*	*5*	*145*
18	20	460	14	7	14	13		552
		625	24	21	5	14		750
		500	11	7	38	10		600
		525	31	46	10	12		630
		208	11	7	4	5		249.6
		419	17	7	9	20		502.8
		486	16	18	42	33		583.2
	Mean	*460*	*18*	*16*	*17*	*15*	*17*	*553*
	Std. Dev.	*128*	*7*	*14*	*16*	*9*	*1*	*154*
18	0	505	31	14	12	31		651
		293	14	4	14	13		378
		326	8	28	20	17		421
		565	27	14	16	41		729
		577	71	136	22	19		744
		500	20	22	16	18		645
		400	6	25	10	23		516
	Mean	*452*	*25*	*35*	*16*	*23*	*25*	*583*
	Std. Dev.	*114*	*22*	*45*	*4*	*10*	*8*	*146*
18	-20	429	13	9	15	34		515
		457	11	7	7	7		548
		450	16	23	12	16		540
		420	15	35	51	18		504
		495	13	35	41	20		594
		448	43	31	0	20		538
		548	19	56	21	38		658
	Mean	*464*	*19*	*28*	*21*	*22*	*22*	*557*
	Std. Dev.	*44*	*11*	*17*	*19*	*11*	*4*	*53*

Table A-1. Glass Bead Wicking Analysis (con't).

Truck Application Speed [mph]	Bead Gun Angle [degrees]	Bead Diameter [μm]	Wicking along Axes				Mean [μm]	'True' Bead Diameter [μm]
			Left [μm]	Top [μm]	Right [μm]	Bottom [μm]		
18	-40	362	15	9	10	10		442
		371	8	6	21	17		453
		300	19	16	18	15		366
		450	53	70	31	50		549
		400	5	13	10	17		488
		448	4	10	15	20		547
		488	59	52	34	53		595
	Mean	*403*	*23*	*25*	*20*	*26*	*24*	*491*
	Std. Dev.	*64*	*23*	*25*	*10*	*18*	*3*	*78*
18	-60	317	11	17	6	6		380
		445	20	9	12	20		534
		419	10	18	13	5		503
		314	13	9	11	15		377
		571	7	13	18	15		685
		390	20	36	41	40		468
		639	25	40	32	20		767
	Mean	*442*	*15*	*20*	*19*	*17*	*18*	*531*
	Std. Dev.	*123*	*7*	*13*	*13*	*12*	*2*	*148*

APPENDIX B
EXAMPLE SEM IMAGES FROM ACCELERATED WEAR STUDY

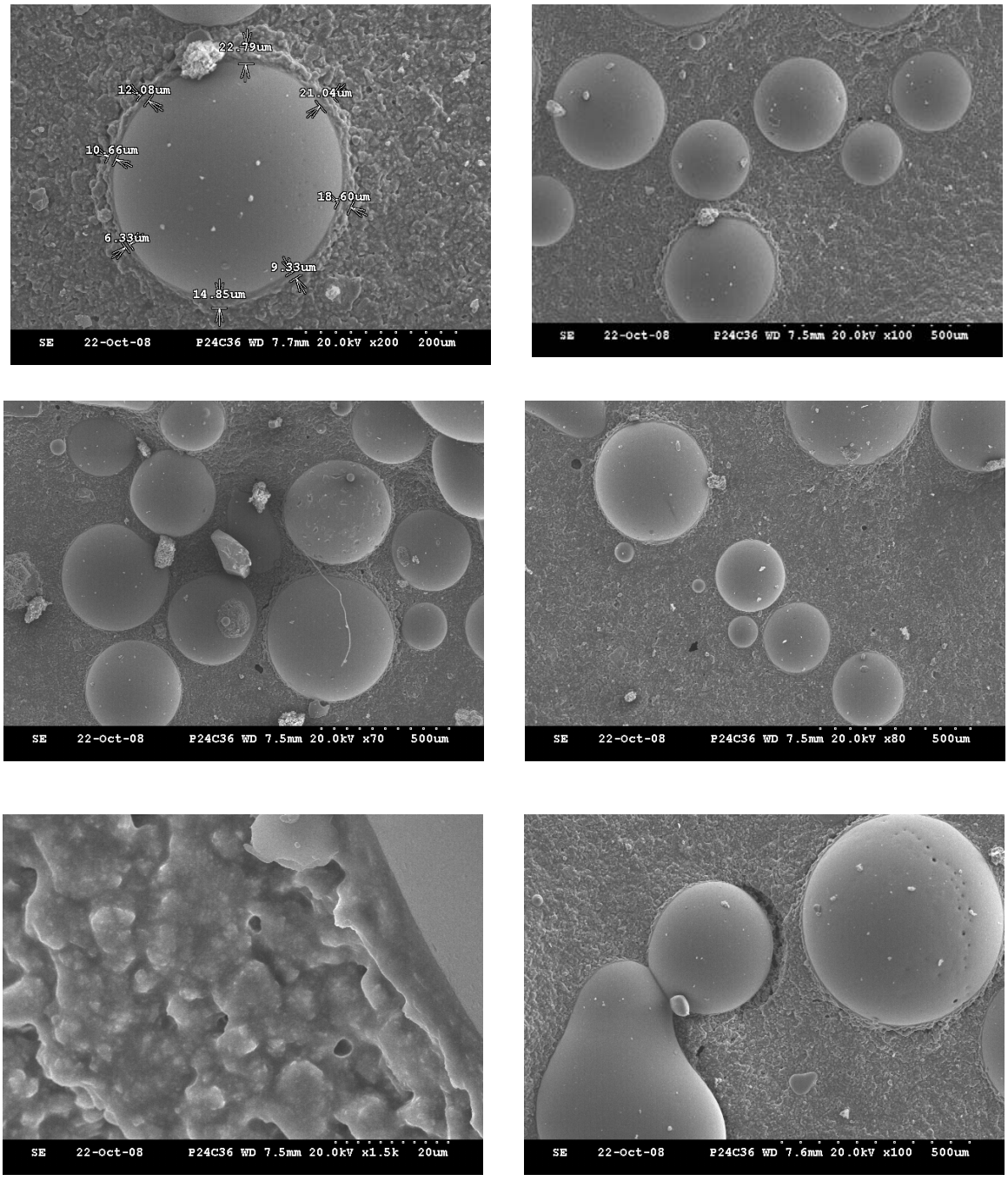

Figure B-1. SEM Images for Baseline Condition.
(Note: Truck Application Speed is 18 mph and Bead Gun Angle is -40 degrees)

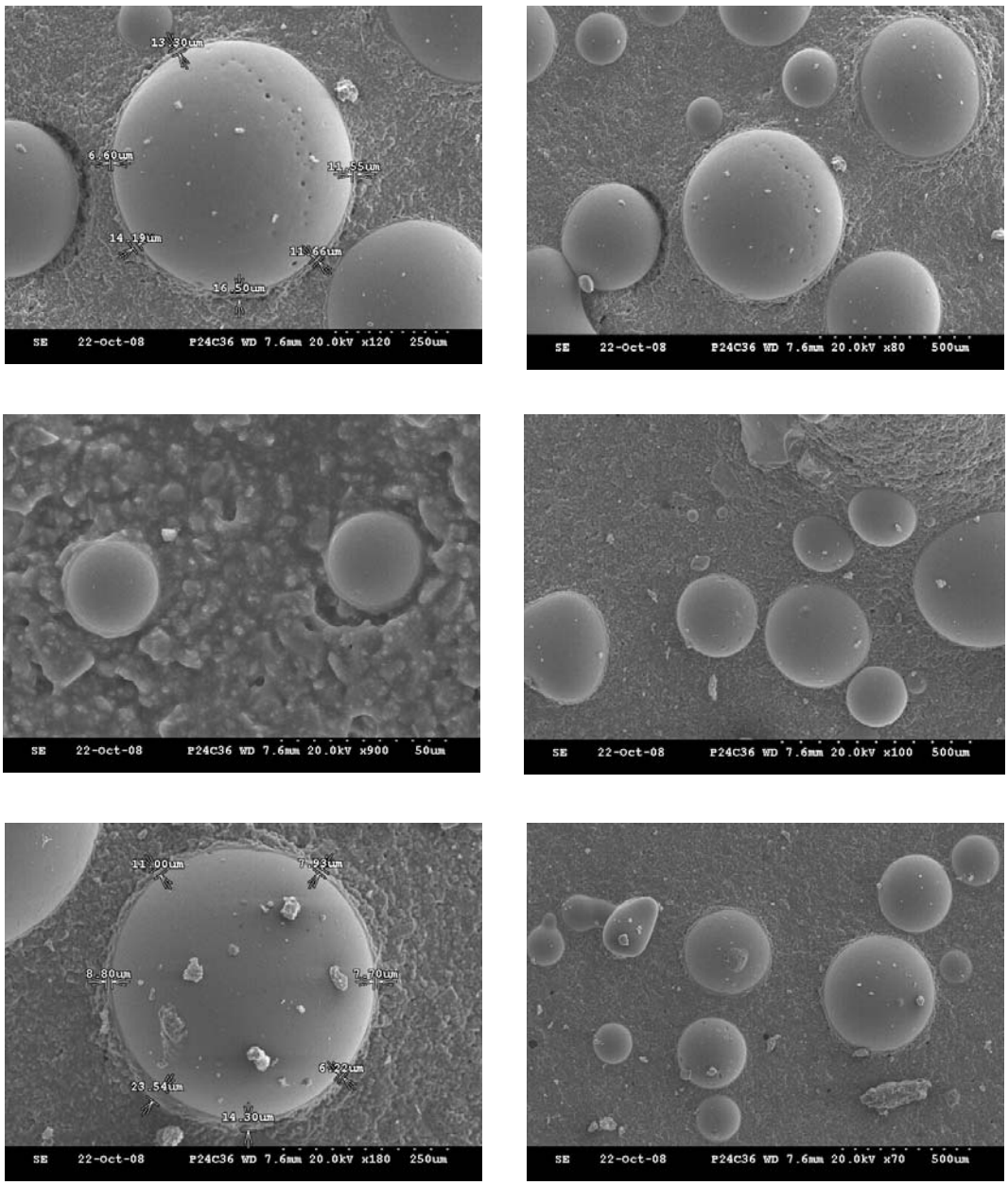

Figure B-1. SEM Images for Baseline Condition (con't).
(Note: Truck Application Speed is 18 mph and Bead Gun Angle is -40 degrees)

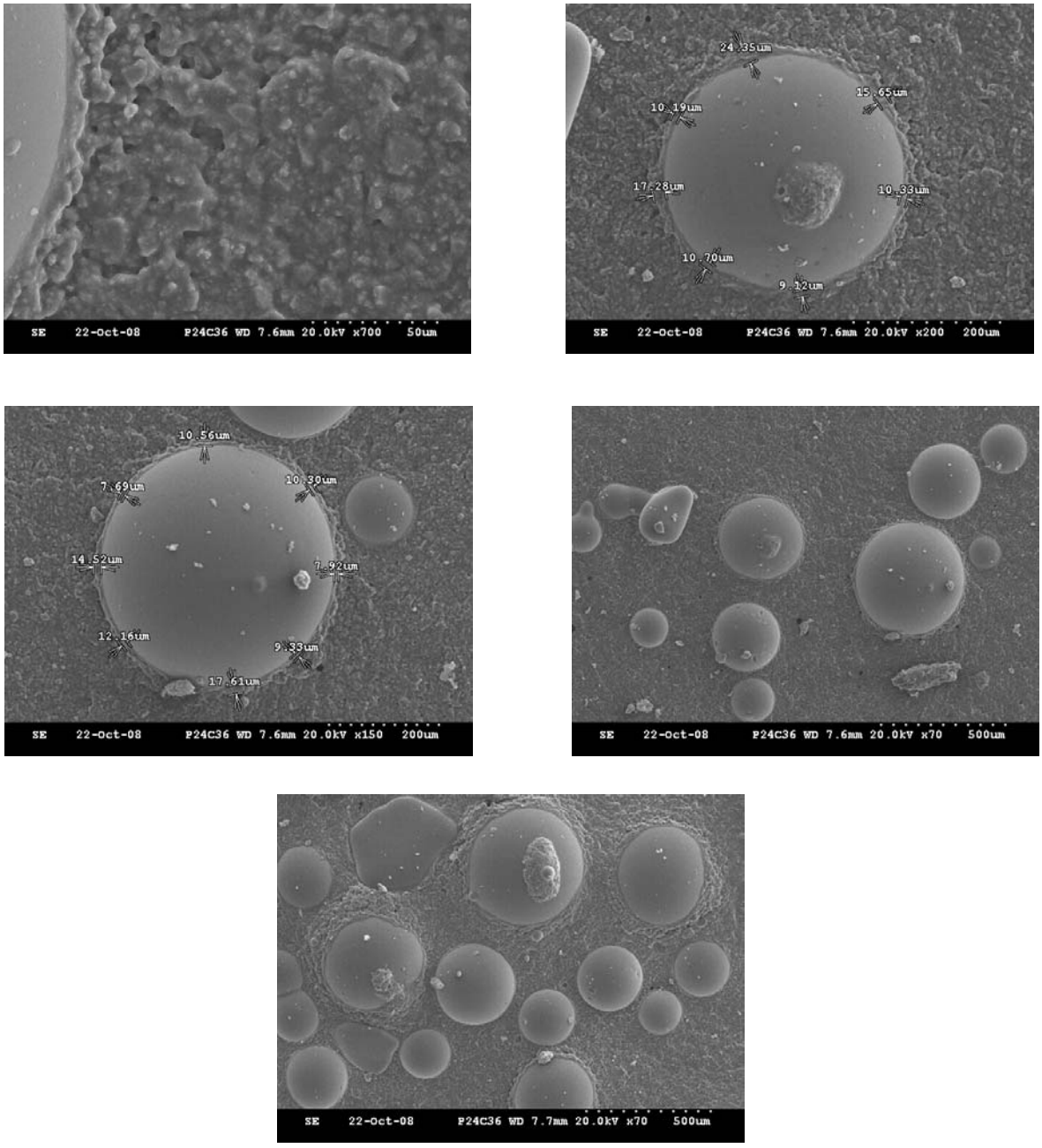

Figure B-1. SEM Images for Baseline Condition (con't).
(Note: Truck Application Speed is 18 mph and Bead Gun Angle is -40 degrees)

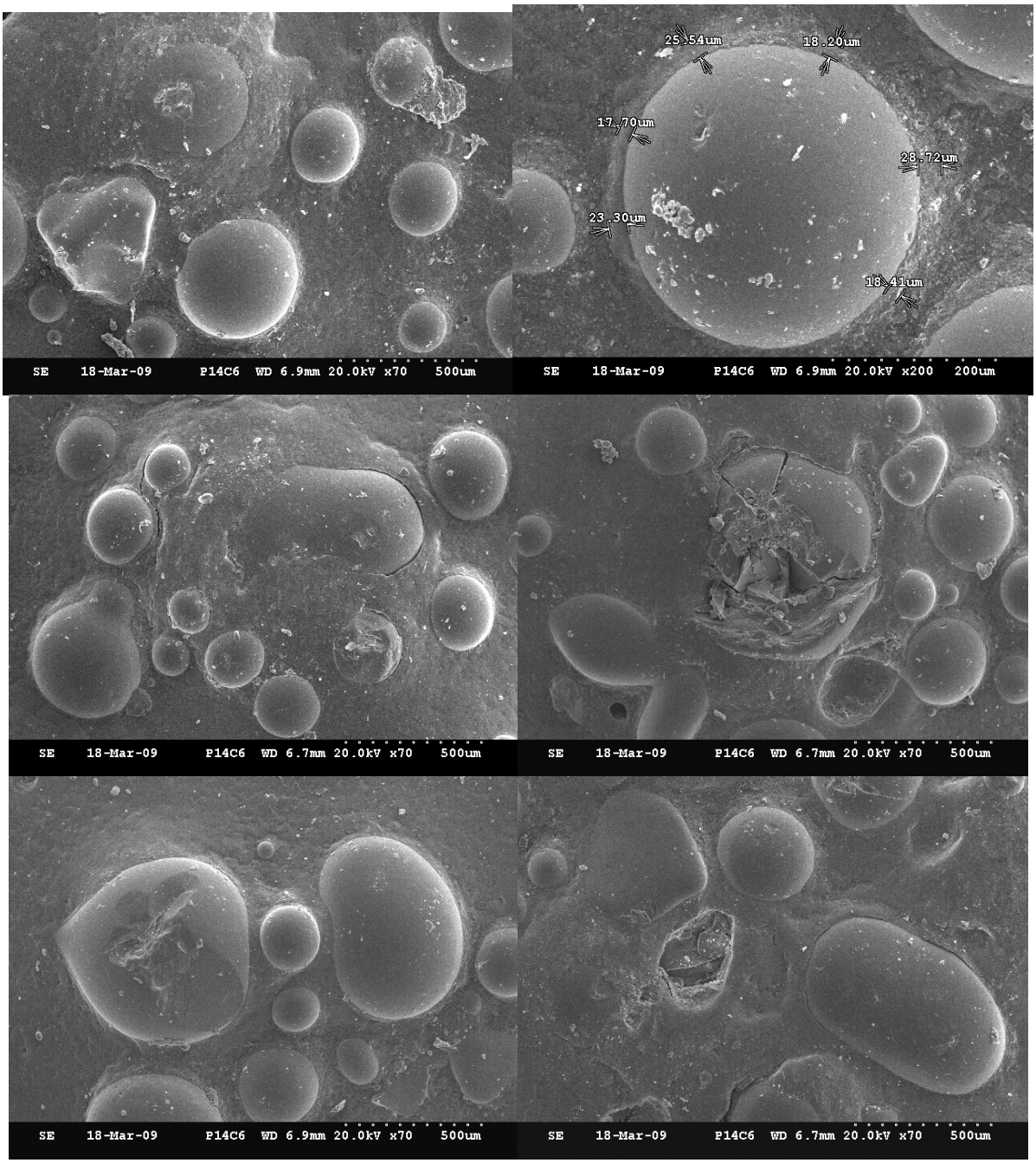

Figure B-2. SEM Images after 1.2 million MMLS3 Cycles.
(Note: Truck Application Speed is 18 mph and Bead Gun Angle is -40 degrees)

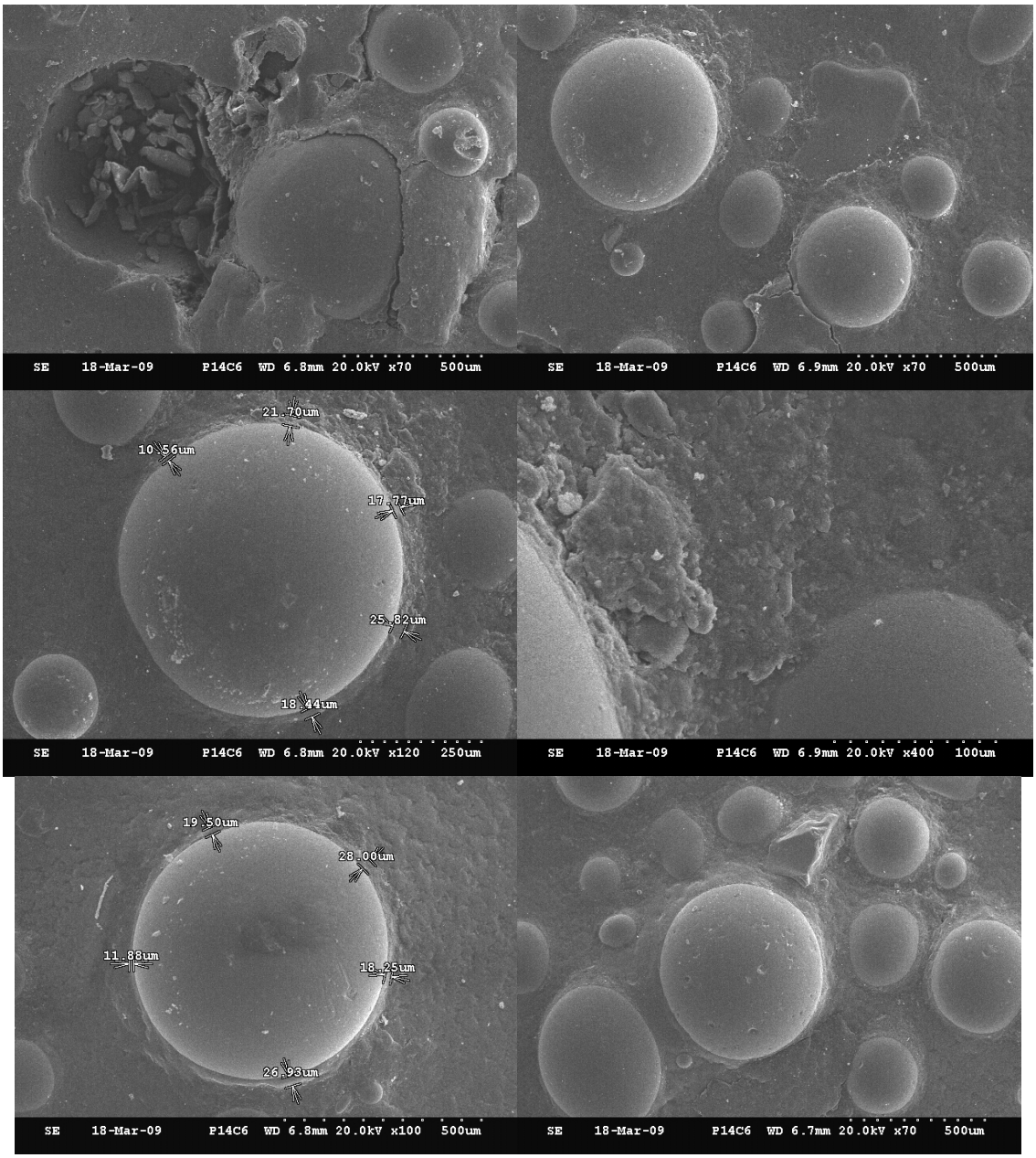

Figure B-2. SEM Images after 1.2 million MMLS3 Cycles (con't).
(Note: Truck Application Speed is 18 mph and Bead Gun Angle is -40 degrees)

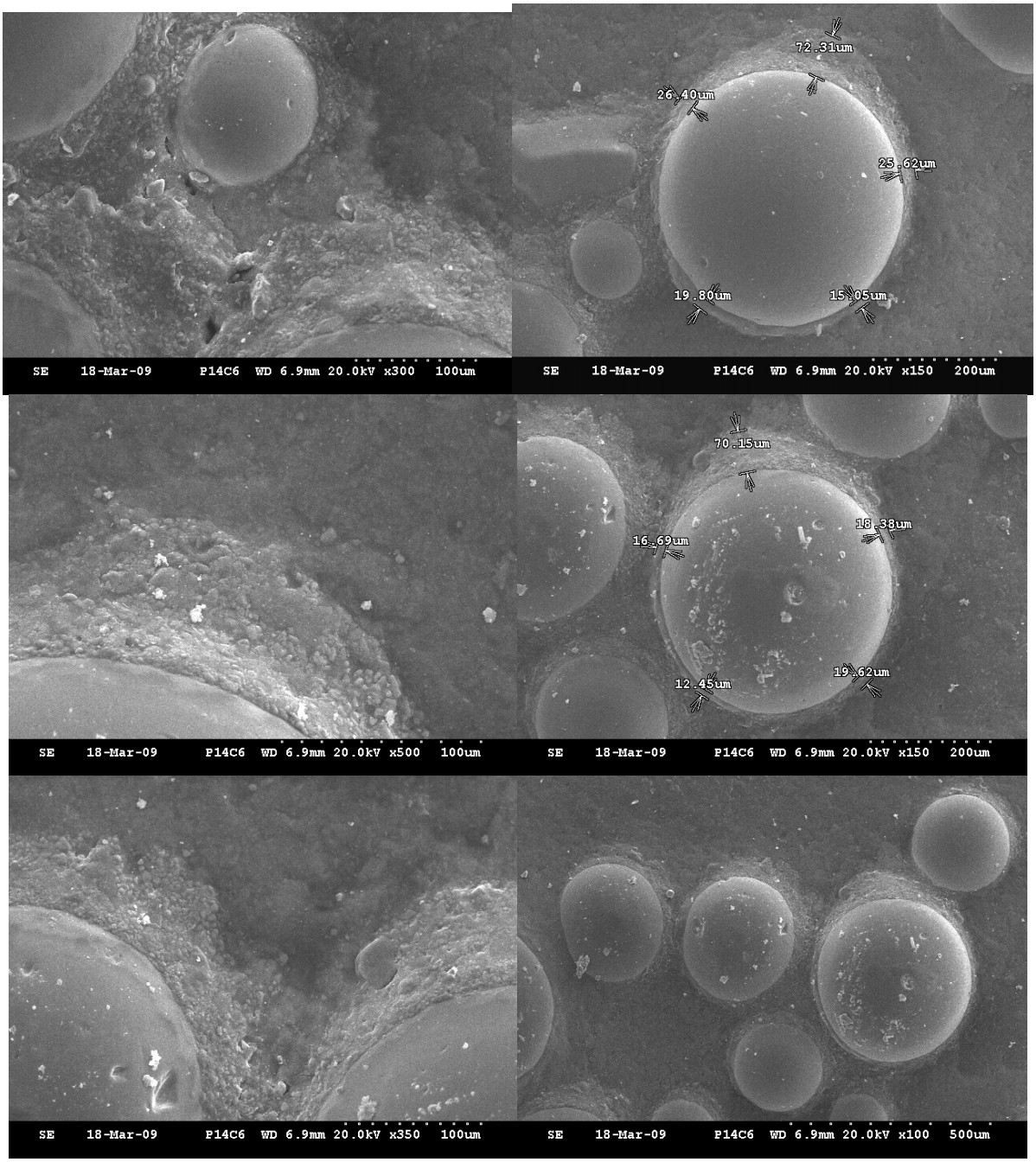

Figure B-2. SEM Images after 1.2 million MMLS3 Cycles (con't).
(Note: Truck Application Speed is 18 mph and Bead Gun Angle is -40 degrees)

APPENDIX C
EXAMPLE SEM IMAGES FROM WEATHERING STUDY

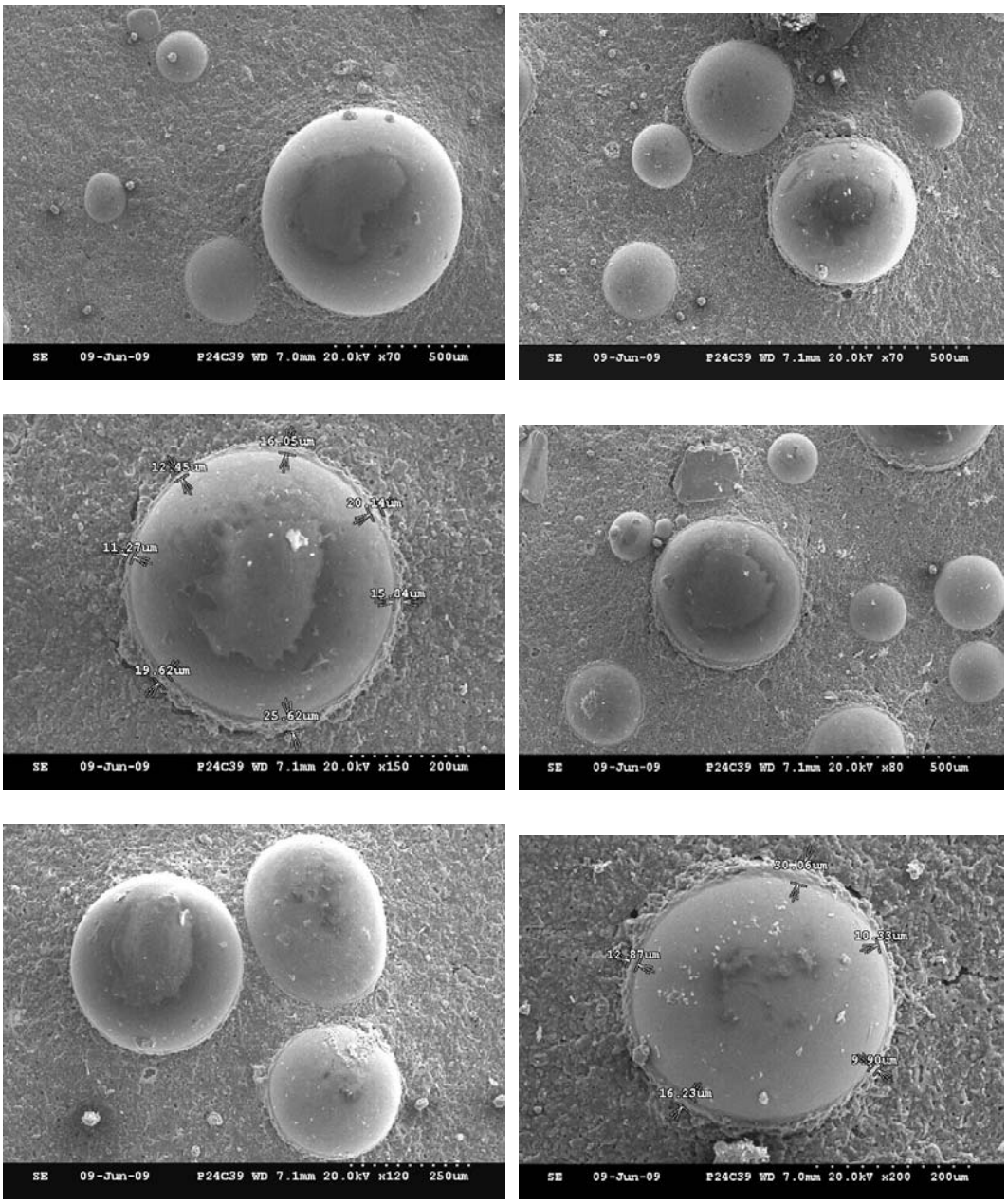

Figure C-1. SEM Images after One Year of Weathering.
(Note: Truck Application Speed is 18 mph and Bead Gun Angle is -40 degrees)

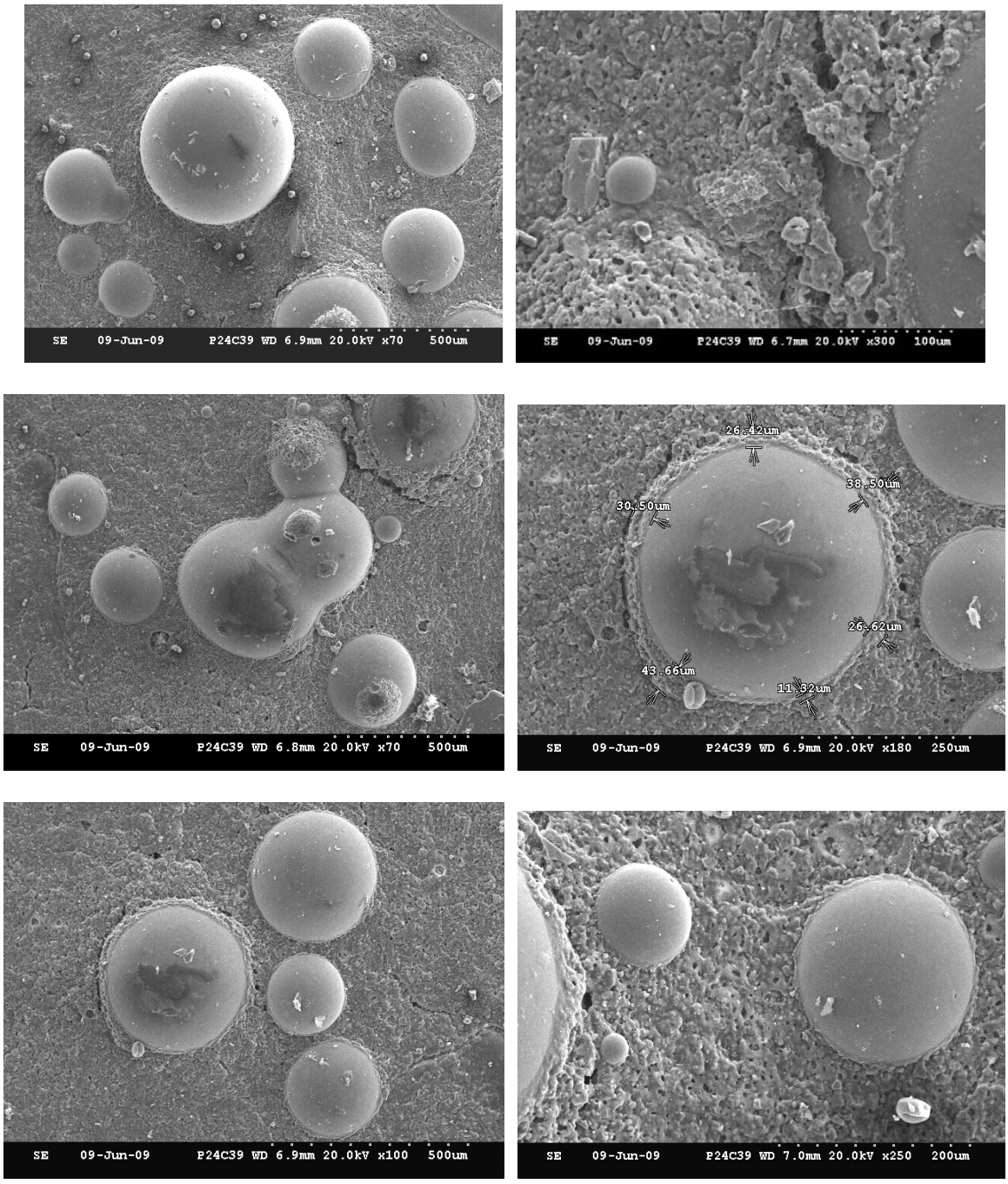

Figure C-1. SEM Images after One Year of Weathering (con't).
(Note: Truck Application Speed is 18 mph and Bead Gun Angle is -40 degrees)

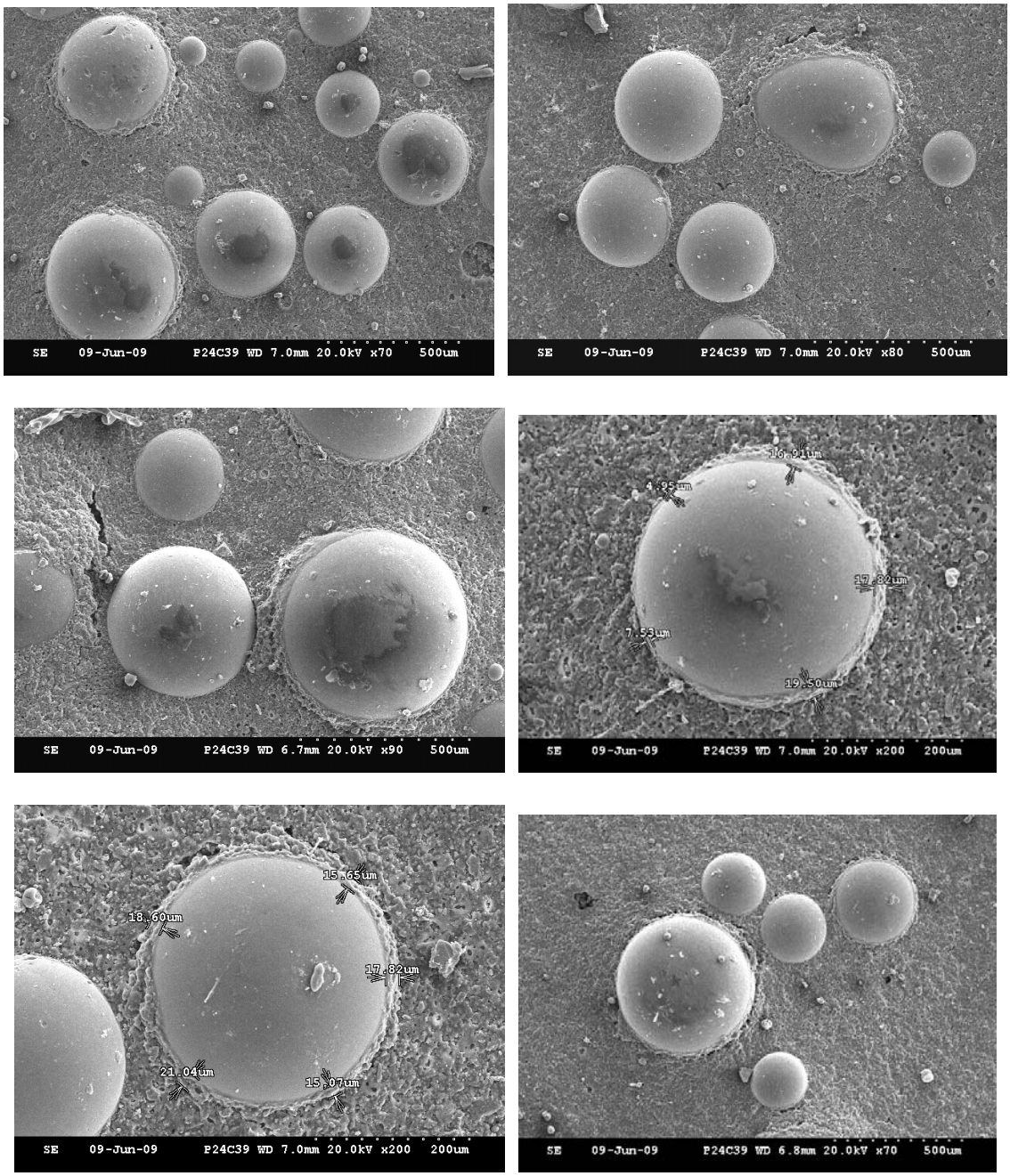

Figure C-1. SEM Images after One Year of Weathering (con't).
(Note: Truck Application Speed is 18 mph and Bead Gun Angle is -40 degrees)